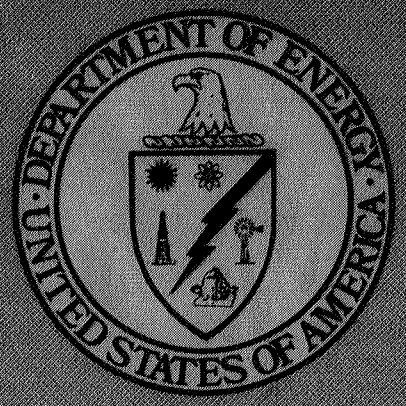

DOE/MC/08216-1378
(DE83008489)

NUMERICAL MODEL DEVELOPMENTS FOR STIMULATION TECHNOLOGIES IN THE EASTERN GAS SHALES PROJECT

By
Timothy G. Barbour
Donald E. Maxwell
Chapman Young

January 1980

Work Performed Under Contract No. AM21-78MC08216

For
Morgantown Energy Technology Center
Morgantown, West Virginia

By
Science Applications, Incorporated
Fort Collins, Colorado

TECHNICAL INFORMATION CENTER
UNITED STATES DEPARTMENT OF ENERGY

DISCLAIMER

Available from the National Technical Information Service, U. S. Department of Commerce, Springfield, Virginia 22161.

Price: Printed Copy A05
Microfiche A01

Codes are used for pricing all publications. The code is determined by the number of pages in the publication. Information pertaining to the pricing codes can be found in the current issues of the following publications, which are generally available in most libraries: *Energy Research Abstracts, (ERA); Government Reports Announcements* and Index (*GRA* and I); *Scientific and Technical Abstract Reports (STAR);* and publication, NTIS-PR-360 available from (NTIS) at the above address.

DOE/MC/08216-1378
(DE83008489)
Distribution Category UC-92a

NUMERICAL MODEL DEVELOPMENTS FOR STIMULATION TECHNOLOGIES IN THE EASTERN GAS SHALES PROJECT

BY

Timothy G. Barbour, Donald E. Maxwell and Chapman Young

Science Applications, Incorporated
202 West Magnolia Street
Fort Collins, Colorado 80521

January 1980

Prepared For

United States Department of Energy
Morgantown Energy Technology Center
Morgantown, West Virginia

Under Contract No. DE-AM21-78MC08216

EXECUTIVE SUMMARY

The continued acceptance and commercial application of explosive well stimulation techniques and the occasionally spectacular results obtained by both conventional and novel explosive stimulation methods in Devonian shale wells indicate that the fracture systems generated by explosive loading can interact quite effectively with the natural fractures and permeabilities controlling shale well production. In contrast to hydraulic fracturing technology, only minimal research and development efforts have been given to explosive well stimulation since hydraulic fracturing began to be the preferred technique in the great majority of hydrocarbon reservoirs. Consequently, the current state-of-the-art for explosive well stimulation, as practiced by many Devonian shale operators, is unchanged from that which was employed thirty years ago. Because of the potential for improved explosive stimulation treatments to be applied to Devonian shale wells in a cost effective manner, increased research efforts should be directed towards both a better definition of shale production characteristics and a better understanding and optimization of the effects of explosive stimulation treatments. Science Applications, Inc. (SAI) has completed the first year of a continuing research and development program to better understand the effects of explosive stimulation treatments.

During the first year of the SAI program, research efforts have been concentrated almost exclusively upon the development and application of numerical modeling techniques to simulate and thus better understand the effects of explosive treatments. The foundation for the SAI program has been the explicit finite-difference numerical programs previously developed by SAI. These programs, identified by the acronym STEALTH*, are based upon and are numerically quite similar to the HEMP and TOODY codes developed at the Lawrence Livermore Laboratory and Sandia Laboratories, respectively. The STEALTH codes are capable of treating one- and two-dimensional solid/fluid mechanics problems incorporating large strains and non-linear material

---

* STEALTH (Solids and Thermal hydraulics code for EPRI Adapted from Lagrange TOODY and HEMP) was developed by Science Applications, Inc. under EPRI contract RP-307.

response. The STEALTH code is ideally suited for the inclusion of complicated explosive/propellant loading conditions and complicated rock fracturing behavior. Due to the lack of suitable computer routines (constitutive equations) describing rock fracture and fragmentation around an explosively loaded wellbore, a large portion of the SAI program was devoted to the development of appropriate descriptions of rock fracturing processes. The computer routines or numerical model for rock fracture has been designated CAVS (Crack and Void Strain). The strains associated with tensile failure and fracturing are critical to a proper description of the continuum mechanics response of the loaded fracturing material and have been coupled, based on elastic theory, with the general three-dimensional stress state.

During the course of the CAVS tensile failure model development and demonstration, improvements have been made to more realistically describe the cracking phenomenon in explosive wellbore stimulation. A tensile failure criteria has been introduced to represent multiple fracture development by introducing logic that adjusts the material's tensile strength (both for crack initiation and crack propagation) according to the degree of cracking that has occurred. Crack propping, either by asperity interference or introduced proppants, has been incorporated to model its effect on crack reclosure. Crack pressurization has been introduced enabling communicating cracks, i.e., communicating with the high fluid pressure of the borehole, to be opened and extended as a result of this additional crack driving mechanism.

For the purpose of demonstrating the capabilities of the CAVS model for studying explosive stimulation techniques and in support of the NTS mineback experiments being conducted by Sandia Laboratories, numerous numerical simulations have been made of the Dynafrac technique being deployed in the NTS tuff in the Sandia experiments. These simulations have been carried out both as parameter sensitivity calculations so as to illustrate the explosive and rock fracturing/yielding properties which might significantly influence experimental results and as predictive

calculations of the effects which should be expected from the specific Dynafrac experiment in NTS tuff.

Several important conclusions have been drawn as a result of these calculations. Exceeding the yield strength, particularly near the borehole, results in irretrievable deformation (plastic flow) and/or compaction and should be minimized as it causes stress redistribution that can severely limit tensile fracture. A lower yield strength will result in a larger plastic deformation around the borehole causing stress redistributions which will result in more crack development near the borehole but less crack development away from the borehole. A larger yield strength by contrast will cause less stress redistribution and reduces the number of cracks and extend them further away from the borehole into the formation. Modeling the compaction equation-of-state as linear and elastic without describing different paths for unloading and reloading results in less near-field compaction and the creation of a small number of long cracks. Modeling compaction as non-linear and non-elastic, a more realistic description of compaction behavior, results in more near-field compaction and the creation of a large number of short cracks near the borehole.

Crack propping directly influences the residual crack void strain and indirectly influences crack extension through crack pressurization. As the shock wave passes the zones immediate to the borehole the hoop tensile stresses generated by the shock are relaxed and the stresses again become compressive. Without a propping mechanism, either natural or introduced, a "skip-zone" commonly occurs around the borehole where cracks that were once open reclose, cutting off communication of the borehole with cracking that has occurred and remains open further from the borehole. By introducing a propping mechanism the cracks remain open and residual void strain is accordingly increased. The increased void strain does not directly influence crack extension but because a non-zero crack void strain exists crack pressurization is possible which assists the crack extension.

Crack pressurization has the most beneficial effect on crack extension of the parameters analyzed. During early times (less than 250 μsec) in the NTS Dynafrac simulations, the shock wave caused by the dynamic explosive loading in the borehole initiates and propagates cracks to about 40 cm. Late time (after 250 μsec) cracking continues to about 80 to 120 cm from the borehole depending on the pressure profile in the crack.

The numerical modeling development and resultant calculations conducted within the first year of this program have illustrated several important factors:

- Numerical simulation methods based upon finite-difference modeling techniques can be effectively utilized to study the fracturing effects of explosive stimulation methods.
- A proper description of the rock fracturing processes is essential to these numerical simulations.
- The fracture patterns developed are extremely sensitive to other rock failure mechanisms such as compaction and yielding.
- The rate and amplitude of wellbore loading can significantly alter the fracture patterns developed especially when yielding and/or compaction are readily activated in the rock.
- Fracture pressurization whether by the explosive reaction products or a liquid pad in the wellbore is critically important to the extension of fractures to significant distances from the wellbore.
- Depending upon the natural fracture control of shale well production characteristics, explosive/propellant stimulation techniques of the tailored-pulse-loading type could prove an effective and viable approach to shale well stimulation.

PREFACE

The Eastern Gas Shales Project (EGSP) of the Department of Energy (DOE) has the goal of examining marginal gas resources and to determine what methods would be required to extract vast amounts of natural gas trapped in eastern Devonian shales. As part of this project the Morgantown Energy Technology Center (METC) is conducting a research program to evaluate stimulation technologies in these relatively impermeable gas shales. One aspect of this program is concerned with numerical model development which would be used in assessing the suitability of various stimulation treatments. Part of this study is being conducted by Science Applications, Incorporated (SAI) under contract to METC. This report presents the results of the recent numerical model development, with particular emphasis on fracture model development and its application to various wellbore fracturing techniques.

CONTENTS

		Page
SECTION 1	INTRODUCTION.	1
	1.1 Eastern Gas Shales Program	1
	1.2 Purpose and Scope of Study	1
SECTION 2	CAVS - A TENSILE FAILURE MODEL.	3
	2.1 Introduction	3
	2.2 Computational Sequence	6
	2.3 Tensile Failure Criteria	7
	2.4 Crack Jumbling	13
	2.5 Crack Pressurization	17
SECTION 3	CAVS - DEMONSTRATION.	20
	3.1 Parameter Sensitivity.	20
	3.2 Model Geometry	20
	3.3 Unaugmented DYNAFRAC	24
	3.4 Material Properties.	24
	3.5 Calculation Results.	33
SECTION 4	SIMULATIONS OF NTS MINEBACK EXPERIMENTS	42
	4.1 Introduction	42
	4.2 Calculation Results.	43
SECTION 5	SUMMARY, CONCLUSIONS AND RECOMMENDATIONS.	76
	5.1 Summary.	76
	5.2 Conclusions.	77
	5.3 Recommendations.	79
REFERENCES.		82
APPENDIX A.		84

TABLES

Table		Page
1	Calculational Matrix for EGSP Wellbore Stimulation Methods	21

LIST OF FIGURES

Figure		Page
1	CAVS Crack Modes	4
2	CAVS Tensile Failure Model	8
3	CAVS Tensile Strength Criterion	10
4	CAVS Crack Initiation, Propagation and Odometer Update	12
5	CAVS Jumbling Model	15
6	CAVS Crack Pressurization Model	19
7	Configuration used in One-Dimensional Cylindrical Geometry Calculations of the DYNAFRAC (unaugmented) Experiment in the NTS Multi-Frac Test Series	23
8	Nitromethane Equation-of-state	26
9	Water Equation-of-State	27
10	Ash-Fall Tuff Yield Models	29
11	Ash-Fall Tuff Compaction Models	30
12a	CAVS Crack Plot - Basline Yield	34
12b	CAVS Crack Plot - Yield #1	35
12c	CAVS Crack Plot - Yield #2	36
13	CAVS Crack Plot - Compaction	37
14	CAVS Crack Plot - Cracks Unpropped	39
15a	CAVS Crack Plot - Cracks Pressurized - Case 1	40
15b	CAVS Crack Plot - Cracks Pressurized - Case 2	41
16a	NTS DYNAFRAC - Nitromethane Pressure-Time History	45
16b	NTS DYNAFRAC - Water Pressure-Time History	46
16c	NTS DYNAFRAC - Borehole Wall Pressure-Time History	47
16d	NTS DYNAFRAC - Radially 1½' Pressure-Time History	48
16e	NTS DYNAFRAC - Radially 2½' Pressure-Time History	49
16f	NTS DYNAFRAC - Radially 3½' Pressure-Time History	50

LIST OF FIGURES (cont.)

Figure		Page
17a	NTS DYNAFRAC - Borehole Wall Radial Stress-Time History	51
17b	NTS DYNAFRAC - Radially 1½' Radial Stress-Time History	52
17c	NTS. DYNAFRAC - Radially 2½' Radial Stress-Time History	53
17d	NTS DYNAFRAC - Radially 3½' Radial Stress-Time History	54
18a	NTS DYNAFRAC - Borehole Wall Hoop Stress-Time History	55
18b	NTS DYNAFRAC - Radially 1½' Hoop Stress-Time History	56
18c	NTS DYNAFRAC - Radially 2½' Hoop Stress-Time History	57
18d	NTS DYNAFRAC - Radially 3½' Hoop Stress-Time History	58
19a	NTS DYNAFRAC - Borehole Wall Acceleration-Time History	59
19b	NTS DYNAFRAC - Radially 1½' Acceleration-Time History	60
19c	NTS DYNAFRAC - Radially 2½' Acceleration-Time History	61
19d	NTS DYNAFRAC - Radially 3½' Acceleration-Time History	62
20a	NTS DYNAFRAC - Borehole Wall Peak Acceleration-Time History	63
20b	NTS DYNAFRAC - Radially 1½' Peak Acceleration-Time History	64
20c	NTS DYNAFRAC - Radially 2½' Peak Acceleration-Time History	65

LIST OF FIGURES (cont.)

Figure		Page
20d	NTS DYNAFRAC - Radially 3½' Peak Acceleration-Time History	66
21a	NTS DYNAFRAC - Radial Stress Snapshot at 50 μsec	67
21b	NTS DYNAFRAC - Radial Stress Snapshot at 100 μsec	68
21c	NTS DYNAFRAC - Radial Stress Snapshot at 500 μsec	69
22a	NTS DYNAFRAC - Hoop Stress Snapshot at 50 μsec	70
22b	NTS DYNAFRAC - Hoop Stress Snapshot at 100 μsec	71
22c	NTS DYNAFRAC - Hoop Stress Snapshot at 500 μsec	72
23a	NTS DYNAFRAC - Acceleration Snapshot at 50 μsec	73
23b	NTS DYNAFRAC - Acceleration Snapshot at 100 μsec	74
23c	NTS DYNAFRAC - Acceleration Snapshot at 500 μsec	75

SECTION 1
INTRODUCTION

1.1 Eastern Gas Shales Program

The Devonian shales, underlying extensive areas of the eastern United States, are estimated to contain trillions of cubic feet of natural gas but only a small fraction of this is economically retrievable using existing well completion and stimulation technologies. Realizing the potential in these reserves, the Morgantown Energy Technology Center (METC) has, since, 1976, undertaken the Eastern Gas shales Project (EGSP) to examine methods of retrieving this resource and to develop, evaluate and field demonstrate new gas recovery methods and stimulation technologies.

Because of the Devonian shale's low permeability, all of the improved formation stimulation techniques have been directed toward increasing the shales permeability and borehole communication with the gaseous formation. Towards this end, much of the recent technology development has been concerned with rock fracture and fragmentation via wellbore fracturing treatments. To comparatively evaluate the various proposed stimulation methods, it has been necessary to quantitatively analyze the many factors influencing rock fracture and their interactions. The parametric analyses reported on here were performed using a time-explicit finite-difference code with a tensile failure model to describe fracture development and to evaluate these factors and interactions for each of the EGSP wellbore fracturing methods.

1.2 Purpose and Scope of Study

The purpose of this report is to summarize the results of numerical calculations using the time-explicit finite-difference code STEALTH with the recently developed Crack and Void Strain (CAVS) tensile fracture model. A brief technical description of the capabilities of the STEALTH (6,7) system of computer codes is presented in Appendix A. The theoretical basis of CAVS (10) is discussed in Section 2. These calculations were performed to

1) evaluate the sensitivity of explosive borehole fracturing using variations in the submodels of CAVS; including crack propping, crack pressurization and tensile failure criterion.

2) evaluate the sensitivity of various geometries and material properties in the borehole models.

3) evaluate the effect of the borehole loading (e.g., high explosive and propellant pulse shape) on the formation fracture pattern.

4) predict fracture patterns, accelerations, and stresses for the Nevada Test Site (NTS) Multi-Frac Mineback Test Series (14).

This report first describes the general theory of CAVS and its submodels. The fracture model is then demonstrated using a borehole model stimulated by the unaugmented DYNAFRAC (13) wellbore fracturing process. Representative fracture patterns, accelerations and stresses are also presented for this process and should aid in the design and data evaluation of the multi-frac test.

Continuing SAI effort will evaluate the effects of additional borehole fracturing techniques; including the other NTS multi-frac experiments. These include the augmented DYNAFRAC and the single and multiple KINEFRAC (3) processes.

SECTION 2
CAVS - A TENSILE FAILURE MODEL

2.1 Introduction

Typically, tension failure models constrain only the stress tensor and adjust the appropriate stress component(s) without detailed compatibility with the strain tensor. This is expedient for most cases of total disruption, such as spall, but in the case of partial cracking a more detailed model is required to provide a coupled response between the stress tensor and the strain tensor due to crack opening and closing. In this case, the stress component adjustments can be very complicated. A detailed description of the computation sequence of these adjustments will be presented in Section 2.2. First, however, the basic philosophy of the model is presented.

The Crack and Void Strain (CAVS) tensile failure model has been developed as part of this study to provide the appropriate coupling between the state of stress and the straining associated with explosive borehole fracturing and to provide a description of crack initiation, propagation and reclosing in the rock formation experiencing the shock wave. The elastic stress-strain relations for three orthogonal directions provides the general case and as now developed, CAVS allows for cracking in these three orthogonal directions. Because of the axisymmetry of the borehole loading, the principal stress directions in the rock are coincident with the orthogonal cylindrical stresses in the one-dimensional calculations presented. The orthogonal cracks allowed by CAVS thus describes quite well the fracture pattern expected from explosive borehole fracturing. The three CAVS crack modes are shown in Figure 1. Because of the nature of the borehole loading, cracking primarily results from tensile hoop stresses. It is then the radially projecting y-cracks that are of primary concern in this report.

As an example of the fundamental basis for crack development, consider the one-dimensional uniaxial strain case where a crack plane interrupts the normal tensile stress. The crack begins to open, sending

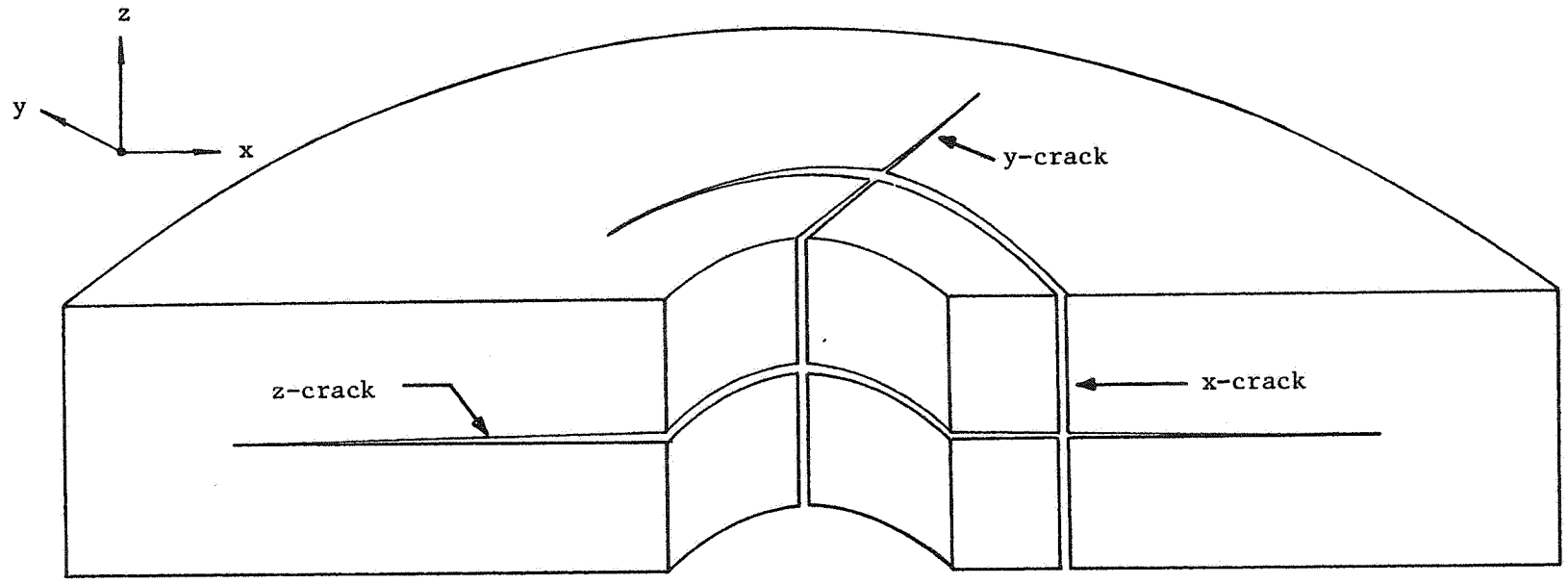

Figure 1. CAVS Crack Modes.

a stress relief wave that decays the tensile stress and the orthogonal stresses (with finite Poisson's ratio). As the crack propagates, a free surface is developed which requires the reduction of the acting tensile stress to zero. This is accomplished by a normal stress decay in the vicinity of the crack and is accompanied by a change (increase) in the rock strain normal to the crack. This rock strain change, due to tensile failure, is manifest as a change of the crack opening, and is identical to what is called "void strain".

The compatibility relations between rock stress and crack void strain are based on elastic theory and provide a simple yet realistic model for fracture initiation and propagation in three orthogonal directions. Material properties that are required for the model are few; a tensile strength and how it varies with crack development, and the bulk and shear moduli. These parameters are easily obtained from simple laboratory experiments, and do not require a description of the inherent flaw size and distribution or flaw nucleation parameters that are usually described in a statistical manner and are required for other computational fracture models (11). These properties represent the microstructural character of the fracturing material and generally are quite difficult to obtain from laboratory testing.

Once a crack has opened and a finite void strain exists, it is possible and quite likely that the crack will reclose if the normal stress becomes compressive. Closure of one crack will in general effect the opening and/or closing of existing orthogonal cracks. The difficulty occurs because of the condition that a void cannot overclose. To prevent this, it is necessary to sub-cycle the closing process to close the crack exactly and not overclose. Additionally, a closing sequence must be defined to properly describe the interaction of cracks closing in one or more directions.

The CAVS model provides for the complications described above and provides side-benefits for crack-wedging (Section 2.4) and crack permeability and pressurization (Section 2.5). The total CAVS tensile failure

model provides for the following basic features:

1) Tensile failure initiation with different criteria for crack initiation and crack propagation (Section 2.3).

2) Odometers, to bookkeep the time-dependent crack description (length and spacing) in three orthogonal directions.

3) Detailed compatibility of the stress tensor adjustments and the crack opening (void strain) in three orthogonal directions.

CAVS is designed for insertion into a standard time-explicit finite-difference code with a minimum of cross-connections to other failure models that may be present, such as plastic yielding, creep, or joint slip constraints on shear stress.

The philosophy behind CAVS is to provide a framework of consistency in which various assumptions of tensile failure, crack propagation, crack propping and pressurization, etc., can be inserted to obtain the detailed and compatible response of the stress tensor and the cracking and crack void strains. It is these submodels that provide for the various responses that may be achieved to predict the observation of laboratory and field demonstrations. After the computational sequence of CAVS and a description of its submodels are presented in Sections 2.2 through 2.5 a demonstration of these responses on the fracture pattern produced from wellbore fracturing will be described in Section 3.

2.2 Computational Sequence

In each of three orthogonal directions the total stress at any time is compared to the current tensile strength in that direction. If the stress exceeds the strength criterion (Section 2.3) cracking is either initiated or continues to propagate, otherwise no change is made in the crack state. To keep track of the cracking, three odometers are defined, one for each of the possible crack directions. Decoding these odometers enables one to determine the number of through cracks, the partial crack length(s) and the crack spacing for each of the model zones. The existing crack spacing is used to establish a time constant, which in turn is used

to define a normal stress decay rate to reduce the acting normal stress to zero as the crack (free surface) develops. The stress decay rate when used with the elastic compatibility relations defines the void strain rate of the crack and for a given time step, the rock stresses, crack void strain and crack spacing are appropriately adjusted. Figure 2 is a flow-chart of this sequence.

Submodels of CAVS allow for propping cracks open when they are re-closed, and for internal pressurization of the cracks. The propping effect models the interference of crack asperities and results in a residual fracture porosity that potentially adds to the material's permeability communicating with the borehole. A detailed description of the concept of propping and a definition of the work required to reclose using this sub-model is described in Section 2.4. The calculation sequence remains the same for crack opening and closing, only the stress relaxation differs; for opening the normal tensile stress is relaxed to zero, for closing the normal compressive stress is modified to satisfy the closing stress-void strain constitutive behavior.

The calculation sequence also remains unchanged when the cracks are pressurized. As described in Section 2.5 the communicating void strain in the cracked rock is internally pressurized and essentially adds to the tensile stress that the crack experiences. As demonstrated in Section 3, the effect is to reduce the number of cracks and extend them further from the borehole.

2.3 Tensile Strength Criterion

Several approaches may be used to define the failure criterion leading to tensile failure and fracture of rock. A purely fracture mechanics approach might be used where zone-to-zone and intra-zone stress gradient, and stress intensity might be computed to compare against the material's fracture toughness. Energy release rate and crack velocity relations may be defined for computing the propagation rate. Another alternative might be to define a distribution on inherent flaws in the

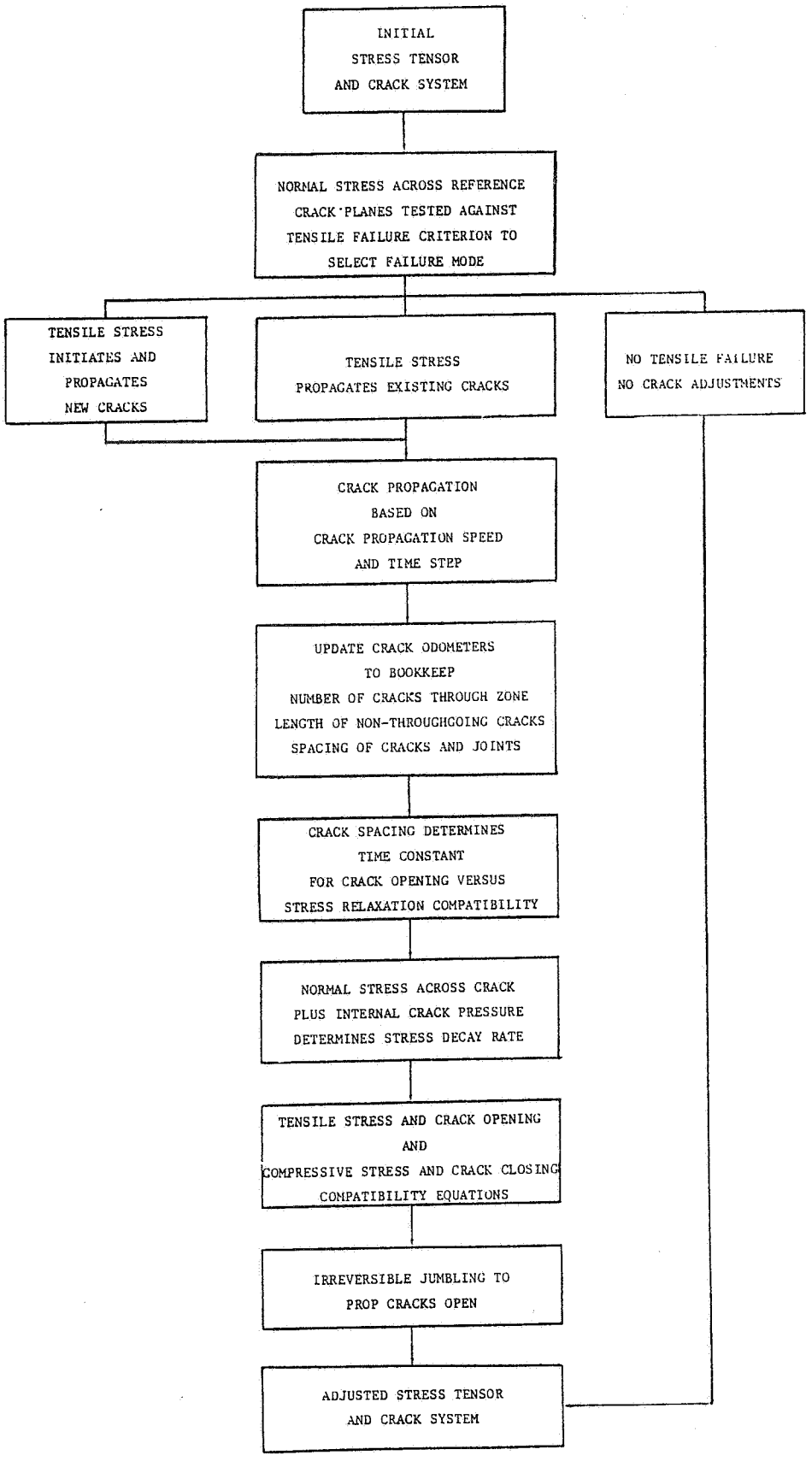

Figure 2. CAVS Tensile Failure Model.

material and flaw growth and nucleation stresses to define flaw growth and coalescence. A somewhat simple, yet descriptive, numerical fracture model might consider only the tensile stress that a zone in the numerical model experiences and compare this to a tensile strength which initiates a crack and a tensile strength which continues to propagate a crack. This is the basis of CAVS as described in sections 2.1 and 2.2

The concept of the tensile failure model of CAVS is to define a single strength at which a crack initiates and another lower strength at which it continues to propagate. Each of these two strengths are incrementally increased as additional cracks develop in a given zone. Increasing the materials tensile strength in this way provides a "weakest-link" behavior where the material initially initiates fractures at a given virgin tensile strength and subsequent initiation of new cracks requires a higher stress. As presently defined in CAVS the ratio of the crack propagation to crack initiation strengths is constant and equal to one-half. The initiation tensile strength as presently defined has the form

$$\sigma_t = C^{NTC}(\sigma_{t_o}) \tag{1}$$

where σ_{t_o} is the uncracked virgin tensile strength, C is a constant (presently 1.05) raised to the NTC (number of through cracks in the zone) power. The propagation tensile strength maintains the incremental increase as additional cracks develop by the ratio mentioned above. Figure 3 shows the variation of the initiation and propagation strengths as a function of time for a zone which has experienced a total of 16 through cracks (NTC).

A continuous variation, rather than the incremental variation as shown in the figure would probably be a more accurate representation and will be included in subsequent representation.

The criteria for crack initiation and propagation described is based on the current crack state in a particular zone. To incorporate the effect of cracking in neighbor zones, the tensile strength of the zone of concern is reduced to a lower crack propagation strength if the number of through

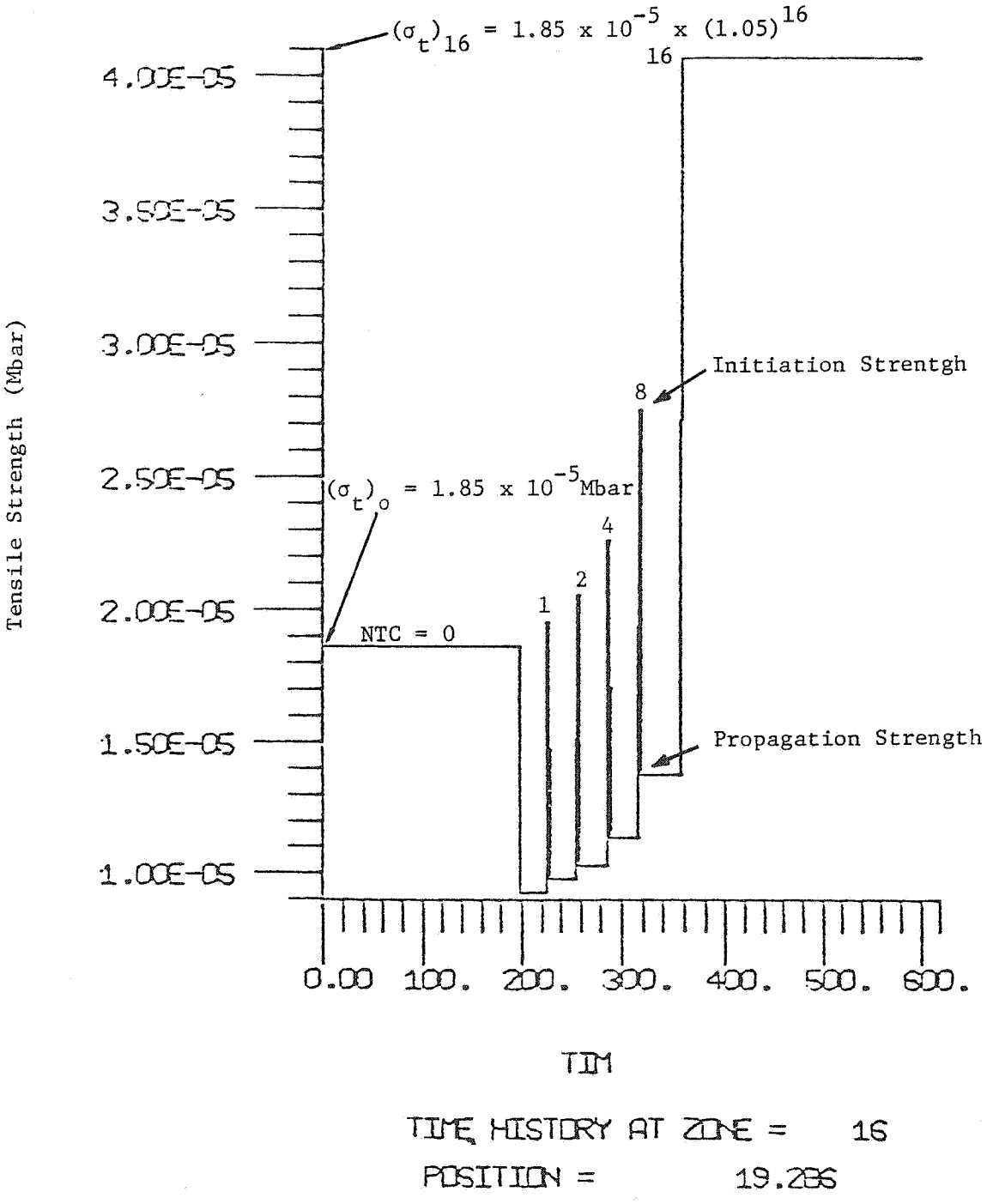

Figure 3. CAVS Tensile Strength Criterion.

cracks for a given direction is greater in a neighbor zone than in the zone in question.

A flowchart of the tensile strength (CTEST) selection and the crack initiation, propagation and odometer update is shown in Figure 4. The crack odometers (F_k), k = 1, 2 or 3, bookkeeps the x, y and z-cracks length (Figure 2) respectively. Extension of the cracks is accomplished at a rate $\dot{F}$ over a given time dt where the $SPEED_k$ is a constant crack propagation velocity and DL_k is the through-crack length of the zone. For each iteration of the calculation, the state of cracking in a zone is determined, from which the zone's tensile strength is defined. The current stress normal (σ_t) on the crack, including internal crack propagation, is then compared to its strength in that direction and propagation or initiation is or is not continued.

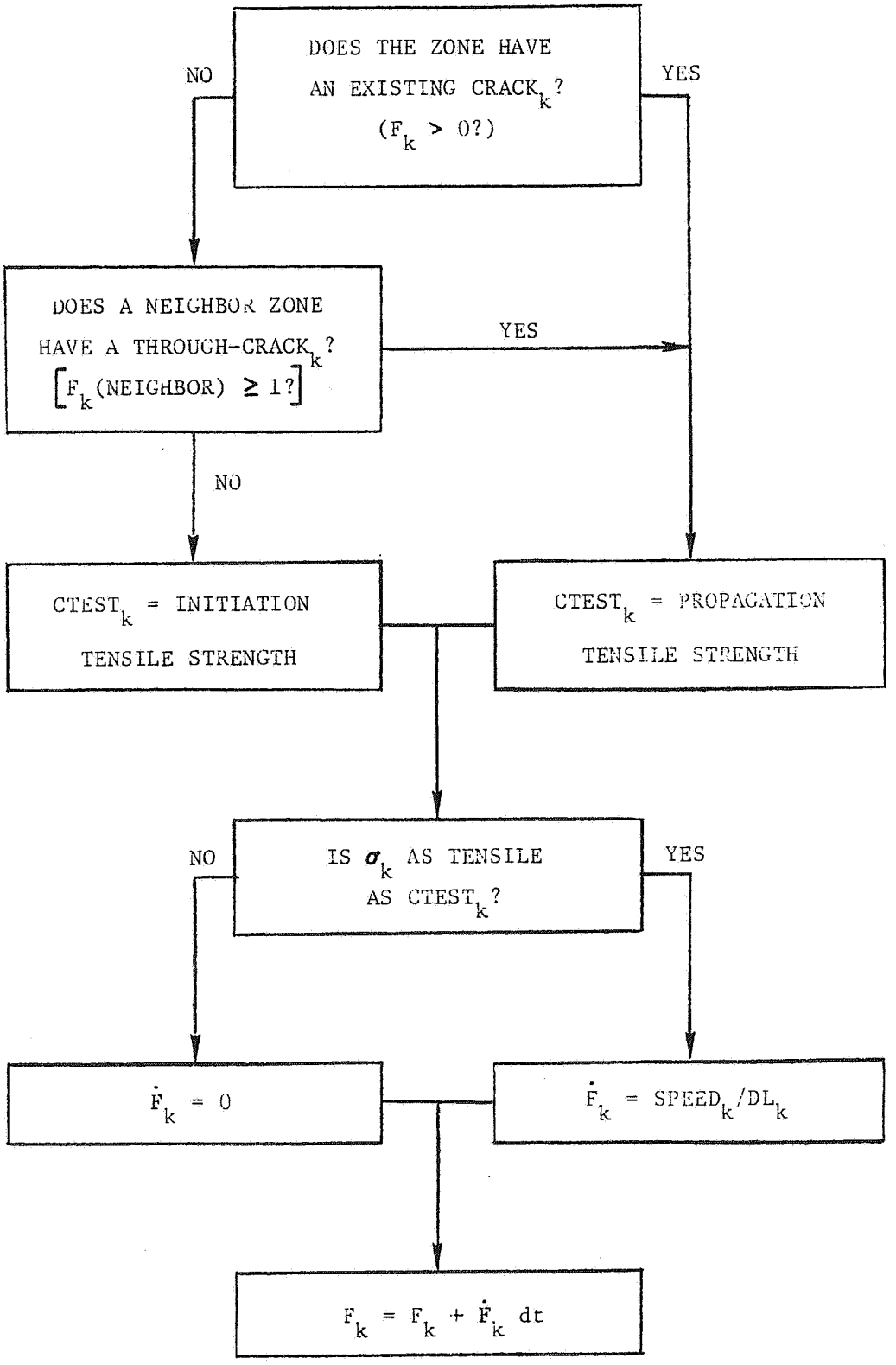

Figure 4. CAVS crack initiation, propagation, and odometer update.

2.4 Crack Jumbling

The jumbling submodel of the CAVS tensile fracture model provides a mechanism to account for the propping action that occurs in a crack or joint when it is opened and then reclosed. Once opened a crack will usually misalign causing the crack to wedge open due to mismatched asperities. The propping action of the model limits complete reclosure, providing an increased residual porosity and permeability of the fractured material. Additionally, the jumbling logic requires energy to be expended in reclosing opened cracks or joints. The amount of work required to overcome the interference to closing chiefly depends on the maximum achieved opening of the crack and the compressive stiffness that the asperities provide against closing.

The amount of bulking (i.e., irrecoverable residual crack void volume) primarily depends on the maximum fracture opening the crack has experienced. The model presented here incorporates this effect by defining a bulking coefficient which limits the degree of reclosure to an appropriate percentage of the maximum achieved crack void volume. The crack closure limit is additionally limited to a maximum value of 12% of absolute strain. Accounting for all three possible cracking directions provided by CAVS, the maximum possible residual porosity is limited to 36%, which is typical of a loose gravel. Irrecoverable crack void strain (VLIM) is defined less than zero, compatible with the code convention that open cracks correspond to values of crack void strain (VSTN) less than zero. The model used in the current calculations is

$$VLIM_k(t) = MAX\left[-0.12,\ MIN\left(VLIM_k(t-dt),\ B\cdot(VSTN_k(t-dt))\right)\right] \qquad (2)$$

where B is a defined bulking coefficient. Here, B is 0.20. This aspect of the model allows for the propping action, defining a residual crack void volume. To completely define the closing phenomenon one must also describe the constitutive stress-strain behavior of the closing crack under compressive normal loading.

In the simplest case, one might define a model which offers no resistance to reclosure. The reclosure limit still would be defined as described above, but the process of reclosing would require no work to be performed. A more realistic model, however, would require energy to be expended to overcome the interference provided by the mismatched asperities. Goodman (5) describes the constitutive behavior of mating and non-mating cracks under compressive normal loading and defines a hyperbolic function to analytically model his experimental observations. The model used here is slightly more complex to enable a more flexible definition of the closing stress (STRCLS) - void strain (VSTN) behavior. Here, a constitutive relationship defined by the summation of a parabola and a hyperbola (Figure 5) is used.

$$\begin{aligned} STRCLS_k(t) = (VSTNMX_k(t)/SF) \; & \Big[\alpha + \beta(VSTN_k(t) - VSTNMX_k(t)) \\ & + \gamma(VSTN_k(t) - VSTNMX_k(t))^2\Big] \\ & + A\Big[VSTN_k(t)/(VSTN_k(t) - VLIM_k(t))\Big]^{\,VSTNMX_k(t)C} \end{aligned} \qquad (3)$$

where

VSTNMX = Maximum achieved void strain that the crack has experienced (i.e., the maximum opening of the crack).

VLIM = Crack closure limit, as defined in Equation 2.

α, β, γ = Coefficients of the parabolic portion of the function, which plays the dominant role during the beginning of crack closure.

A, C = Coefficients of the hyperbolic portion of the function, which plays the dominant role during the end of the crack closure when the crack approaches its closure limit.

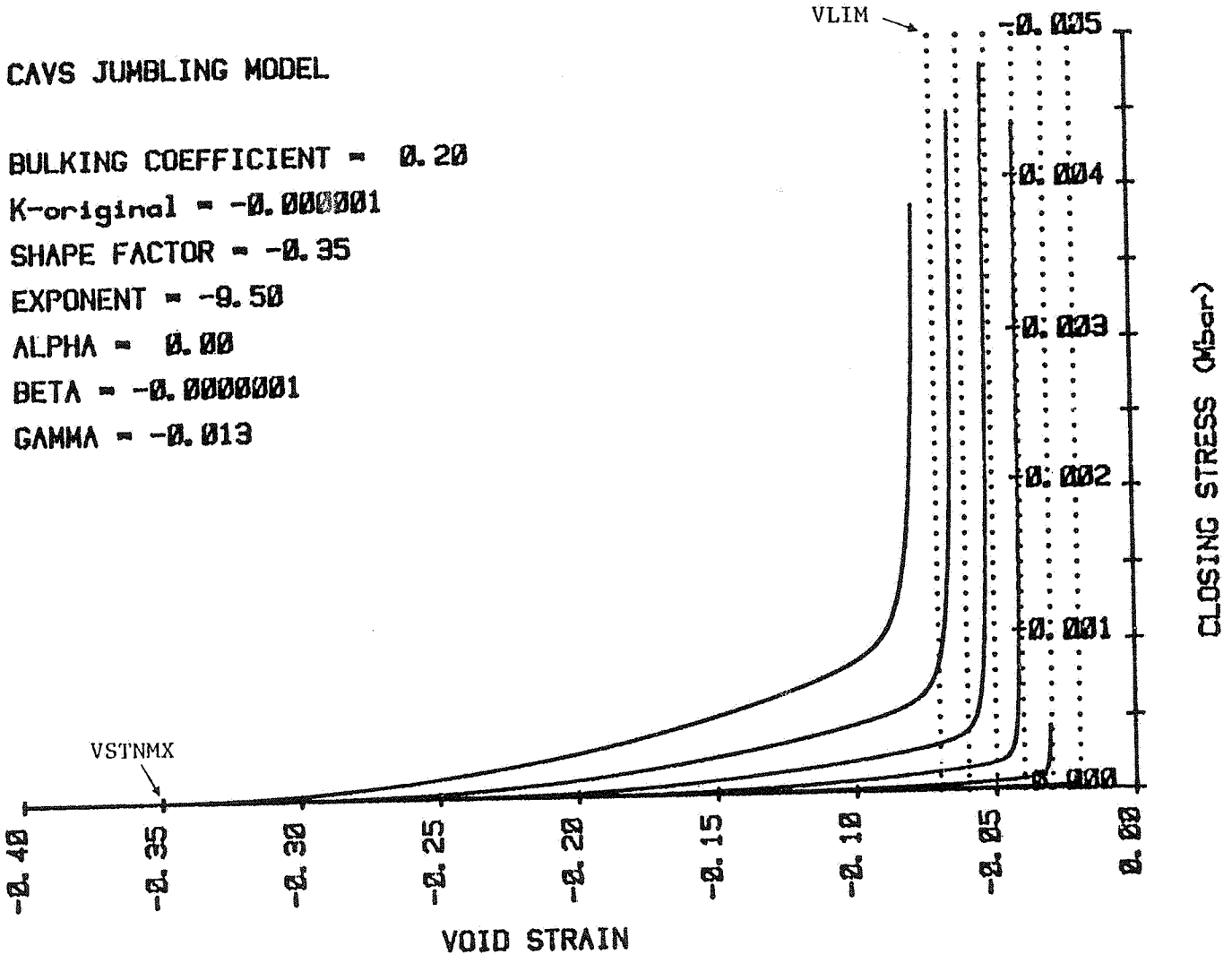

Figure 5. CAVS Jumbling Model.

SF = Shape factor which controls the variation in the shape of the constitutive relationship depending on the maximum achieved crack void strain. This factor was used to initially fit the relationship to the few experimentally obtained data points that were available from dynamic compaction tests on unretorted oil shale with various initial fracture void volumes.

The family of curves that equation 3 describes continuously varies, being chiefly controlled by the maximum achieved crack void strain. As defined, the larger the maximum void strain, the larger the amount of work is required to reclose a crack. Redefining the coefficients, described above, will enable a more accurate fitting of experimental data as it becomes available. When the crack has completely closed (i.e., the void closure limit, VLIM, has been reached) the constitutive behavior is again represented by the equation-of-state description of the bulk unfractured rock.

During crack closure the stress tensor must be adjusted to be compatible with a reduced crack void strain. This is accomplished in the same manner as crack opening, where the tensile stress is relaxed to zero across the free surface of an open crack and the void strain appropriately increased. During crack closing, however, the compressive stress across the crack must be relaxed to be compatible with the constitutive behavior defined by equation 3. When the normal stress across the crack is more compressive than the envelopes of Figure 5 will allow, the excess compressive stress is relaxed to the envelope and a compatible void strain is computed. Instead of relaxing the stress state to zero and allowing a relatively large void strain reduction, the compressive stress is relaxed to the envelope and the void strain reduction is somewhat less. The overall difference is to reduce the amount of closure for a given state of stress, thus requiring additional work to be performed to completely close a crack. When the closing stress is less compressive than the envelope, no change is required in either the crack void strain or compressive stress across the crack.

2.5 Crack Pressurization

Recent numerical (12) and experimental (4) investigations of explosively produced fracture suggest that the explosive gases (or liquids, when the explosive is used with a buffering liquid, such as water) may penetrate fractures and contribute directly to the fracture process, adding a crack opening and extension mechanism to the primary process of tensile failure due to shock wave propagation. The basic interactions between the gases produced by the explosive in the borehole, the penetration of these gases into the cracks and the profile that the crack faces experience is in need of much additional research. The consequences of static, or quasi-static pressurization have been well-treated. Daneshy (2) provides a summary and comparison of several of the analysis methods. As a qualitative measure of the effect of dynamic crack pressurization on the response of the CAVS fracture model, a series of calculations were performed using the unaugmented DYNAFRAC model described in Section 3.2. The calculations were directed towards the sensitivity of the cracking pattern around the borehole as a result of various assumed pressure profiles within the cracks communicating with the gases in the borehole.

Because CAVS allows for both crack opening (void strain increase) and closing (void strain decrease) the first requirement of these calculations was a knowledge of the communicating crack void strain in the rock with the explosively produced fluid pressure in the borehole. For each time-step it was, therefore, necessary to monitor which cracks were opened and which were closed and to bookkeep the total volume of void strain of the opened cracks that could be conceivably pressurized.

Commonly, a "skip-zone" would develop in the crack pattern around the borehole, where immediate to the borehole the stress field would at late times become compressive and reclose the previously opened cracks. This phenomenon, probably a part of borehole crushing, is due to the tensile hoop stress relaxation after the passing of the radially compressive shock wave. This zone of crack reclosure substantially reduces the total communicating void strain and number of cracks that might be pressurized.

Knowing the crack void strain that is in communication with the borehole volume, a new total volume that the gases might occupy is defined and a reduced borehole pressure is computed to maintain the $-P \cdot \Delta V$ energy balance. A reduced pressure is then applied to the crack to increase its opening and extend its length. Variations of the crack pressure profile where then applied, always maintaining a balance with the total available gas energy from the borehole explosive.

As suggested by McHugh (12), if the borehole explosive gases can be assumed to behave as an ideal gas, the maximum gas velocity that may be achieved, for one-dimensional flow in a crack will be greater than, or comparable to, typical crack velocities in rock, suggesting gas penetration into the fractures. At any instance of time during the explosive fracturing, it is likely that the total crack volume will not be penetrated by the gases from the borehole, particularly because of dynamic gas leak-off and variation from the one-dimensional flow assumption. A reduced volume was therefore selected, usually at 95% (2) of the total available crack volume.

The one-dimensional crack representation shown in Figure 6 depicts the 95% gas occupancy at X_c. Figure 6 also shows possible pressure profiles that a crack might experience. P_x is computed pressure calculated at position x which is the mid-position of the cracked zone. P_x is an average pressure applied across the length of the given zone.

As will be discussed in Section 3 adding an internal pressure to a crack significantly effects the developed crack pattern in rock around a borehole. Several calculations were performed to determine the effect on cracking using several of these crack pressurization profiles.

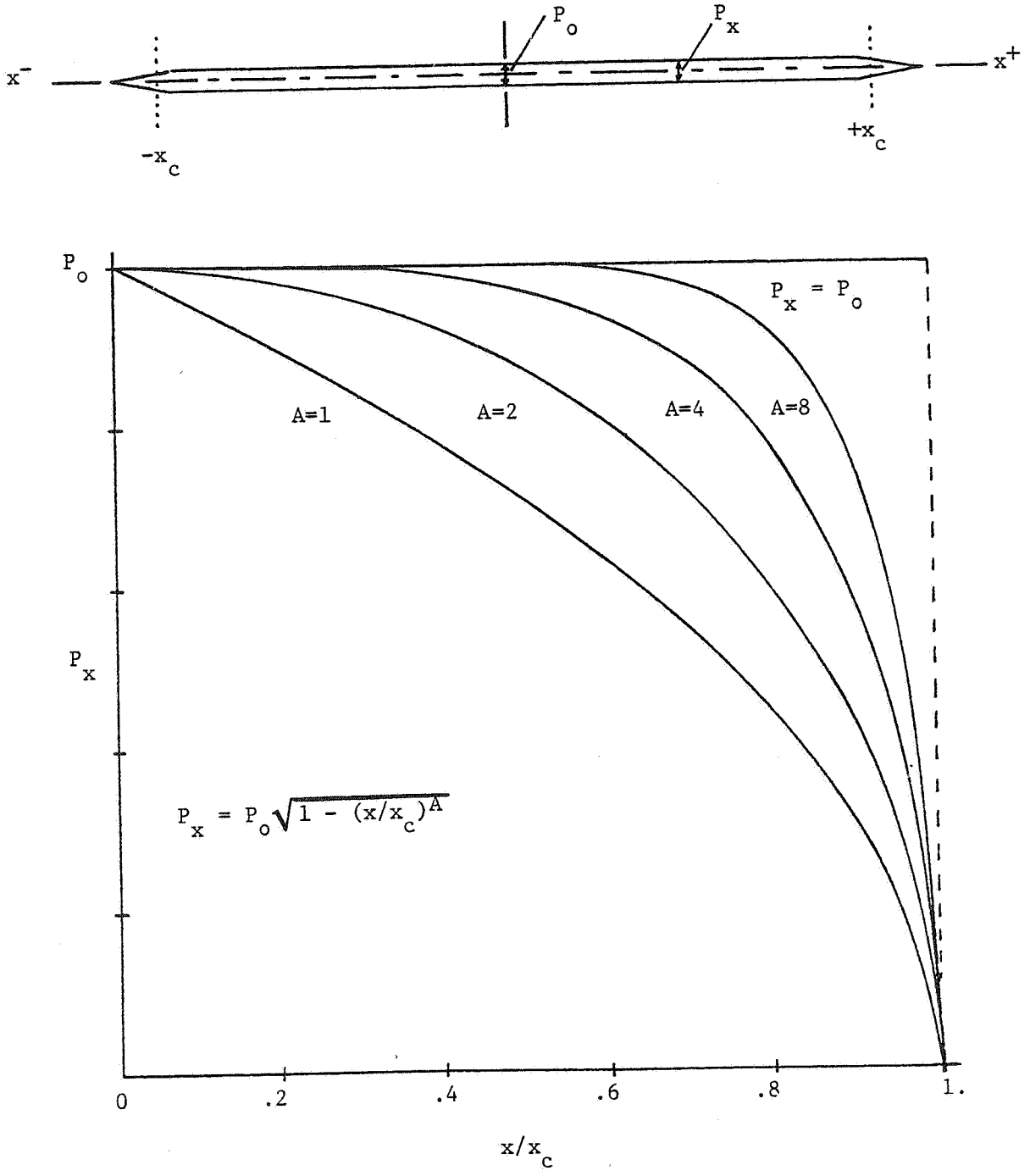

Figure 6. CAVS Crack Pressurization Profiles.

SECTION 3
CAVS - DEMONSTRATION

3.1 Parameter Sensitivity

To evaluate the parameter sensitivity of rock fracture and fragmentation using the CAVS tensile failure model, it was necessary to determine the effect on cracking of the various submodels described in Section 2, of the rock mass characterization and model geometry and of the borehole loading.

In addition to a critical physical evaluation of the rock fracture and fragmentation processes and how the numerical models duplicate these events, a comparative evaluation must be undertaken for the various EGSP wellbore stimulation techniques. The parameters which have been identified for evaluation and which compose the two axes of a matrix of well stimulation methods and related physical processes are given in Table 1. A complete evaluation of the wellbore stimulation technology thus requires first a measure of the dependence of the method upon the various rock and geologic parameters and then, after appropriate normalization, a comparative evaluation with other technologies.

In the demonstration presented in this section only one borehole loading technique, the unaugmented DYNAFRAC, is considered. Evaluation of the other techniques of borehole fracturing, as mentioned in Section 1, have not been completed but are planned and will be presented in future reports.

3.2 Model Geometry

SAI's one-dimensional finite-difference, time-dependent computer code, STEALTH-1D, was used to numerically model the unaugmented-DYNAFRAC wellbore stimulation treatment. This code solves the differential equations of mass, momentum and energy conservation to an accuracy that is determined by zone size and time step used in the finite differencing model.

TABLE 1

CALCULATION MATRIX FOR EGSP

WELLBORE STIMULATION METHODS

DYNAFRAC - unaugmented

DYNAFRAC - augmented

KINEFRAC - single treatment

KINEFRAC - multiple treatment

GAS FRAC - Sandia

Rock Fracture

- Failure criterion
  - Tensile strength
  - Fracture toughness
  - Initiation/Propagation
  - Linear elastic/Non-linear non-elastic
- Anisotropy
  - *In Situ* stress
  - Strength
- Rate dependence

Rock Porosity

- Compaction

Rock Strength

- Yield
- Tensile

Stress Gradients/Differences

Gas evolution

- Crack internal pressurization

Discontinuities

- Joints, faults

Geometry and boundary conditions are selected to model these aspects as they might be found for a particular laboratory or field demonstration. For the purposes of this demonstration these conditions describe the NTS Multi-Frac Test Series. Borehole geometry and *in situ* stresses are defined based on the preliminary design and conditions of these experiments. Data generated by the code (i.e., stresses, accelerations, cracking, etc.) where obtained (reported in Section 4) at radial distances from the borehole where instrumentation is preliminarily planned for these field tests.

Additionally, characterization of the model's materials must be defined and varied to evaluate the parameter's sensitivity on the response of the model. Three materials are involved in the one-dimensional model shown in Figure 7; a nitromethane explosive charge, a surrounding water buffering fluid and the ash-fall tuff rock mass. For these calculations no pre-existing discontinuities have been modeled within the rock mass.

Figure 7 is a representation of the one-dimensional cylindrical geometry configuration used in the calculations summarized in this section. Centered in the borehole, is a charge of nitromethane, which is surrounded by water acting as a buffering fluid used to couple the explosive pulse to the formation in the desired fashion. The geometry ratio of borehole diameter to explosive diameter was selected as 8:1 because it provided the best results in Physics International's investigation (13) in extending cracks without seriously compacting and damaging the immediate rock around the borehole. The rock mass, for purposes of demonstration and as an indication of the response in the NTS Multi-Frac Test Series, was selected as ash-fall tuff.

Its characterization has been preliminarily described by Terra-Tek (1) and Sandia Laboratory (15). Dynamic compaction and yield data as well as tensile strength data are currently being obtained by SAI on the ash-fall tuff.

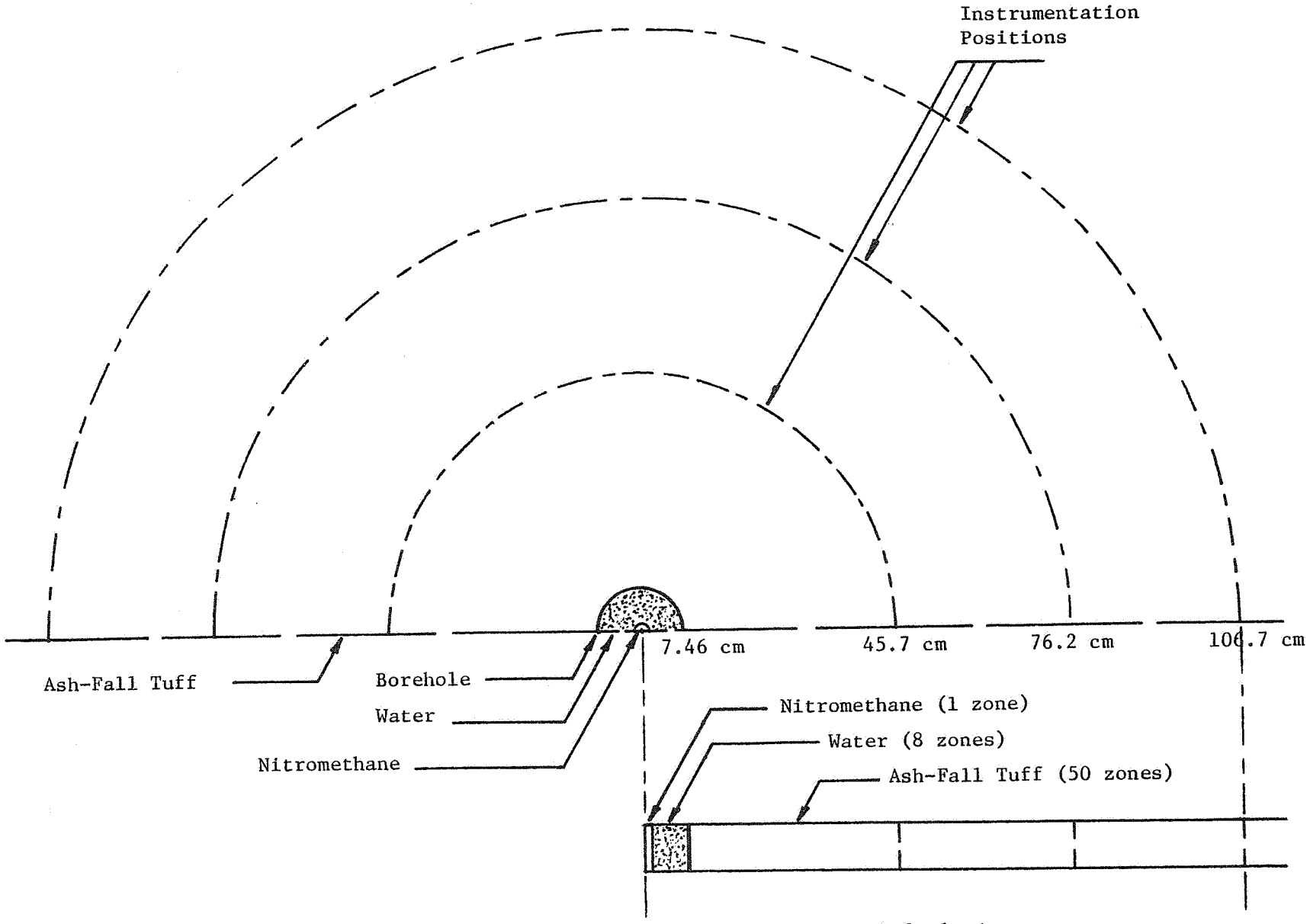

Figure 7. Configuration used in One-Dimensional Cylindrical Geometry Calculations of the DYNAFRAC (unaugmented) experiment in the NTS Multi-Frac Test Series.

3.3 Unaugmented DYNAFRAC

The unaugmented DYNAFRAC wellbore fracturing technique (13) is an explosive fracturing method intended to increase productivity of oil and gas reservoirs. The method is based on generating and extending multiple fractures in an oil or gas formation by using a small downhole explosive source in a controlled manner. The unaugmented process almost instantaneously pressurizes the borehole causing multiple fractures to occur in the formation before stress relief occurs from the tensile failure. The augmented DYNAFRAC process attempts to superimpose a slow burn-rate propellant pulse on the rapid explosive pulse to extend the created multiple fractures by increasing the duration of the borehole pressure loading. A complete and detailed accounting of the processes and the success of the methods in field demonstrations can be found in Reference 13.

3.4 Material Properties

To complete the description of the numerical model representing the unaugmented DYNAFRAC process in the NTS Multi-Frac Test series it is necessary to define the constitutive behavior of each of the materials involved. For the rock mass, this must include the elastic properties, the yield criterion and the plastic properties. Additionally, the rock's fracture properties must be specified. For purposes of this investigation, both the rock mass and rock fracture properties were assumed to be isotropic for the fairly homogeneous NTS ash-fall tuff. The water buffering fluid which couples the energy of the explosive to the borehole is inert and hydrodynamic requiring only a description of its compressibility. The nitromethane explosive requires a description of the amount and rate of energy release.

The model that was selected to describe the behavior of the nitromethane explosive is called the Jones-Wilkins-Lee (JWL) equation-of-state (8). It is based on abundant experimental data and is represented by

$$P = A\left(1 - \frac{\omega}{R_1 \cdot V}\right)e^{-R_1 \cdot V} + B\left(1 - \frac{\omega}{R_2 \cdot V}\right)e^{-R_2 \cdot V} + \frac{\omega E}{V} \text{ (Mbar)} \qquad (5)$$

For nitromethane,

$A = 2.0925$
$B = 0.056895$
$R_1 = 4.4$
$R_2 = 1.2$
$\omega = 0.3$

where P, V and E are the instantaneous pressure, relative volume and energy. The initial total available energy, E_o, is 0.051 Mbar·cc/cc. The STEALTH-1D code has a standard JWL equation-of-state option. Only the constants A, B, R_1, R_2 and ω and the initial energy E_o were required as input. The reference density is 1.128 gm/cc. An implicit time history of the nitromethane PV response is shown in Figure 8.

The equation-of-state of water has been experimentally defined and takes on different forms depending on the range of pressures and temperatures. The model used here (9) is independent of temperature and good up to shocks of about 200 kbars. The implicit time history of the water PV response is shown in Figure 9. The general form of the equation is

$$P = P_o(1 - \frac{G\mu}{2}) + \frac{GE_o}{V} \text{ (Mbar)} \qquad (6)$$

where

$$P_o = A\mu + B\mu^2 + C\mu^3$$

$$G = D \sin(\frac{EV}{F} - H) + I$$

E_o = initial relative energy = 1.85185×10^6 erg/cc for an initial relative density of 0.9982 gm/cc and initial relative volume, V, of 1.0

and μ = compression $(\frac{1-V}{V})$.

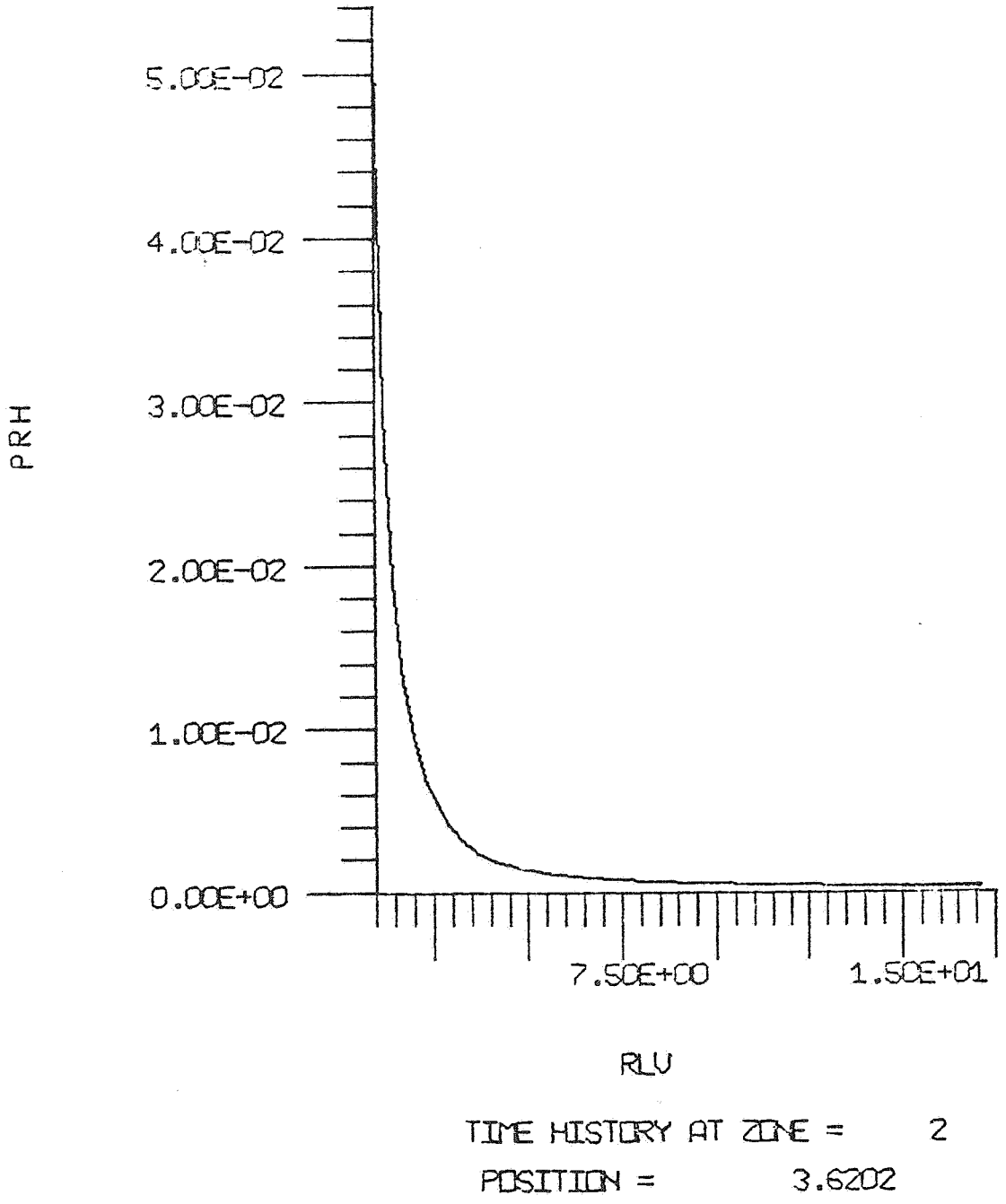

Figure 8. Nitromethane Equation-of-State

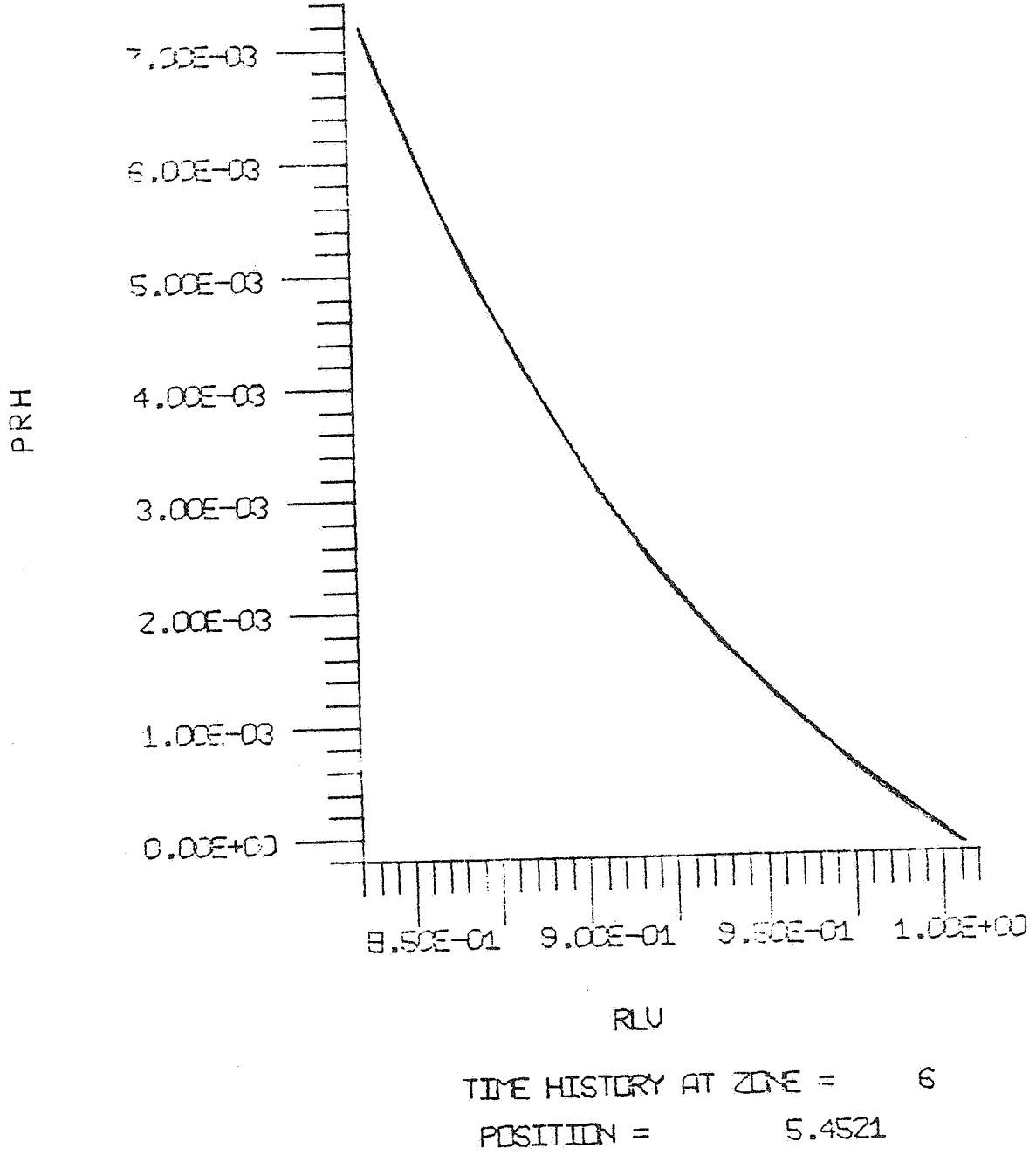

Figure 9. Water Equation-of-State

The equation's constants are

A = 0.21954
B = 0.052138
C = 0.23181
D = 0.41
E = 9.52
F = 0.9982
H = 4.5676
I = 0.94

Ash-fall tuff was chosen as the formation rock. As mentioned above, the tuff behavior was assumed to be isotropic for this demonstration. The parameter sensitivity analysis of this report is concerned with the response of the CAVS fracturing with variation in the constitutive behavior of the rock mass. Of particular concern, are the effects that variations of the yield criterion and the equation-of-state have on the CAVS fracture pattern around a borehole. The NTS ash-fall tuff's characterization has been preliminarily described by Terra-Tek (1) and Sandia Laboratory (15). Dynamic compaction and yield data as well as tensile strength data are currently being obtained by SAI on the ash-fall tuff.

Three yield envelopes were defined in the sensitivity analysis and are shown in Figure 10. The baseline yield function is representative of an ash-fall tuff from the Nevada Test Site (NTS) although the criterion was established (1) on samples taken in locations other than the G-tunnel site of the multi-frac test series. This function is considered typical of the tuff's behavior and serves as an estimate of the yielding in this demonstration. Two other yield surfaces were defined and are purely hypothetical (labeled Yield #1 and Yield #2 on Figure 10). The three criteria were used to evaluate the sensitivity of the rock's yield strength in CAVS cracking. A discussion of these results will be presented in Section 3.5.

Two equations-of-state were defined as a means of comparing the effect of the rocks compressibility on the cracking pattern. The two functions are shown in Figure 11. A simple linear behavior described by a bulk modulus alone (curve #1) served as the baseline behavior. Loading and

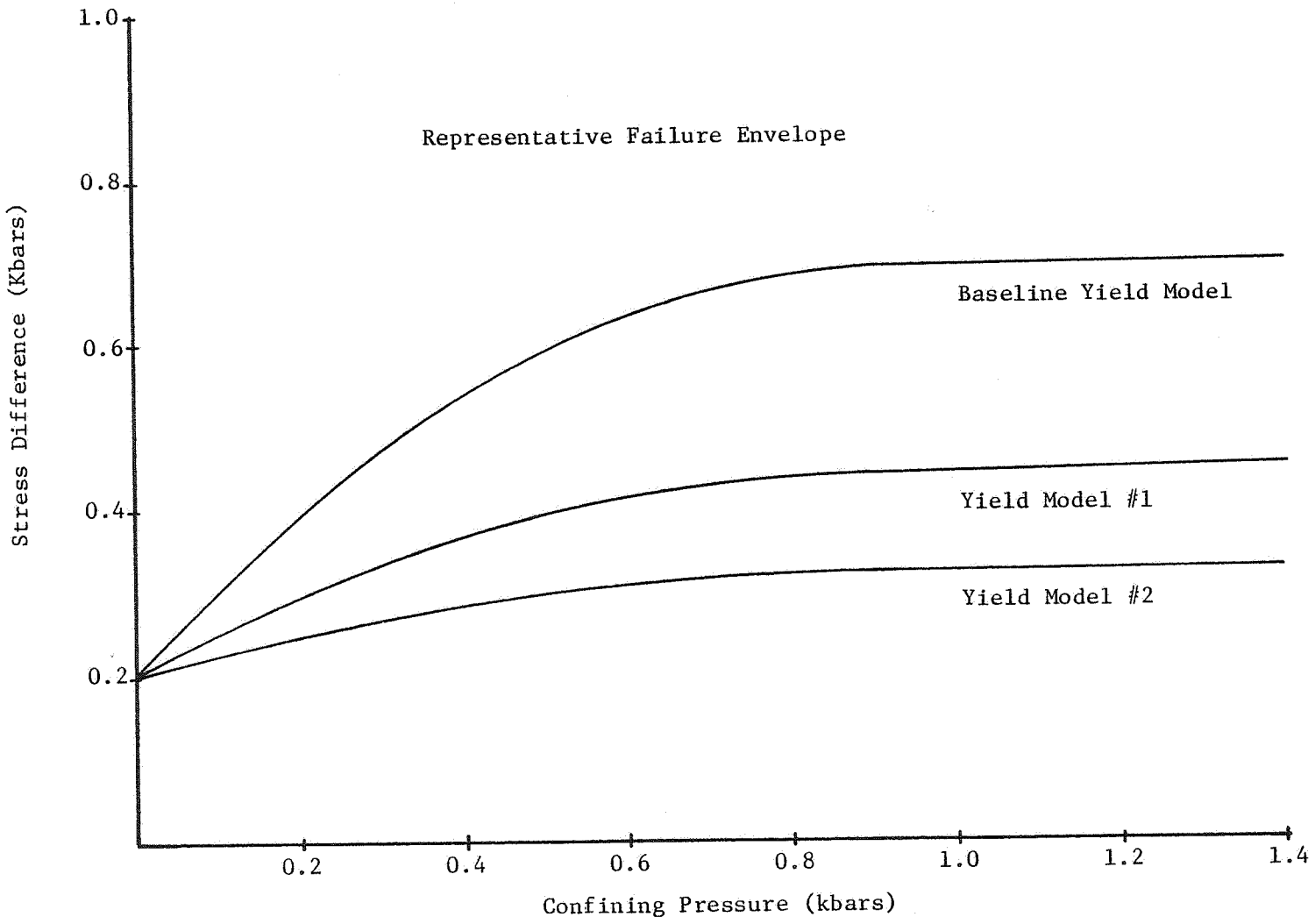

Figure 10. Ash-Fall Tuff Yield Models.

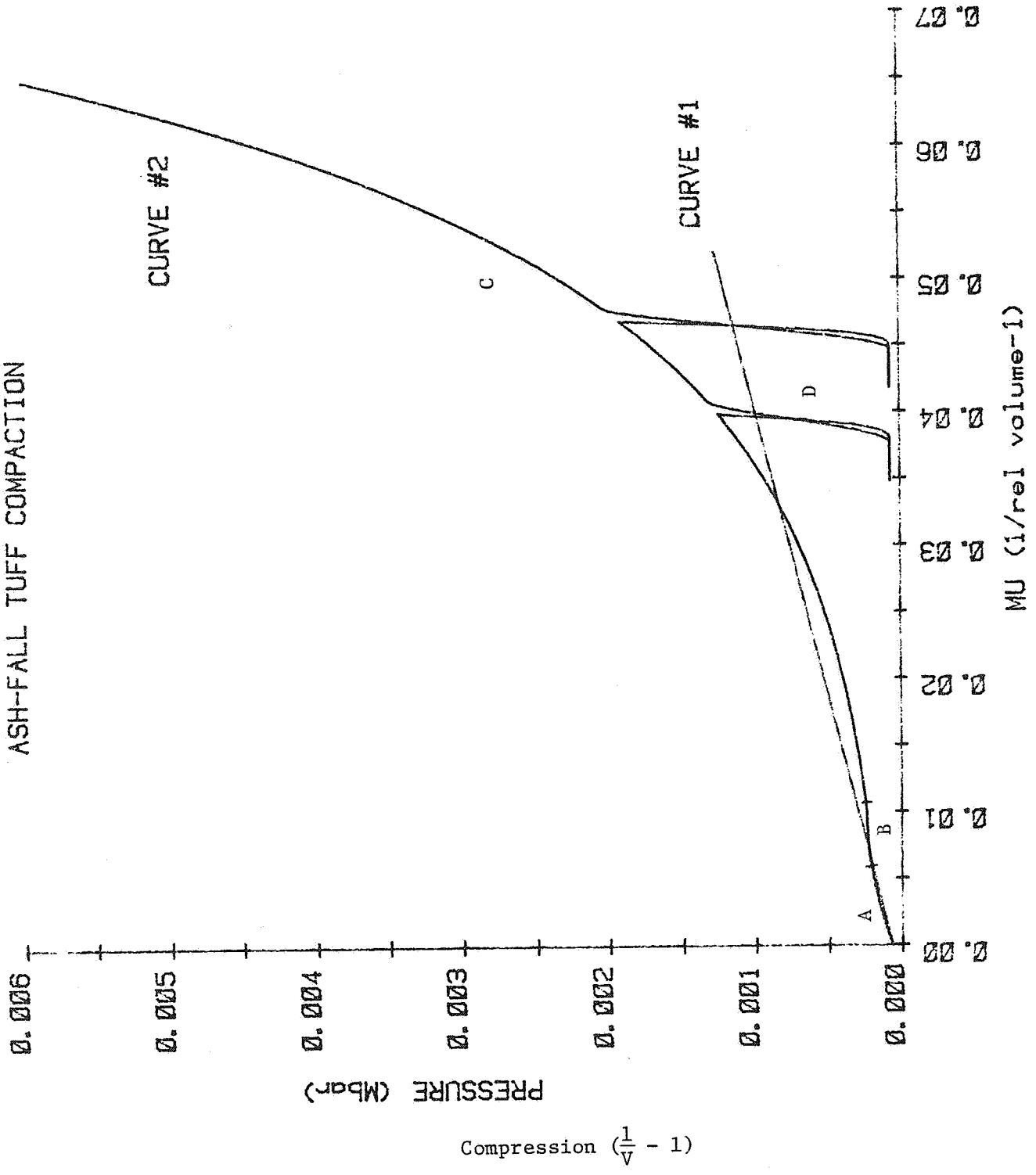

Figure 11. Ash-Fall Tuff Compaction Models.

unloading were assumed to occur along the same path. A more complex function (curve #2) describes the many aspects that might be expected and has been observed (1) in the ash-fall tuff's compaction. The two equations-of-state were used to evaluate the importance of compaction on cracking and the results of these calculations are described in Section 3.5

Curve #2 can be portioned and described by the physical processes that are occurring during the compaction. During initial compression of the porous tuff, a microstructural breakdown between the material grains is represented by Section A of the curve. As the grain-to-grain contacts are broken the tuff becomes less stiff and pore collapse occurs (Section B). During and after pore collapse the ash-fall tuff becomes less compressible as represented by Section C. Unloading and reloading during any portion of the compaction is modeled using two different yet similar curves indicated as Section D of Curve #2.

To complete the description of the ash-fall tuff for the STEALTH calculations the following material properties were defined:

Rock Mass Density = 1.8 gm/cc

Isotropic Elastic Model

Bulk Modulus (curve #1 of Figure 11) = 0.023 Mbar

Shear Modulus = 0.0172 Mbar

Isotropic Plastic Model

Yield Model - (below P = 0.0009) Y = 0.0002 + 1.10P - 610P (Mbar)

(above P = 0.0009) Y = 0.00067 + 0.02P (Mbar)

Flow Rule - non-associated Prantl-Reuss are defined in STEALTH

CAVS Tensile Failure Model

Virgin Tensile Strength of Intact Rock = 1.86×10^{-5} Mbar

Ratio of Initiation-to-Propagation Tensile Strengths = 2.0

Strengths adjusted as described in Section 2.3

In Situ Stresses

Isotropic = 6.89×10^{-5} Mbar

As previously indicated, no joints were present in the models and no pore pressures were modeled.

3.5 Calculation Results

To evaluate the sensitivity of the CAVS fracture model upon the characterization of the fracturing material (ash-fall tuff in this case) a series of STEALTH/CAVS calculations were performed. The yield criterion and the compaction equation-of-state were considered most likely to have the greatest influence in variations of the borehole cracking and thus these parameters were analyzed. Additional evaluation might be directed towards the effect of pore pressures in yielding and compaction and thus on cracking and the effect of a tensile strength criterion as compared to a fracture mechanics type criterion. Additional sensitivity analyses that might be considered are summarized in Section 5.

Figures 12a, 12b and 12c show the crack patterns that have been calculated by CAVS for the three yield surfaces shown in Figure 10. The geometry of the DYNAFRAC model used for these calculations is shown in Figure 7. The highest strength yield model (labeled Baseline Yield on Figure 7) allows the cracks to extend further into the rock than the other two yield models (Yield #1 and Yield #2). Comparing the three CAVS crack plots (Figures 12a, 12b and 12c) and their yield model counterparts indicates that the lower the yield strength the shorter the cracks extend from the borehole. As the yield strength is lowered more cracks are developed immediately around the borehole but extend only a relatively short distance into the rock. Conversely, as the strength is increased and the plastic deformation reduced, stress redistribution is less and the available energy for cracking is increased. The tensile stresses remain high at relatively long distances from the borehole and cracks are extended. In these three calculations, the cracks were propped using the jumbling model but not pressurized.

Figure 13 is a CAVS cracking plot for the compaction sensitivity analysis. The results were obtained with the crack jumbling logic on and the crack pressurization prohibited. Adjacent to the borehole the maximum compression (see Figure 11) was about 2% using the equation of curve #1, and about 6% using the equations of curve #2. The crack pattern for the two compaction curves 1 and 2 (see Figure 13) shows the influence of the

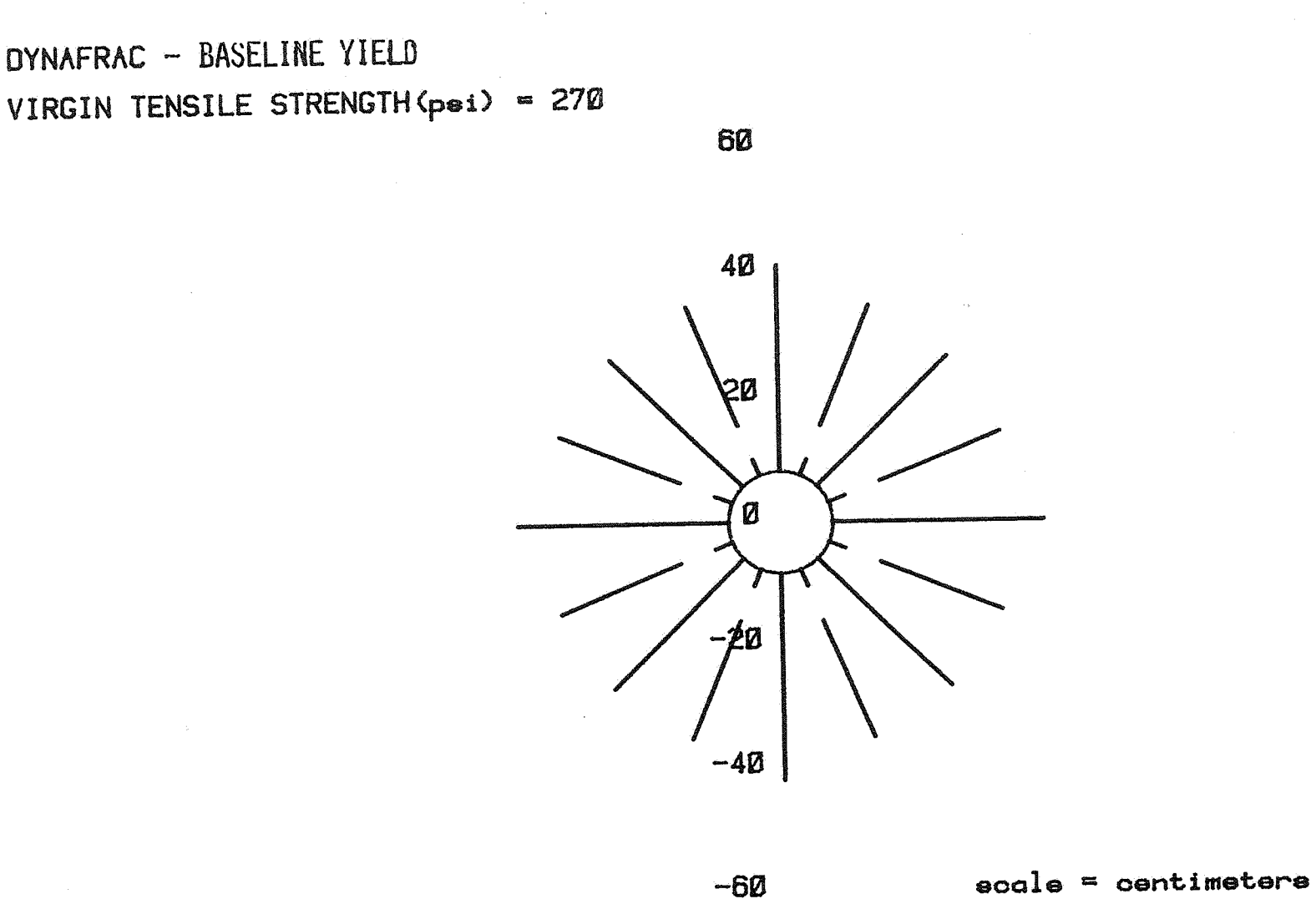

Figure 12a. CAVS Crack Plot - Baseline Yield Criterion.

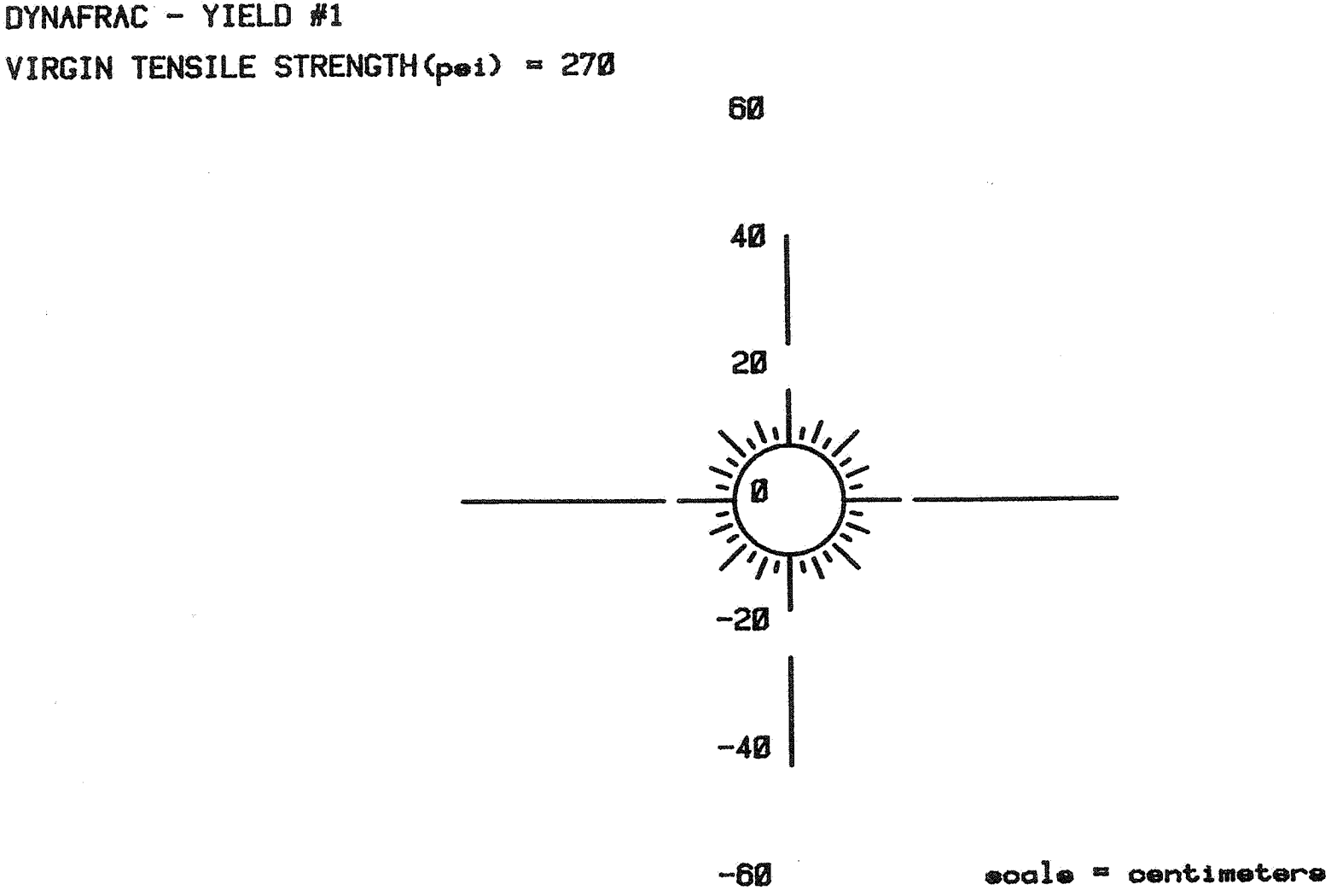

Figure 12b. CAVS Crack Plot - Yield #1.

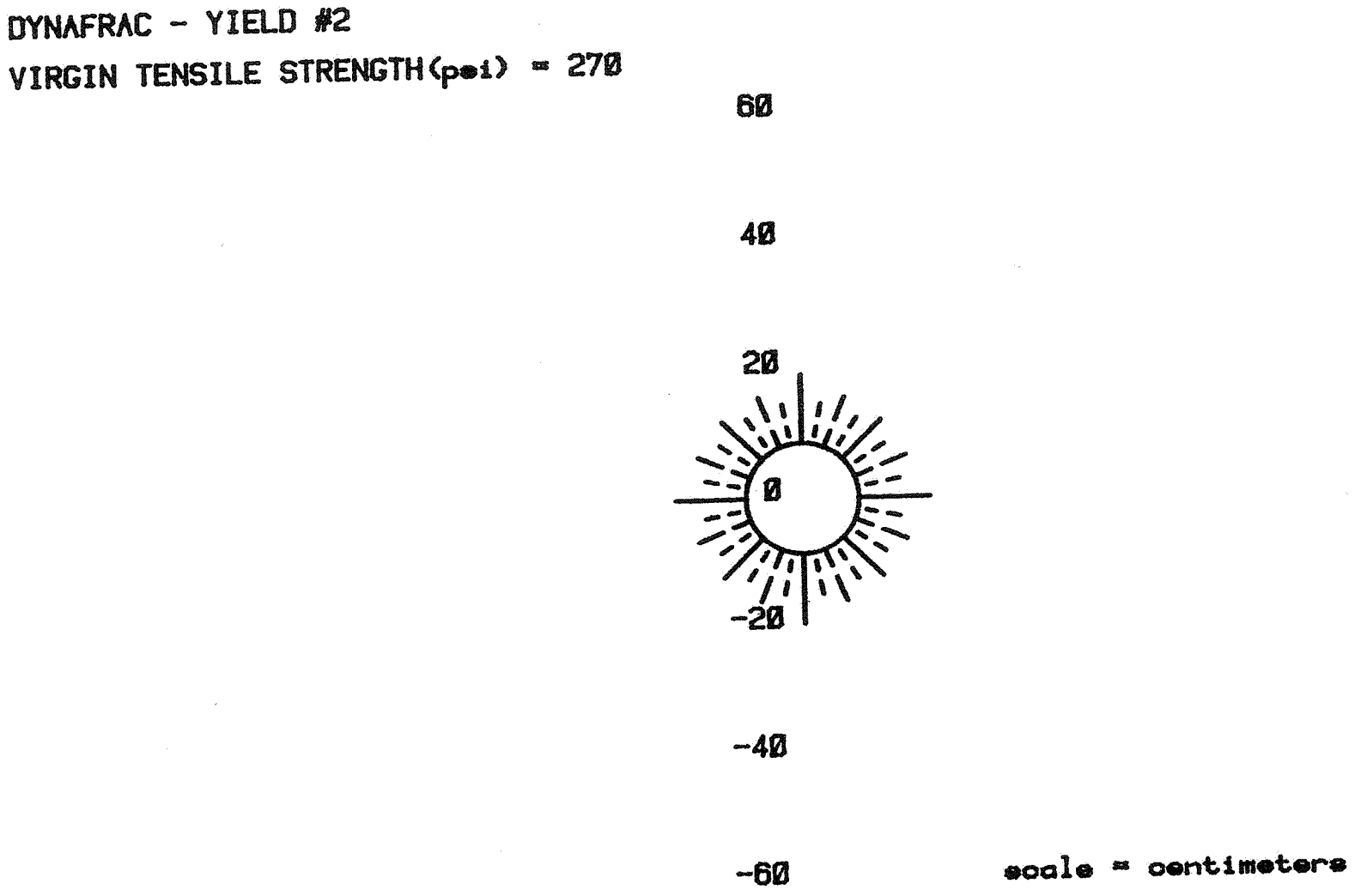

Figure 12c. CAVS Crack Plot - Yield #2.

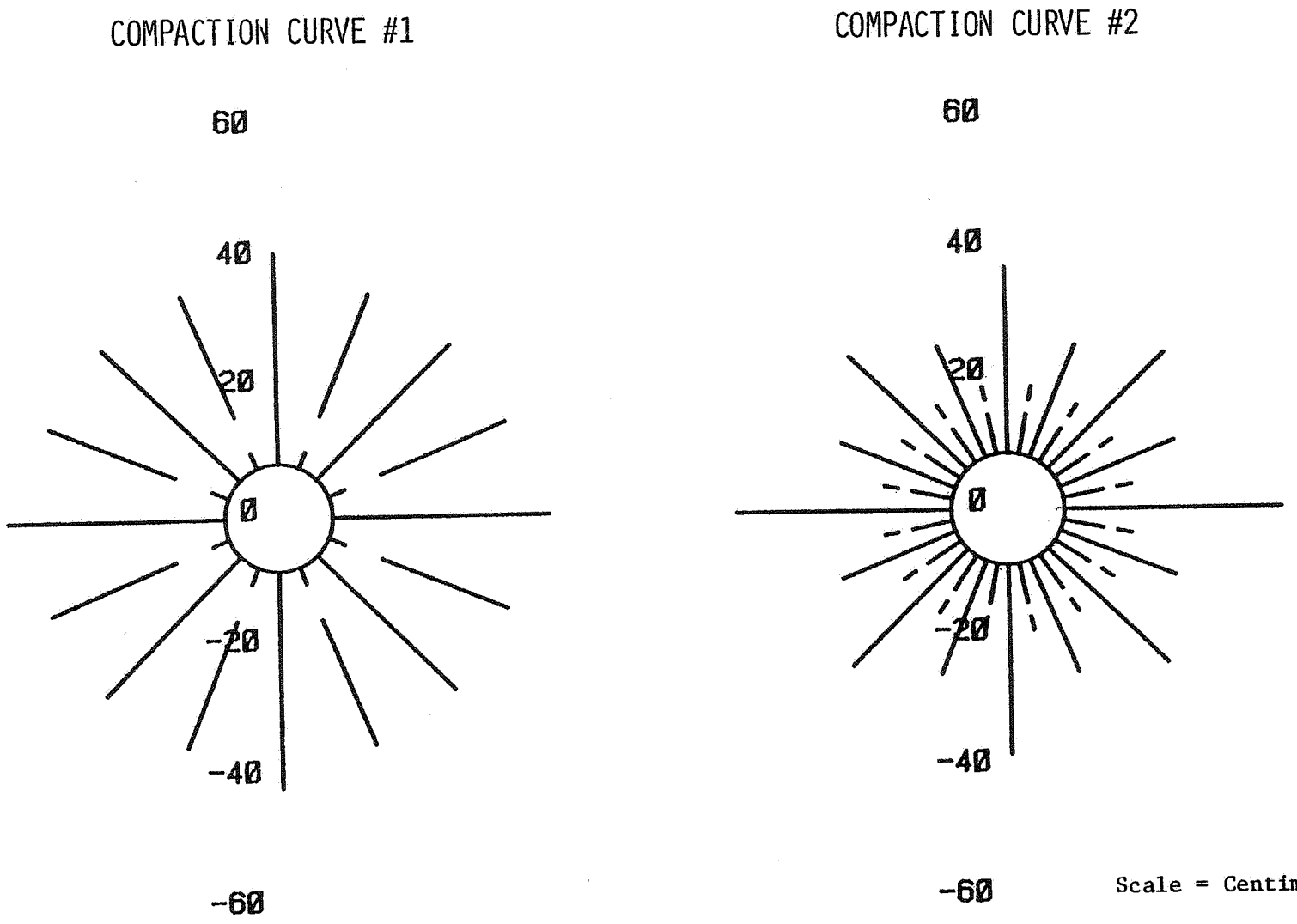

Figure 13. CAVS Crack Plot, Compaction #1 and #2.

additional compaction on the increased near-field cracking. Far-field cracking (where the compaction is less) is essentially the same for both compaction models.

Figure 14 is a CAVS plot of cracking around a borehole, again for the NTS Dynafrac experiment. In this case the jumbling submodel of CAVS was not used and the cracks were able to completely reclose. The dotted lines indicate the cracks that were developed as the hoop tensile wave passed through the rock and were later reclosed as a result of the tensile stress relaxation and the hoop stresses again become compressive causing closure. This plot is the same as Figure 12a were the jumbling logic used to maintain the open cracks except propping is not allowed.

Figure 15a and 15b are CAVS plots of cracking for two cases of crack pressurization. In Figure 15a the cracks were pressurized according to the pressure profile indicated on Figure 6 using A = 2. Figure 15b is a similar plot using A = 8. It should be noted that these two calculations were run for 5000 μsec as compared to 500 μsec for all of the other un-pressurized calculations. The main reason for this is that the cracking continues during late times, caused primarily by the crack pressure, rather than the early time shock wave cracking. This is an important consideration and shows the importance on crack extension of late time crack pressurization.

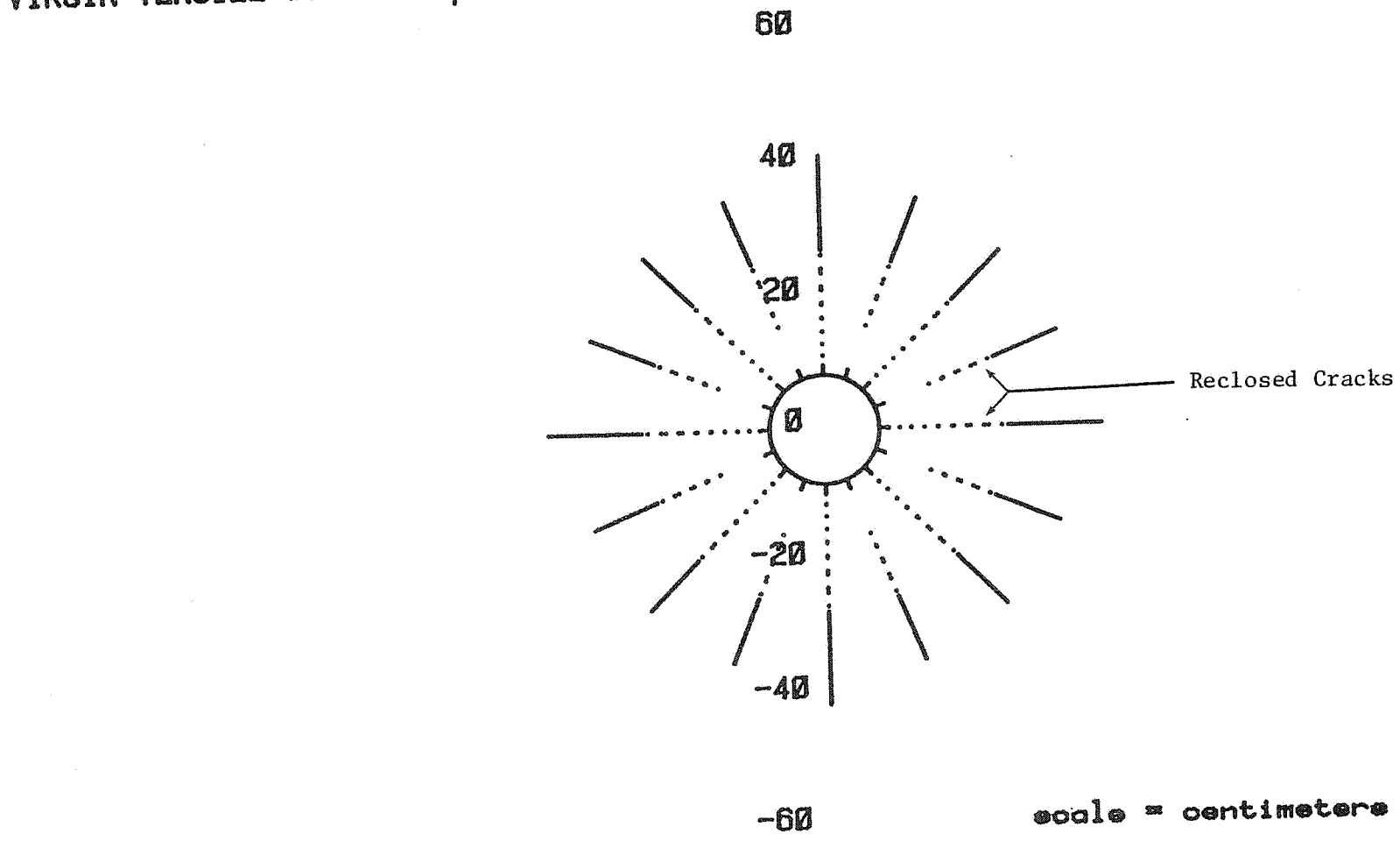

Figure 14. CAVS Crack Plot - Cracks Unpropped.

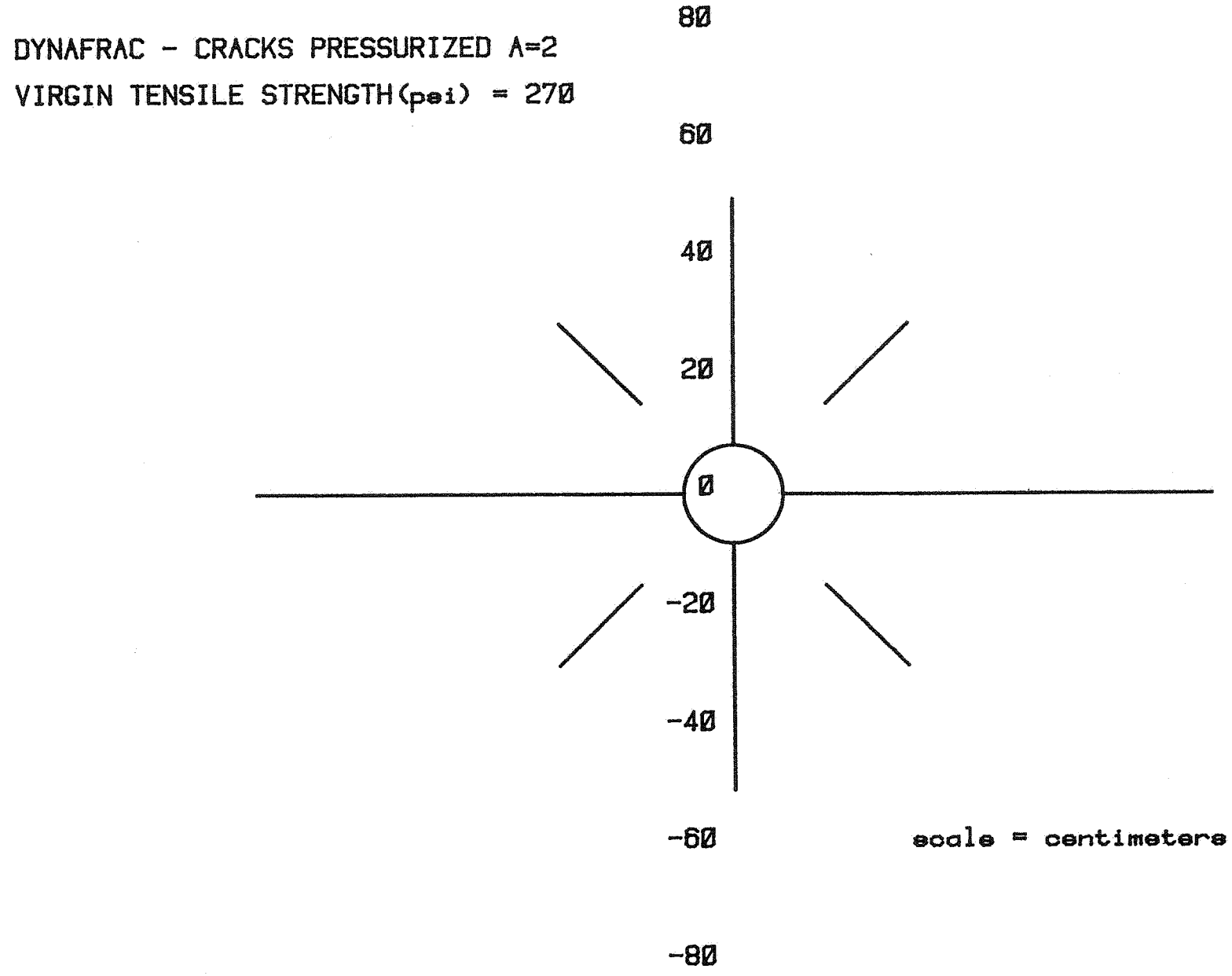

Figure 15a. CAVS Crack Plot - Cracks Prssurized - Case 1.

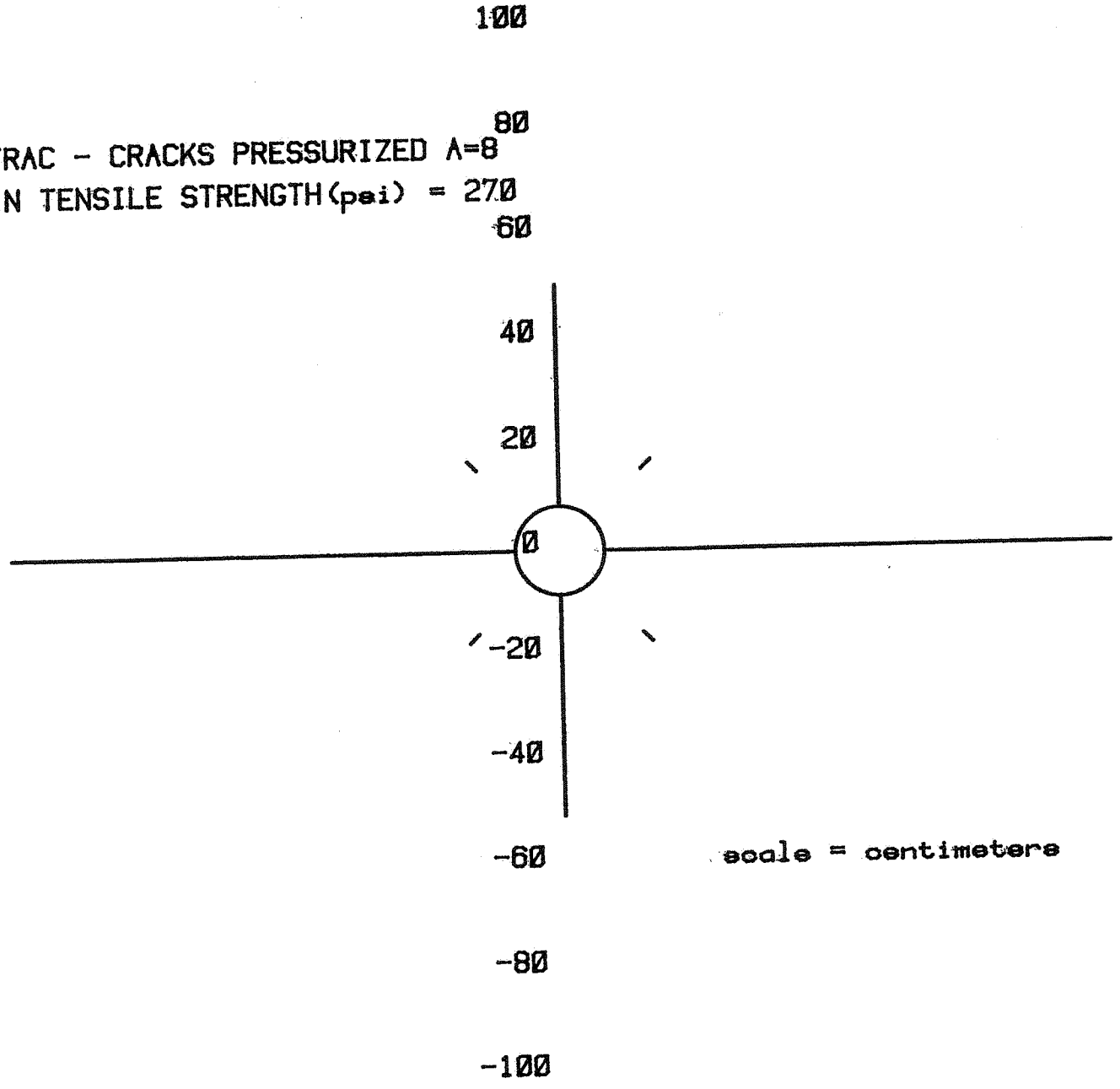

Figure 15b. CAVS Crack Plot - Cracks Pressurized - Case 2.

SECTION 4

SIMULATIONS OF NTS MINEBACK EXPERIMENTS

4.1 Introduction

The Nevada Test Site (NTS) Mineback Experiment Series planned for early in 1980 have as its overall objective to advance our understanding of multiple fracturing in wellbore stimulation treatments (14). Specific objectives for this test series are: (1) to conduct a series of field tests of five different dynamic fracturing concepts under realistic *in situ* conditions, (2) evaluate the test phenomenologically and quantitatively via mineback observations and instrumentation and (3) to utilize the results to assess and/or validate existing models for multiple fracturing.

Five fracturing tests will be conducted: (1) Dynafrac, a decoupled explosive, (2) Augmented Dynafrac, a decoupled explosive combined with a propellant-driven fluid, (3) Kinefrac, a pressure-insensitive propellant under a fluid head, (4) multiple Kinecrac, three sequential applications of the single Kinefrac process in a single borehole, and (5) High Energy Gas Frac, a propellant designed to maximize gas generation.

The test location is in G-tunnel in Rainier Mesa at DOE's Nevada Test Site. The site provides an overburden of approximately 1400 feet. The specific location has known *in situ* stresses and is a good region in terms of uniformity of properties and absence of joints or major faulting.

Planned instrumentation for these tests include dual fluid-coupled-plate transducers to measure the pressure-time behavior in the wellbore cavity and accelerometers and stress guages to measure the response of the surrounding ash-fall tuff. The fracture systems will be directly examined by mining back through the shot points with a rotating-head Alpine mining machine. Approximate measures of created fracture volume and permeability will be made post-shot, but prior to mineback.

Thus, cavity pressures, acceleration and stress data, post-shot cavity sizes and permeabilities, and a detailed description of the fracture systems will be the primary output of this test series. These data, along with material property data currently being gathered and the *in situ* stresses will be used in the analysis of the experiment results.

4.2 Calculation Results

The unaugmented Dynafrac wellbore stimulation experiment was modeled using STEALTH 1-D with the geometry and material properties previous described in Sections 3.2 through 3.4. The yield model used was the failure envelope labeled "baseline" in Figure 10. The compaction model used was the equation-of-state labeled "curve #1" in Figure 11.

Calculations were run with and without CAVS cracking as a means of observing the differences in the ash-fall tuff's acceleration and stress response. Significant differences were not observed with and without cracking, although when cracking was allowed the accelerations in the tuff were slightly higher. The calculation results for the no-cracking case have been presented here and should serve as an estimate of the NTS unaugmented Dynafrac response.

Figures 16 through 23 are plots of the NTS Dynafrac experiment response generated by STEALTH 1-D. Figures 16a and 16b are pressure-time histories for the nitromethane explosive and buffering water, respectively. Figures 16c through 16f are pressure-time histories for the ash-fall tuff at the borehole wall and at radial distances from the borehole center of 1½', 2½', and 3½'. Figures 17a through 17d are radial stress-time histories at the same locations in the tuff. Figures 18a through 18d are hoop-stress-time histories. Figures 19a through 19d are radial acceleration-time histories. Figures 20a through 20d are peak radial acceleration-time histories. Figures 21a through 21c are snapshots of the radial stress versus radial position at 50 μsec, 100 μsec and 500 μsec. Figures 22a through 22c at similar snapshot plots at 50 μsec, 100 μsec and 500 μsec. Figures 23a

through 23c are acceleration snapshots at the same times. Note that in all cases the units of stress are megabars, the units of distance are centimenters, the units of time are microseconds and the units of acceleration are centimenters/microseconds^2.

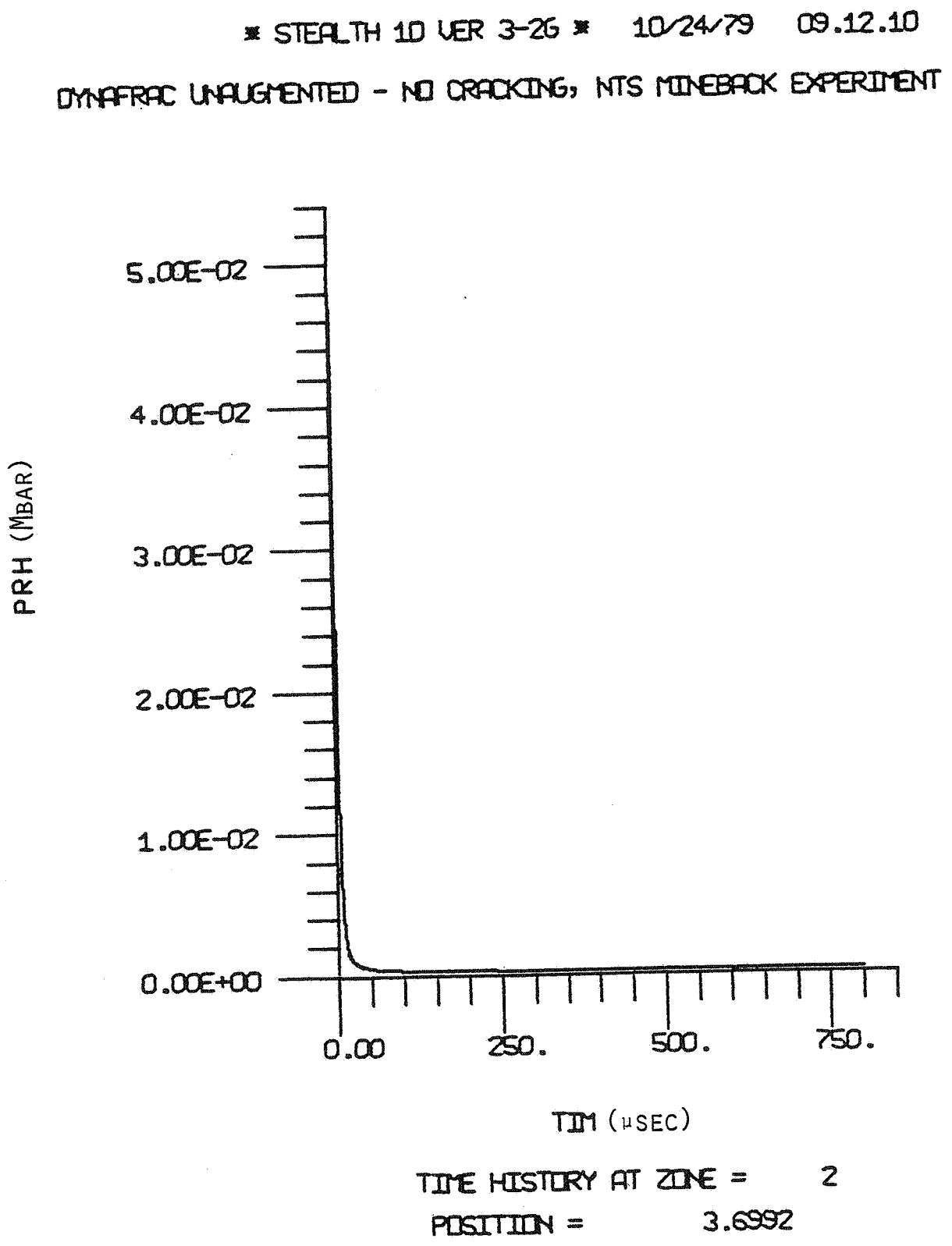

Figure 16a. NTS DYNAFRAC - Nitromethane Pressure-Time History.

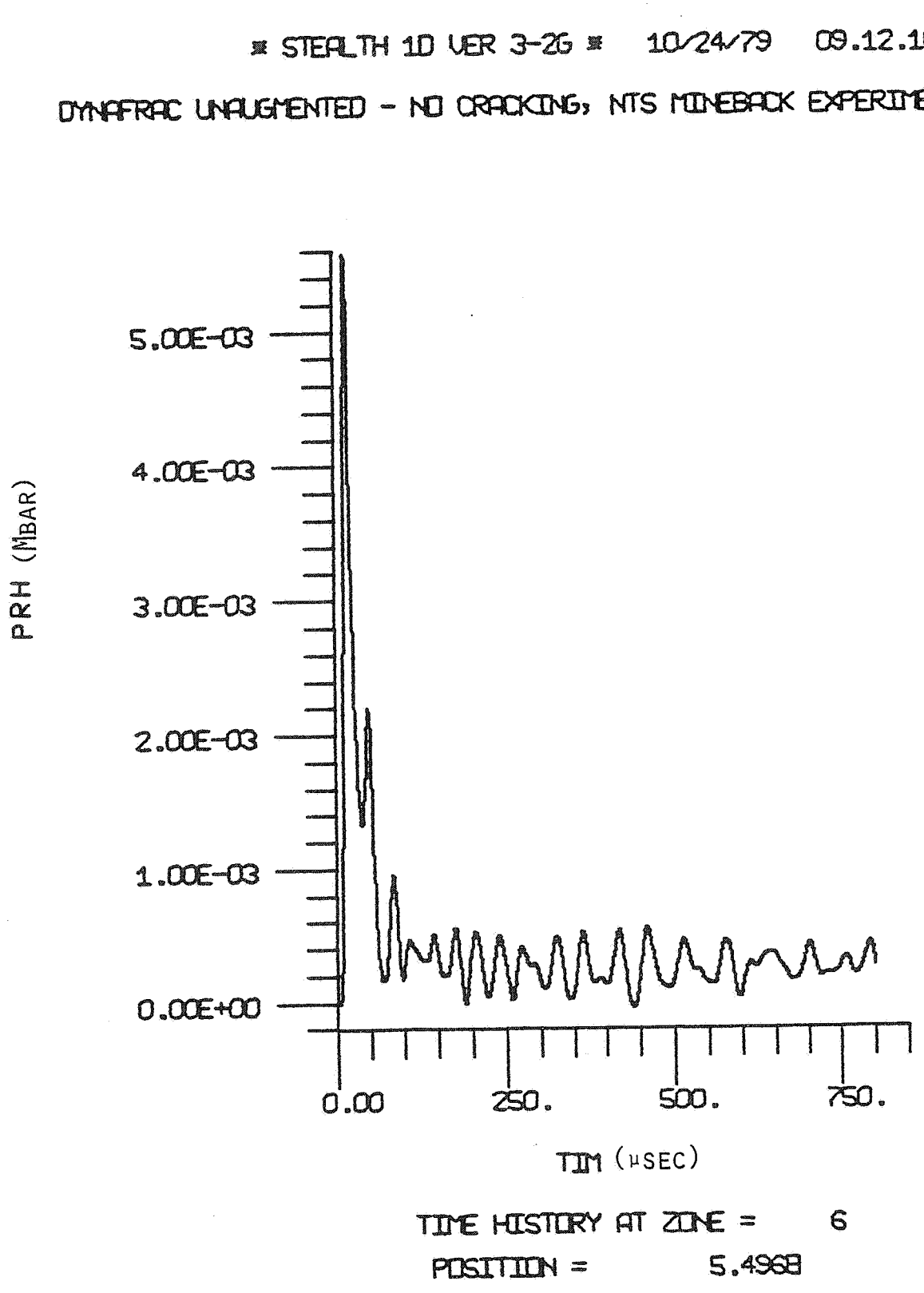

Figure 16b. NTS DYNAFRAC - Water Pressure-Time History.

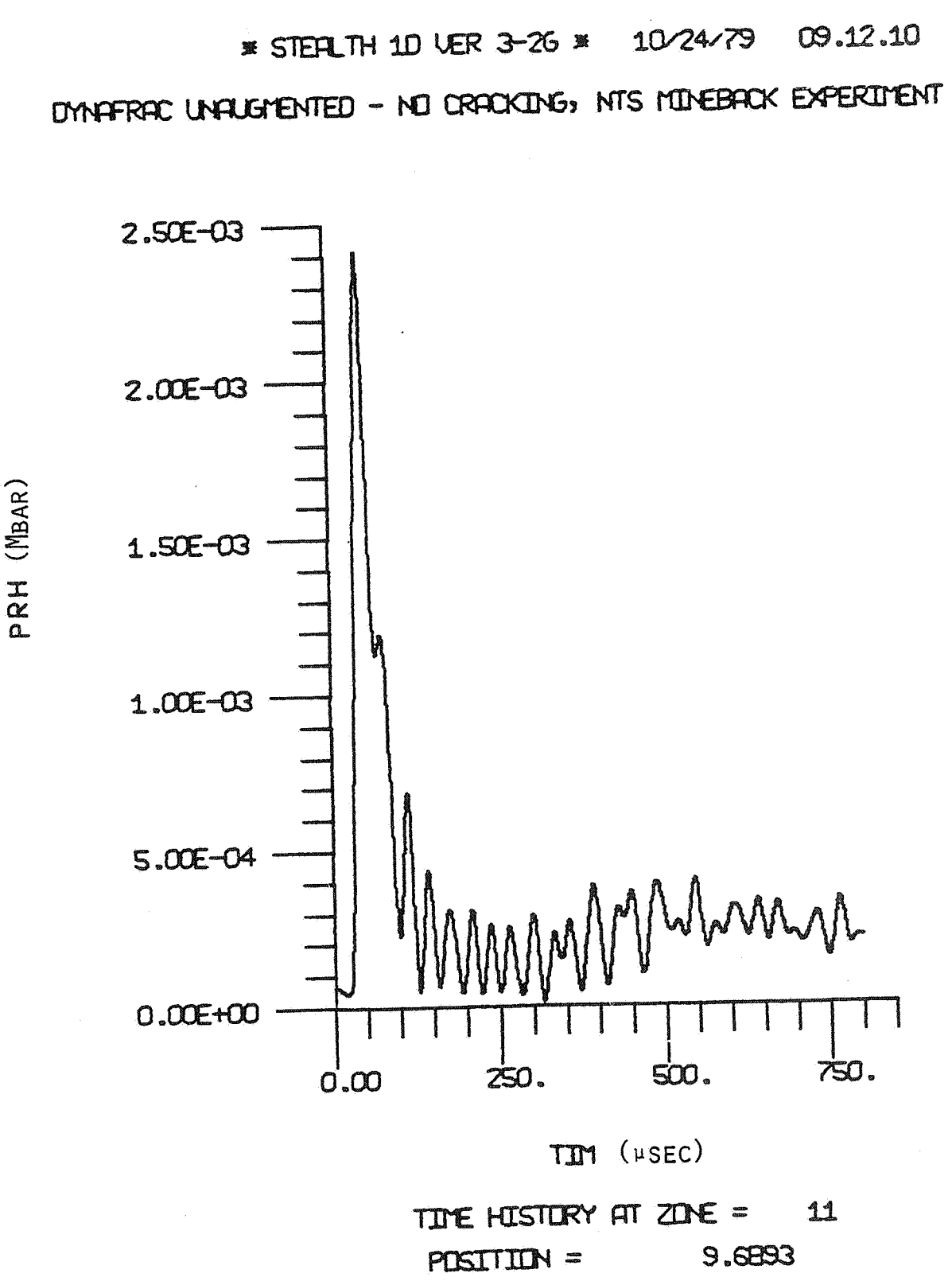

Figure 16c. NTS DYNAFRAC - Borehole Wall Pressure-Time History.

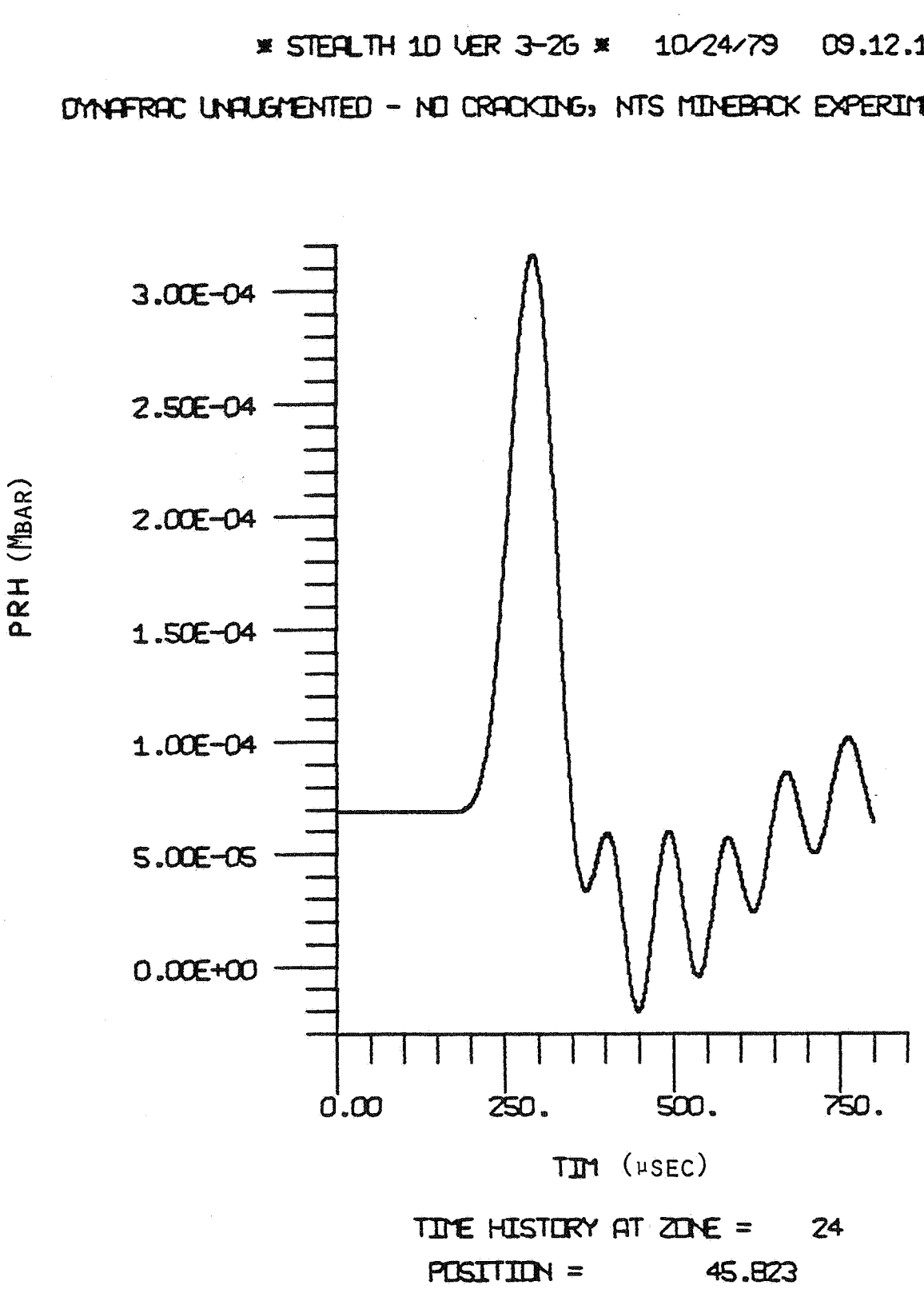

Figure 16d. NTS DYNAFRAC - Radially 1½' Pressure-Time History.

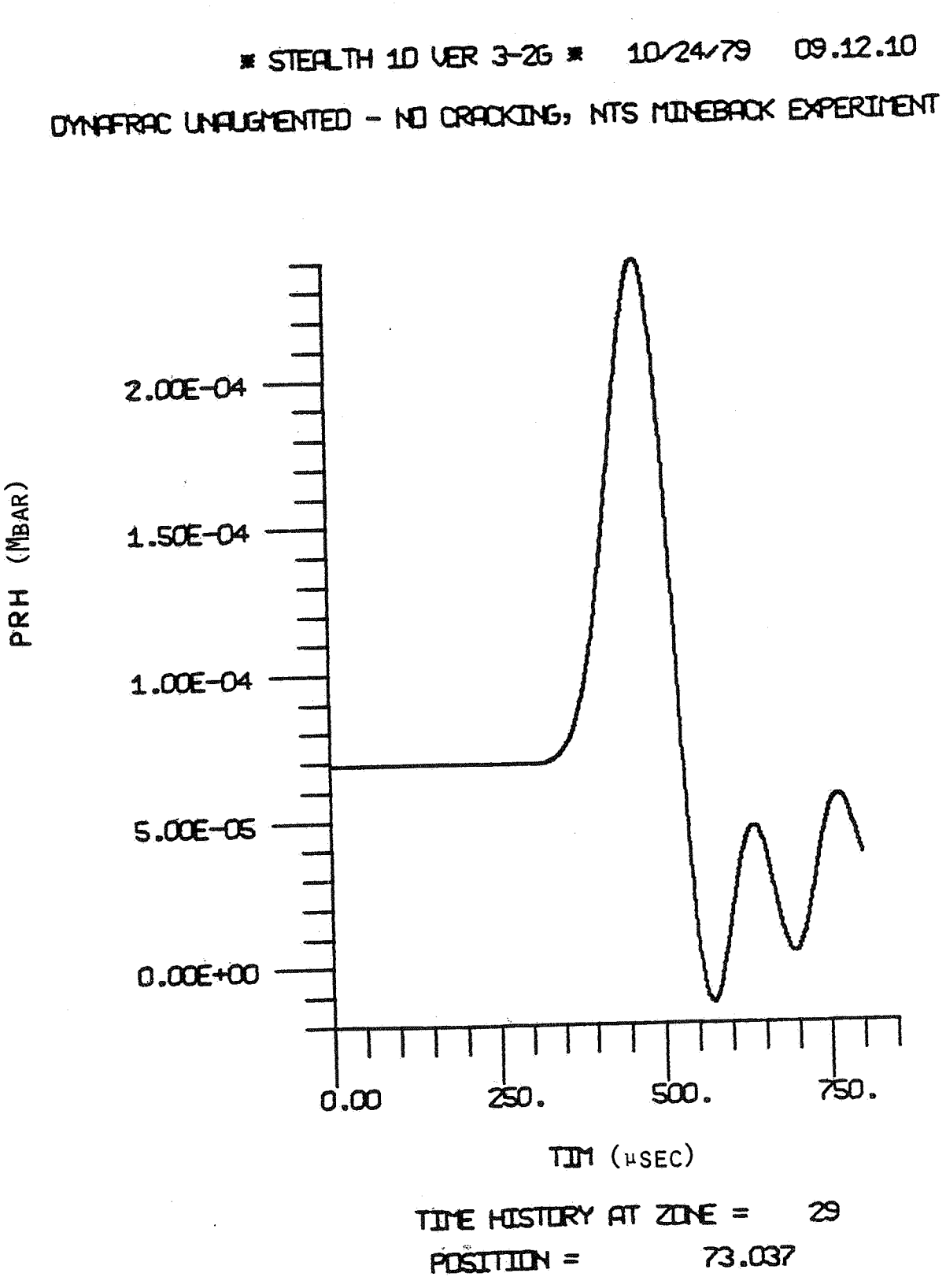

Figure 16e. NTS DYNAFRAC - Radially 2½' Pressure-Time History.

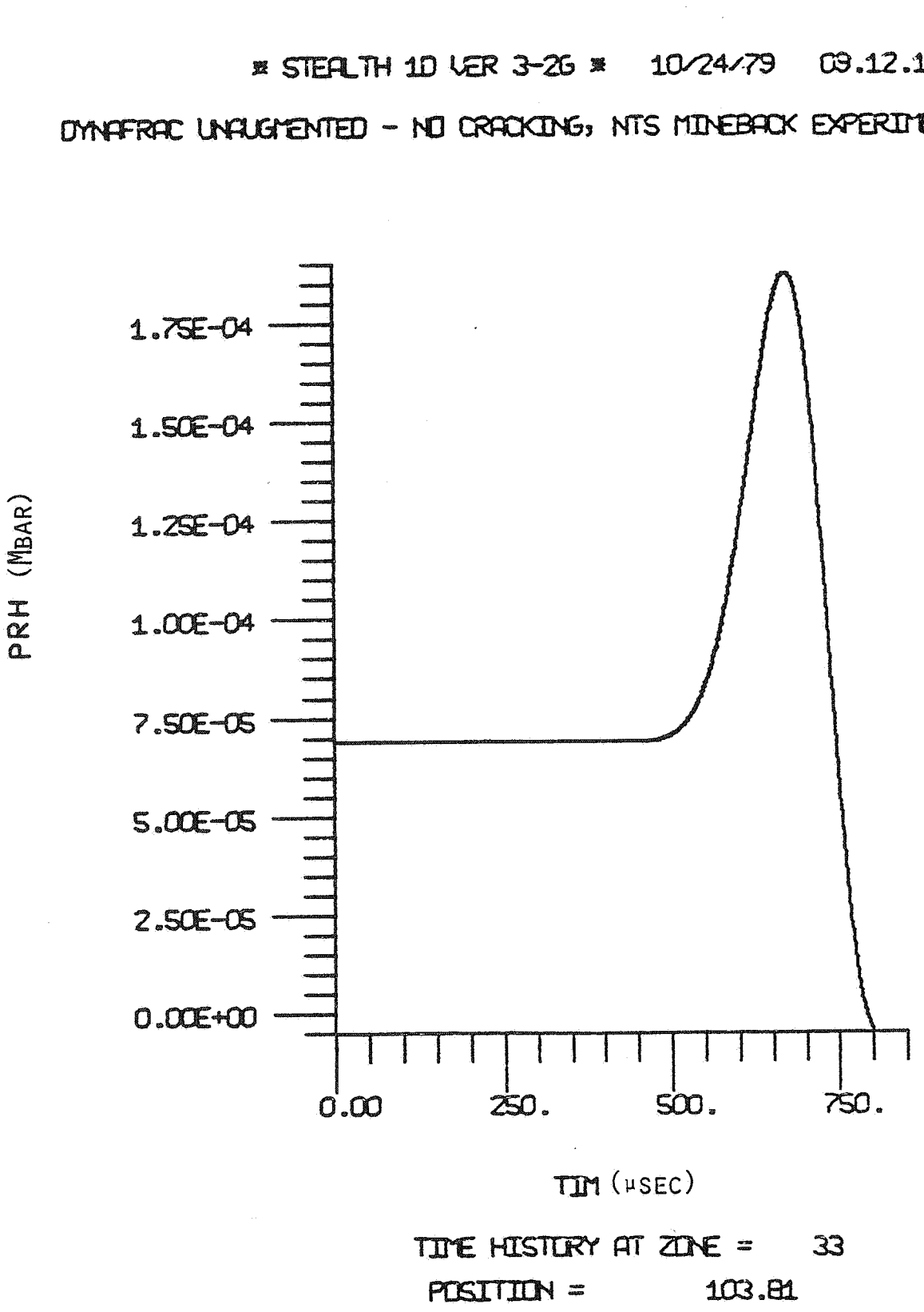

Figure 16f. NTS DYNAFRAC - Radially 3½' Pressure-Time History.

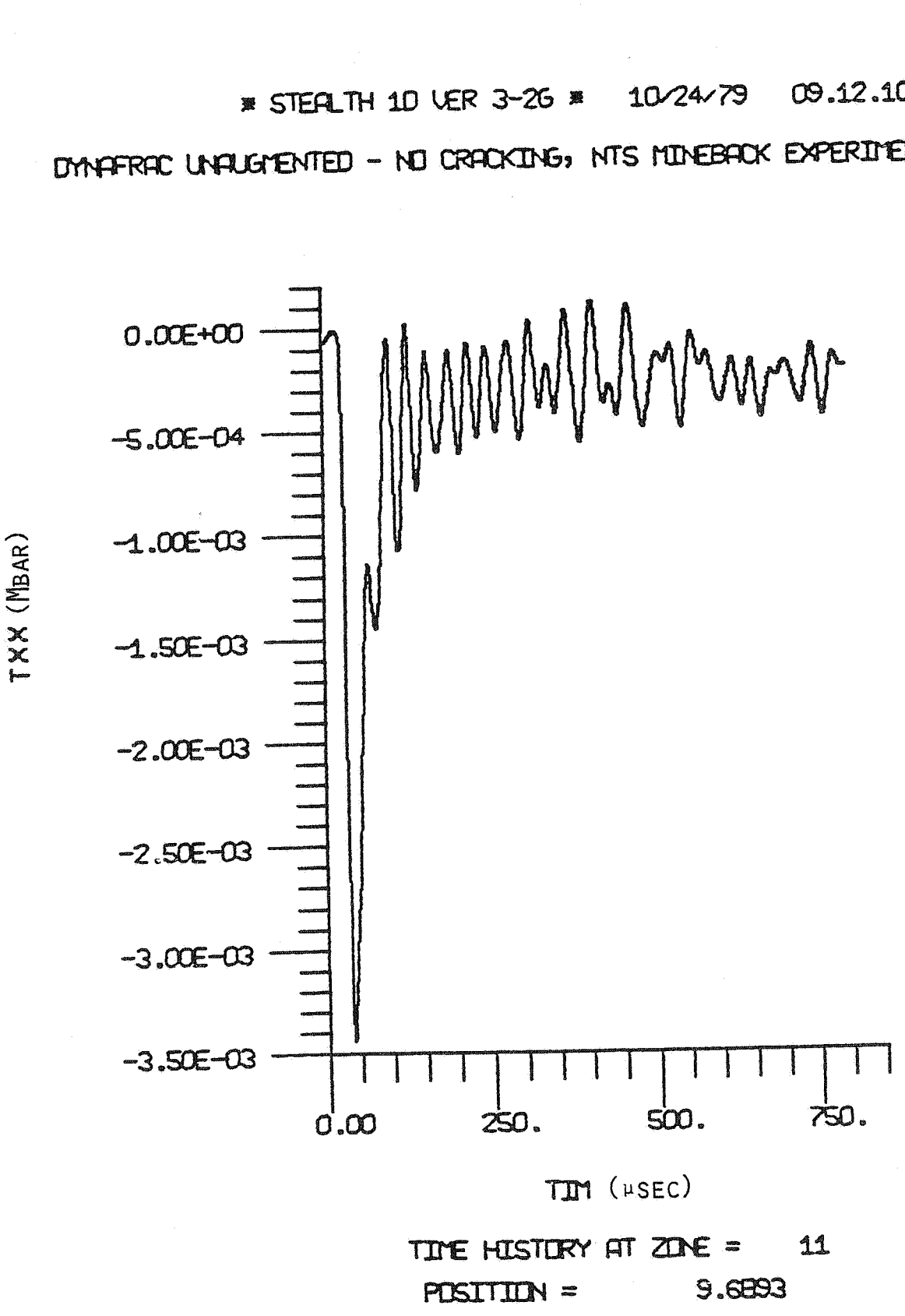

Figure 17a. NTS DYNAFRAC - Borehole Wall Radial Stress-Time History.

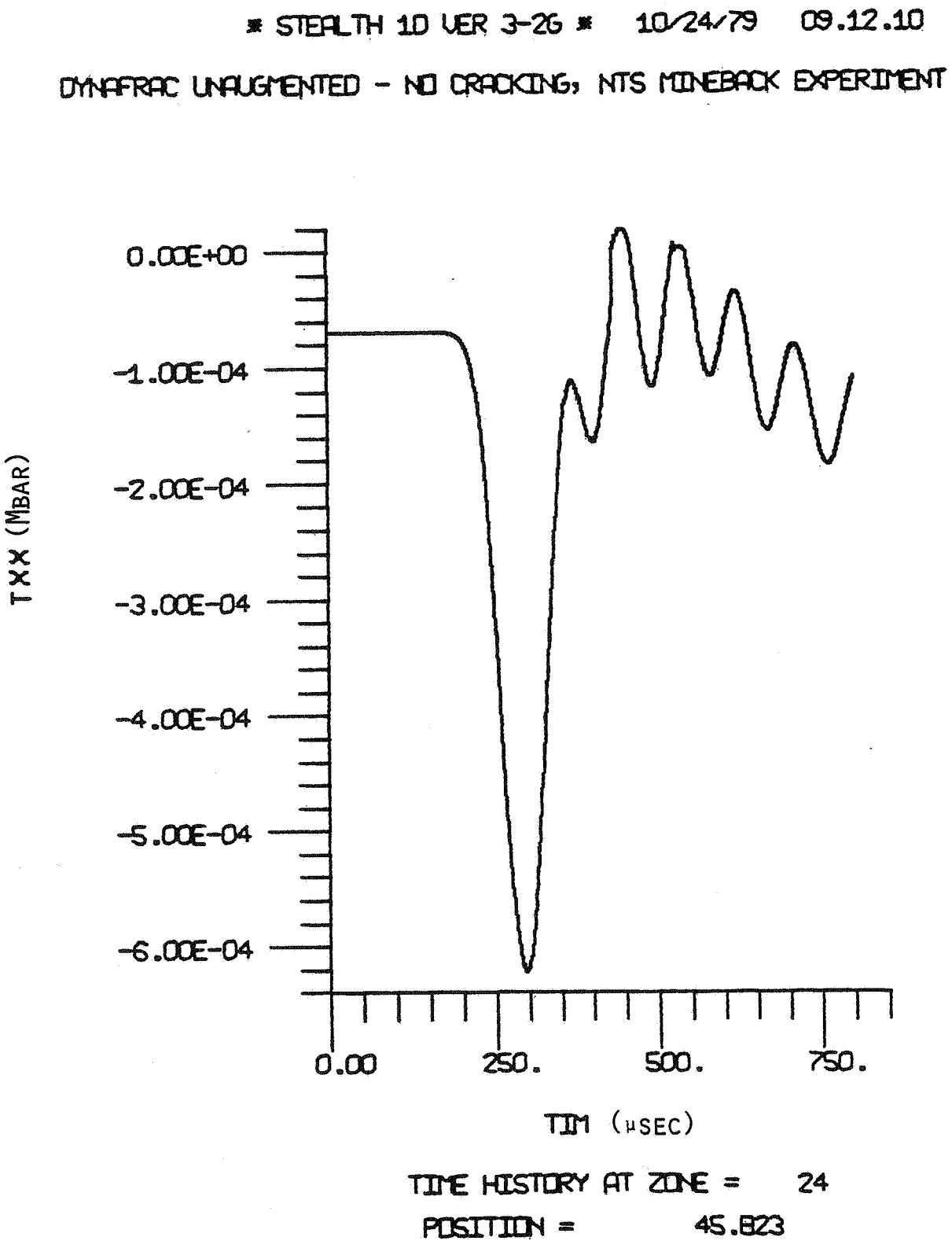

Figure 17b. NTS DYNAFRAC - Radially 1½' Radial Stress-Time History.

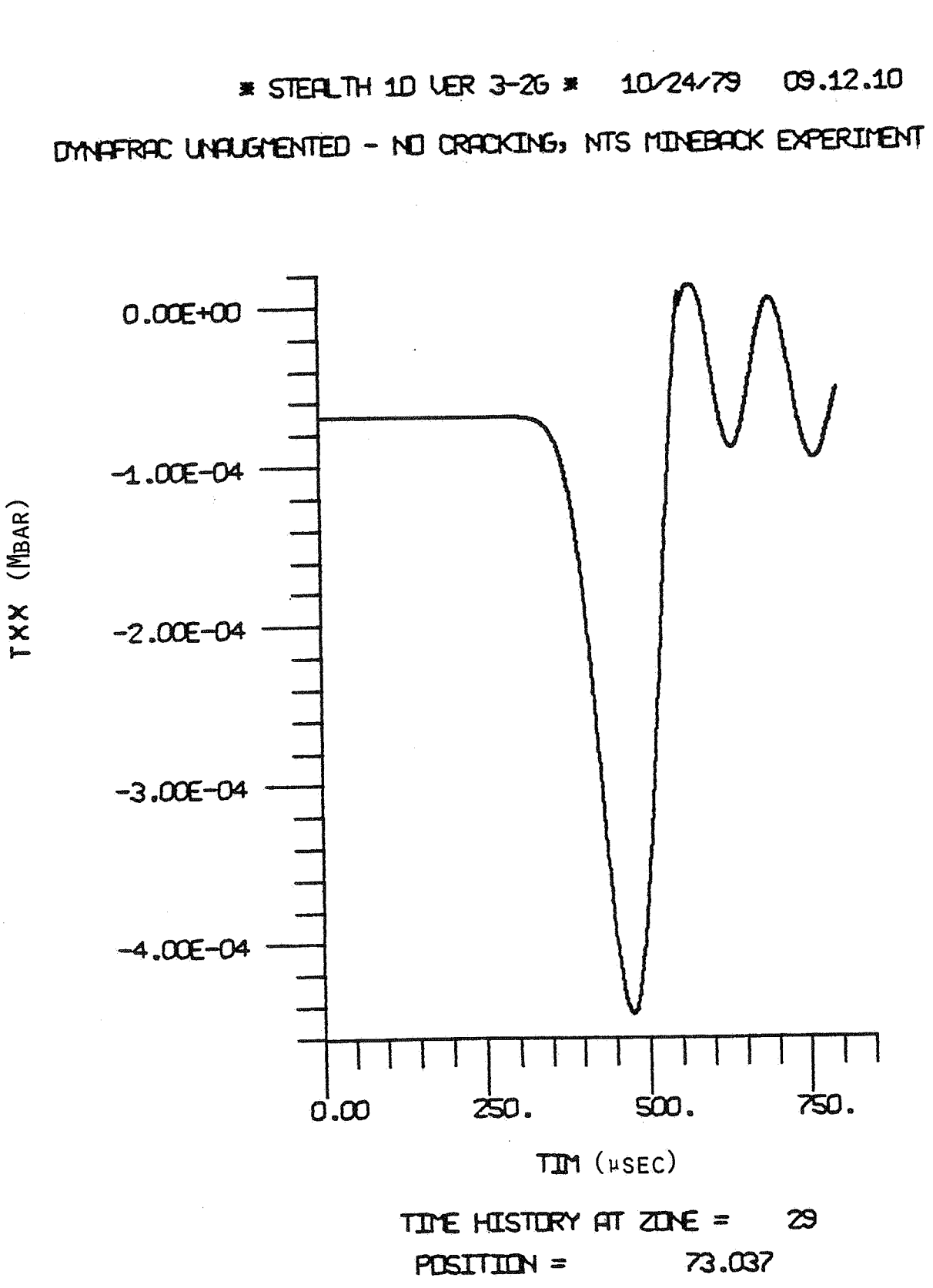

Figure 17c. NTS DYNAFRAC - Radially 2½' Radial Stress-Time History.

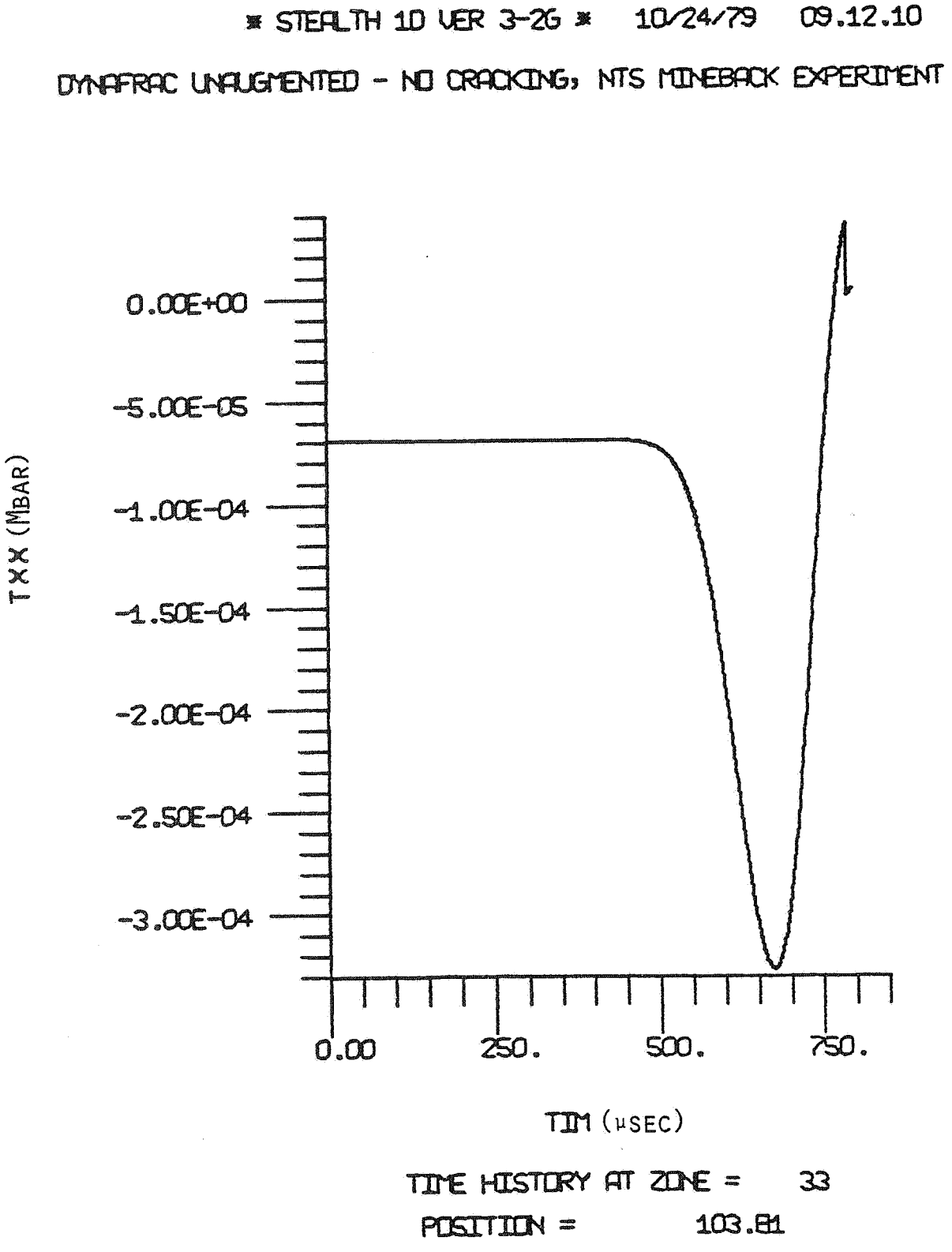

Figure 17d. NTS DYNAFRAC - Radially 3½' Radial Stress-Time History.

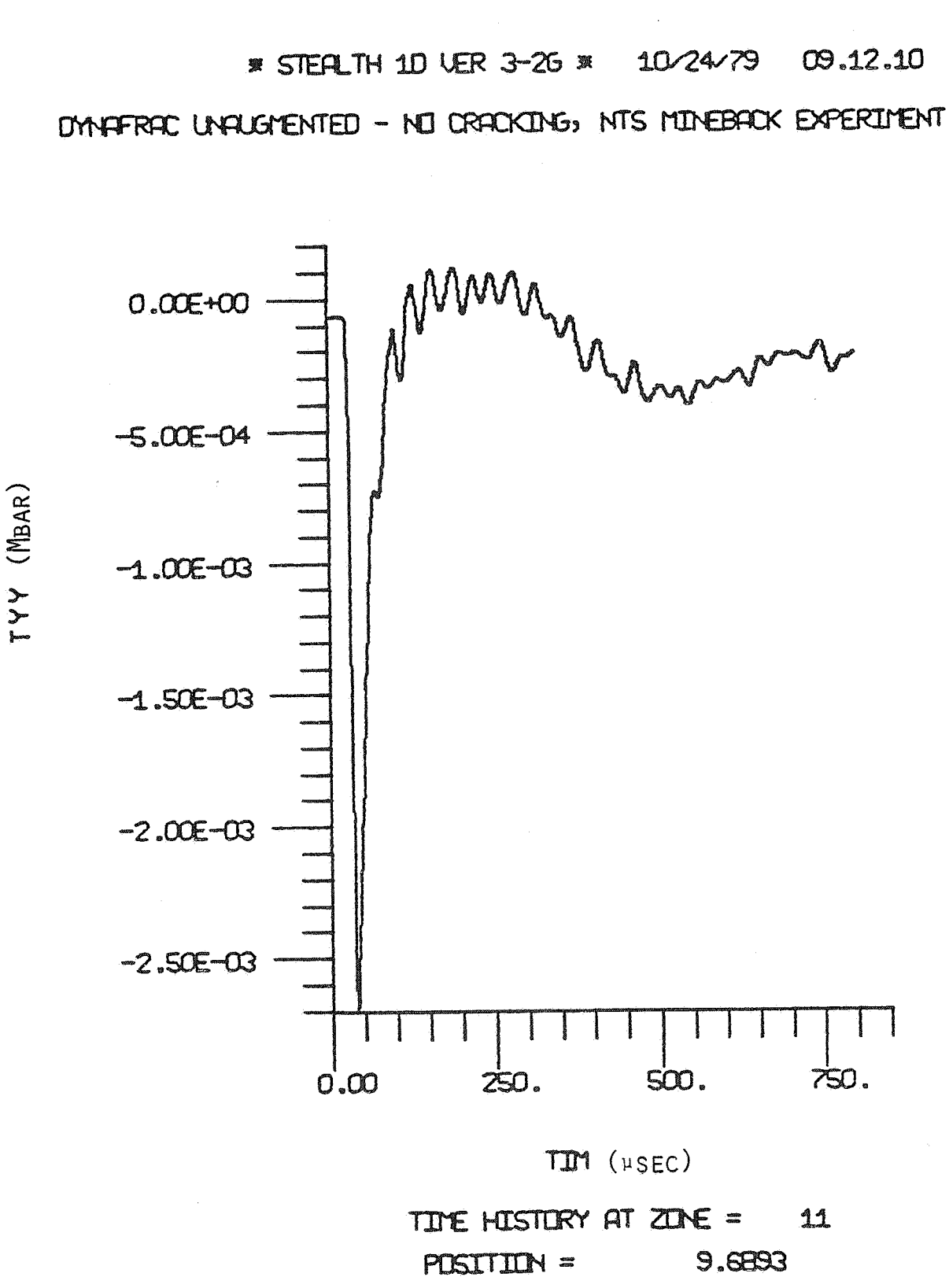

Figure 18a. NTS DYNAFRAC - Borehole Wall Hoop Stress-Time History.

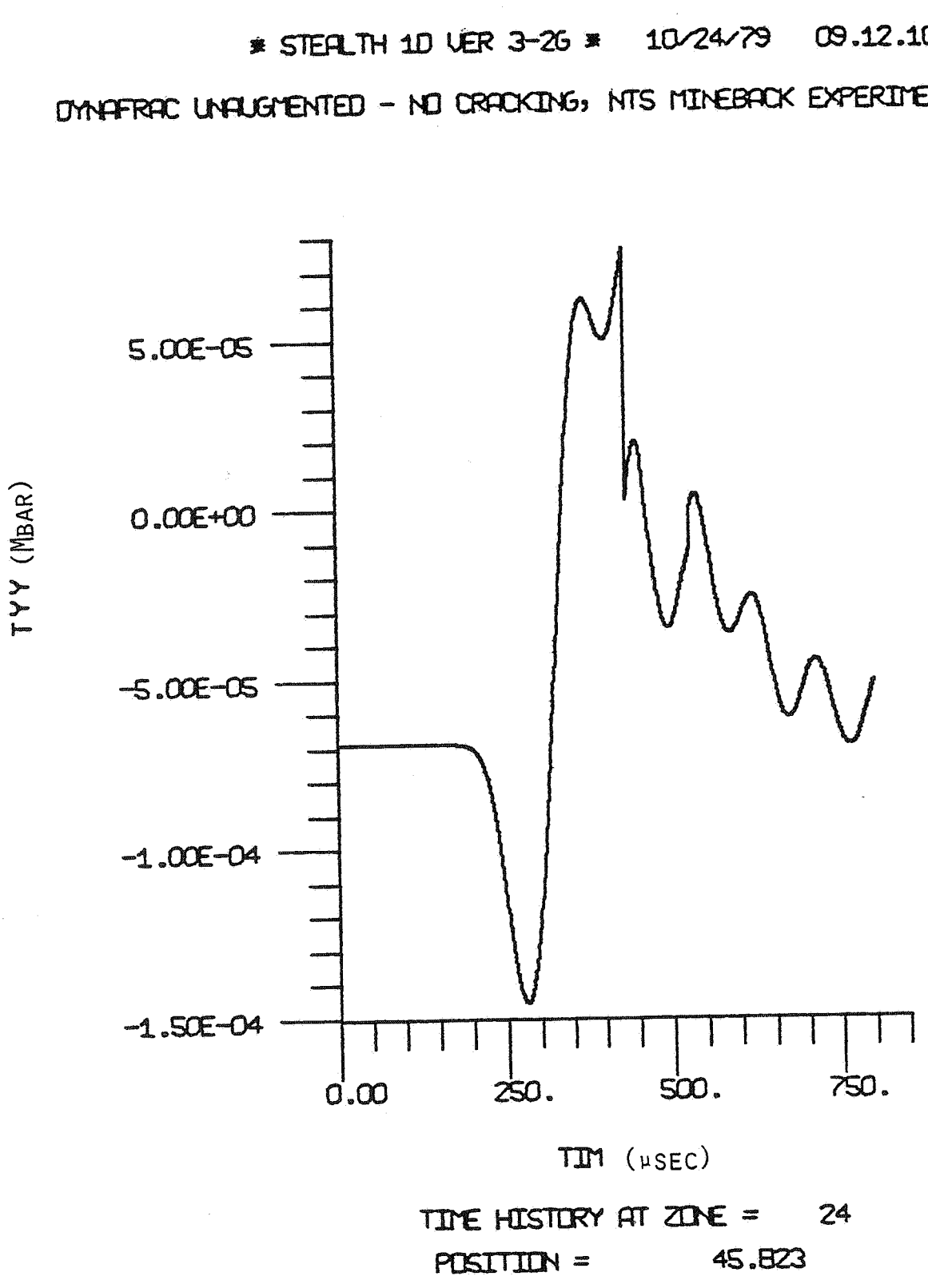

Figure 18b. NTS DYNAFRAC - Radially 1½' Hoop Stress-Time History.

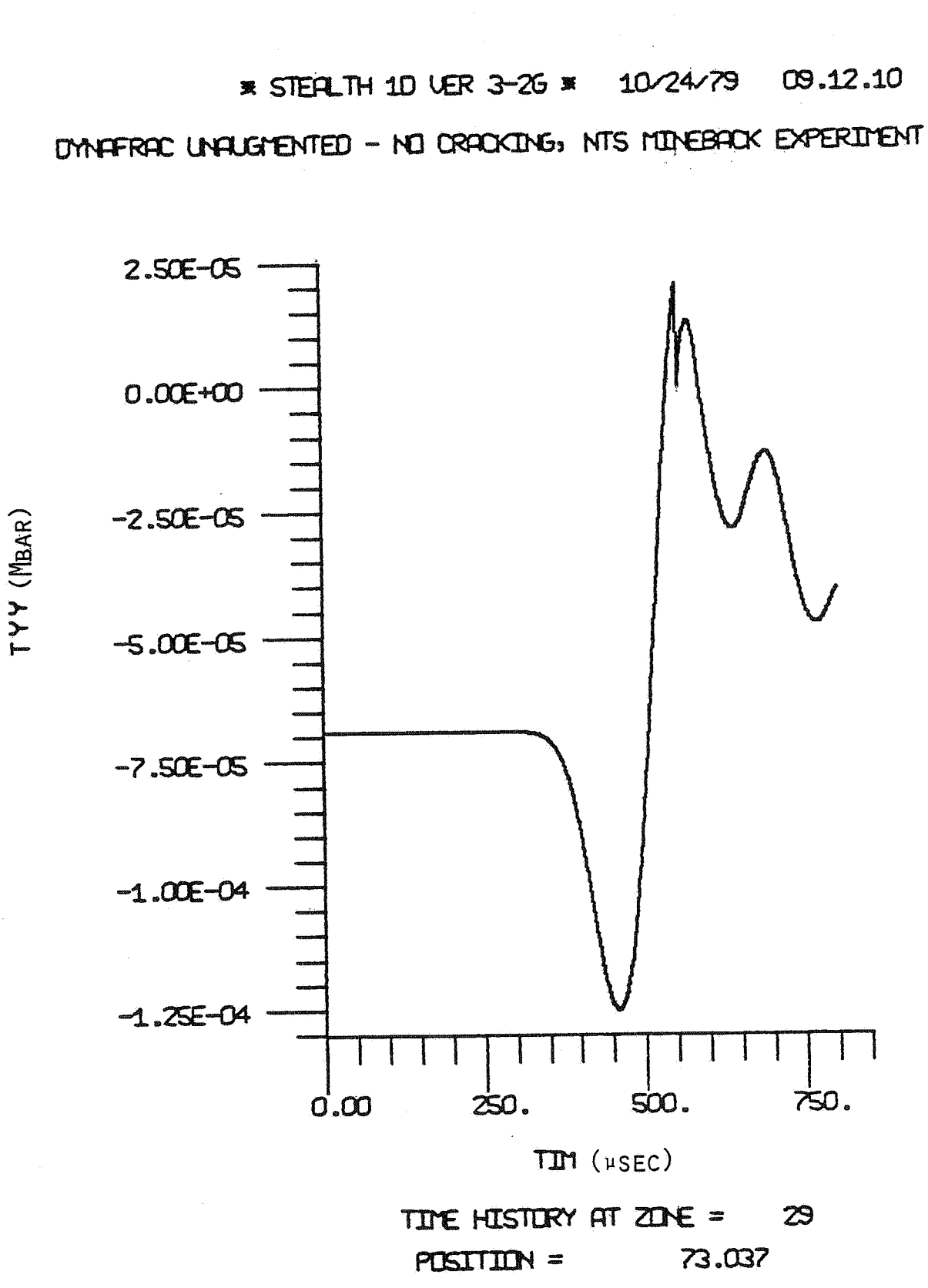

Figure 18c. NTS DYNAFRAC - Radially 2½' Hoop Stress-Time History.

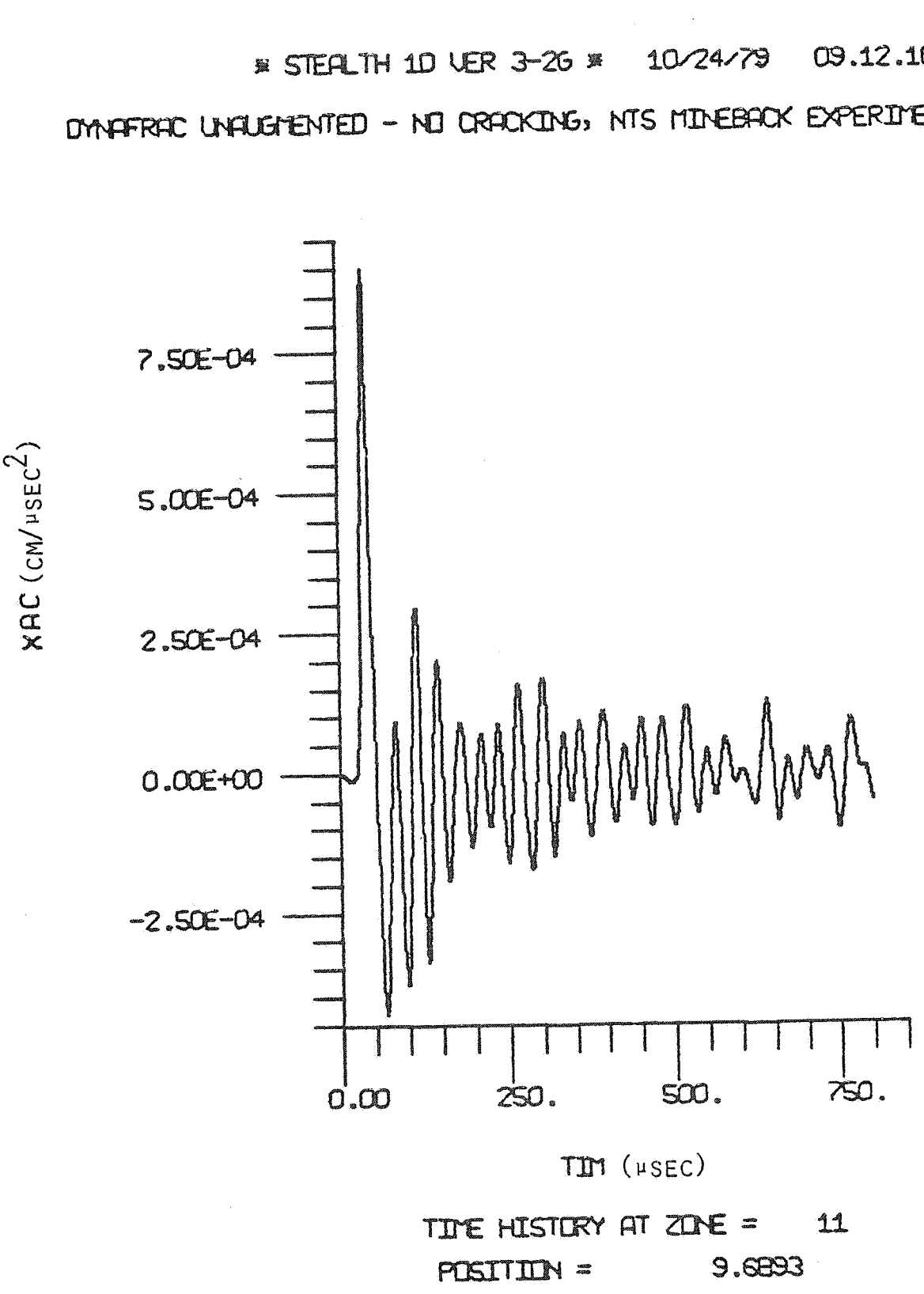

Figure 19a. NTS DYNAFRAC - Borehole Wall Acceleration-Time History.

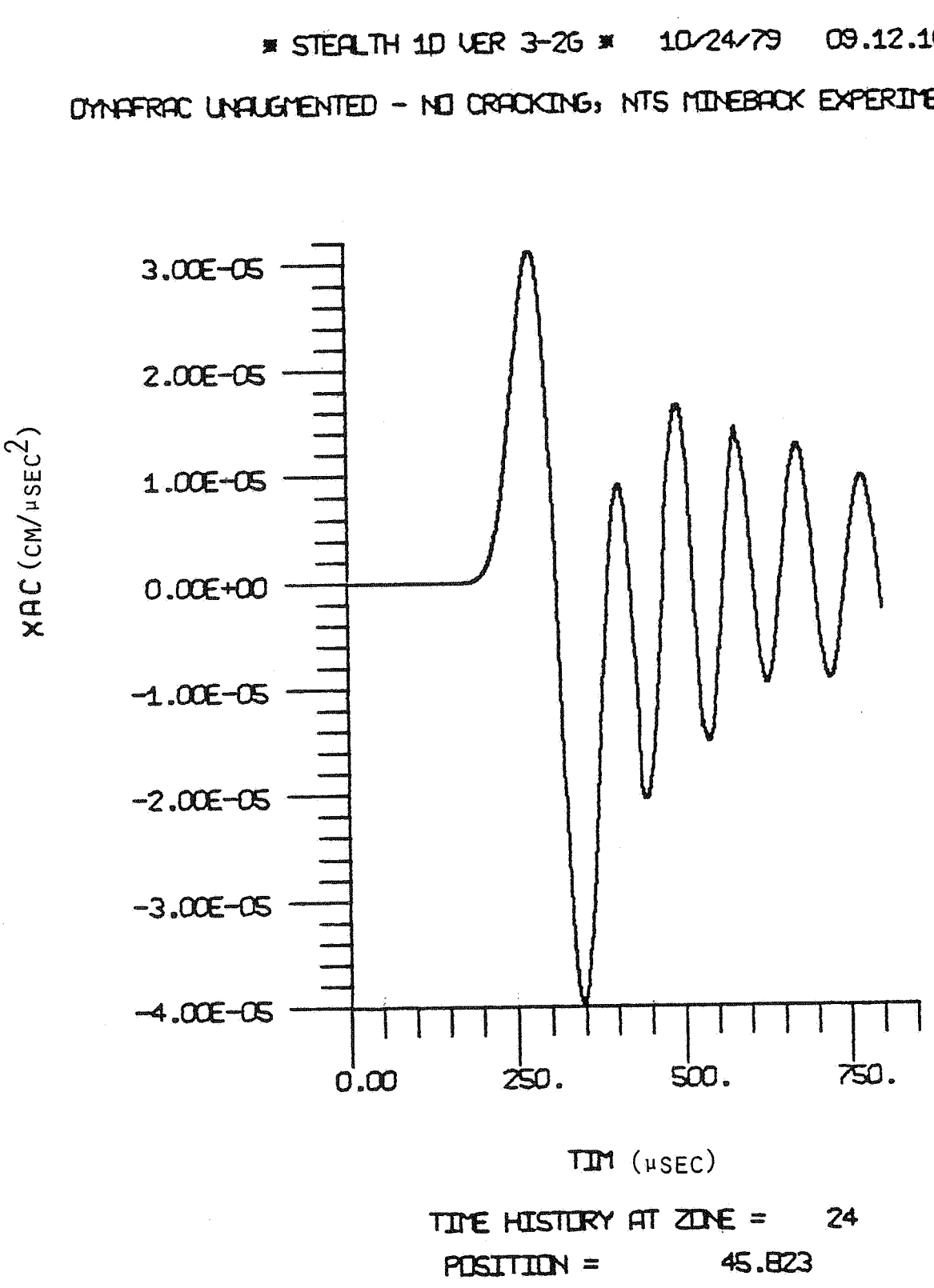

Figure 19b. NTS DYNAFRAC - Radially 1½' Acceleration-Time History.

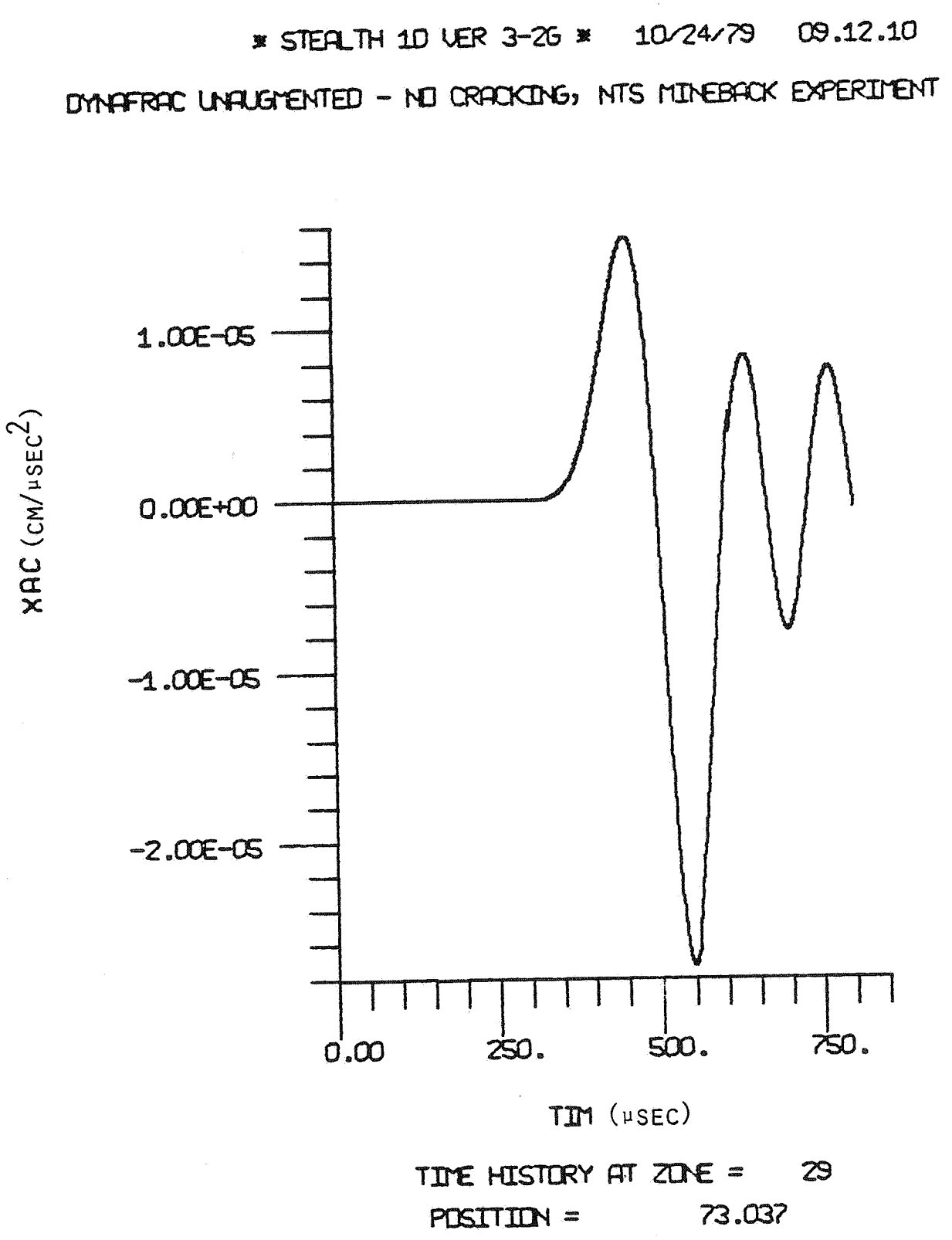

Figure 19c. NTS DYNAFRAC - Radially 2½' Acceleration-Time History.

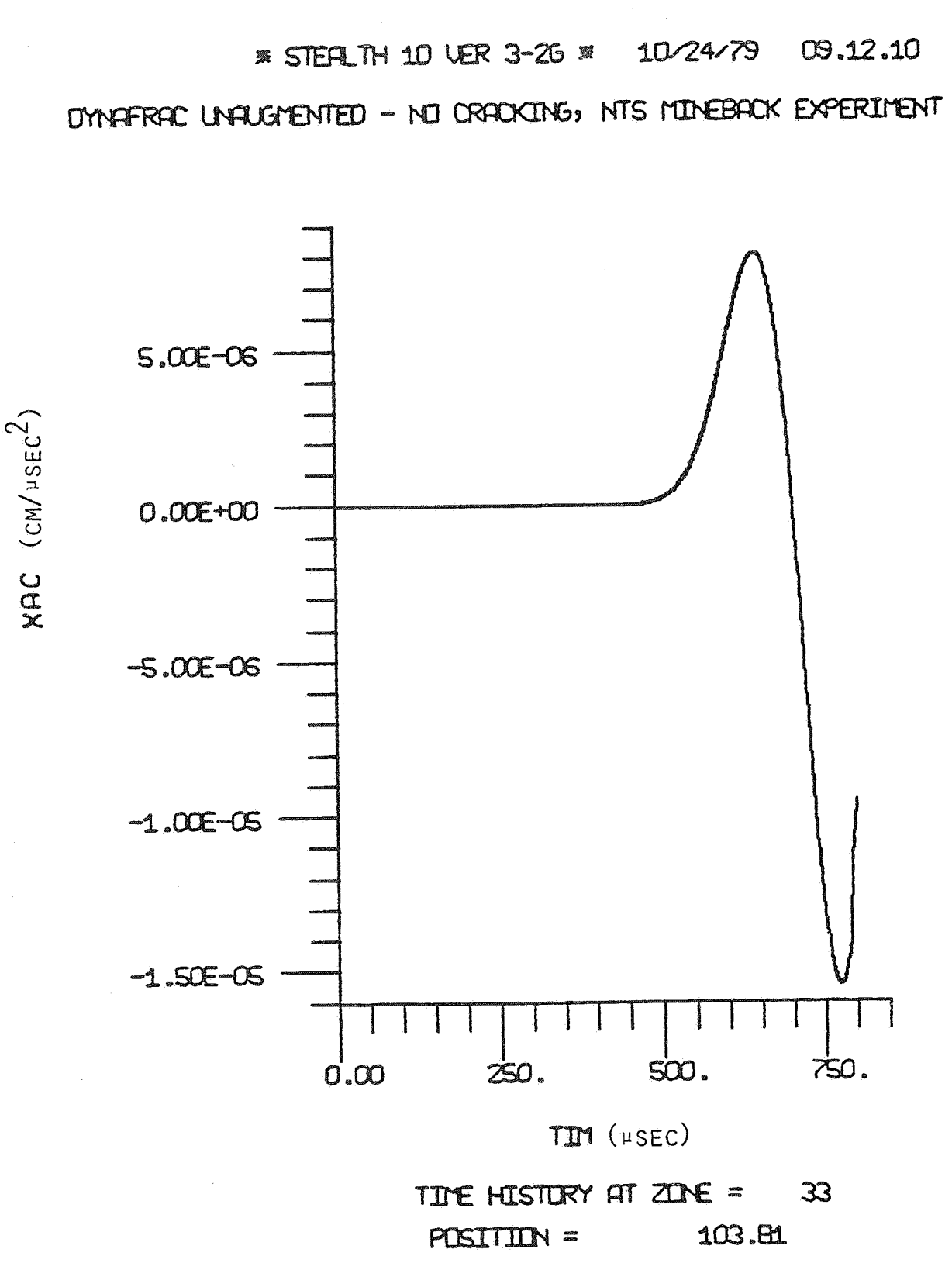

Figure 19d. NTS DYNAFRAC - Radially 3½' Acceleration-Time History.

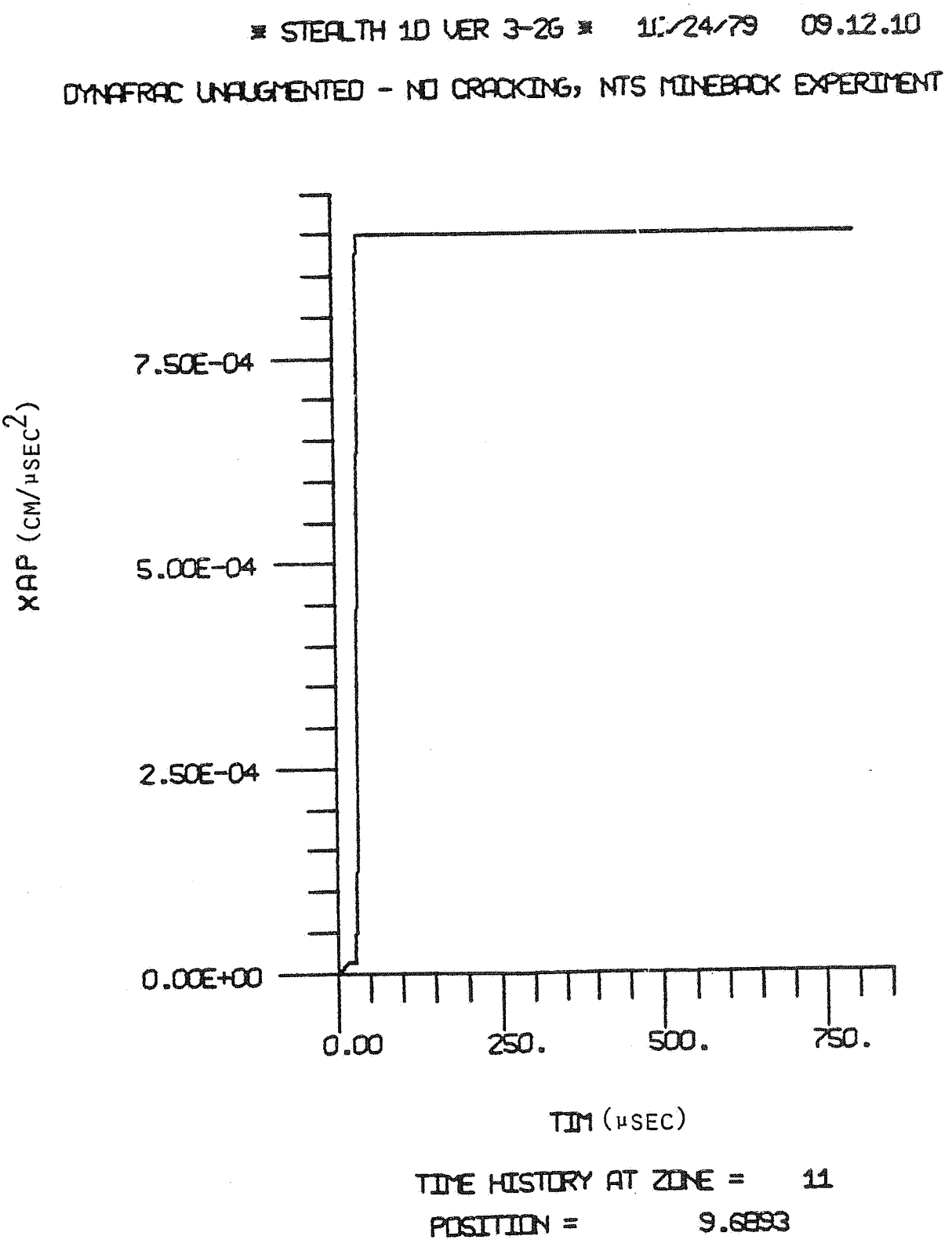

Figure 20a. NTS DYNAFRAC - Borehole Wall Peak Acceleration-Time History.

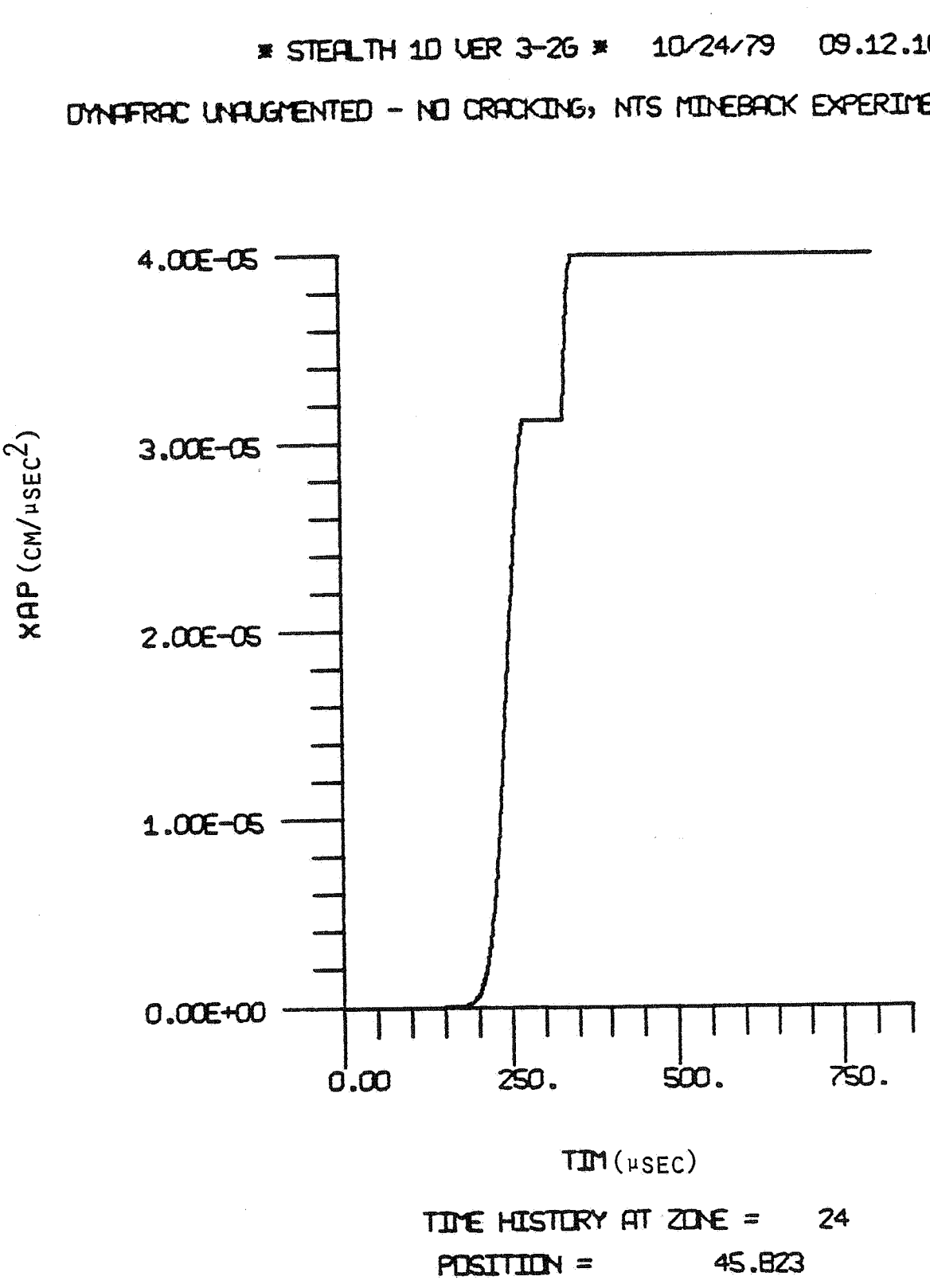

Figure 20b. NTS DYNAFRAC - Radially 1½' Peak Acceleration-Time History.

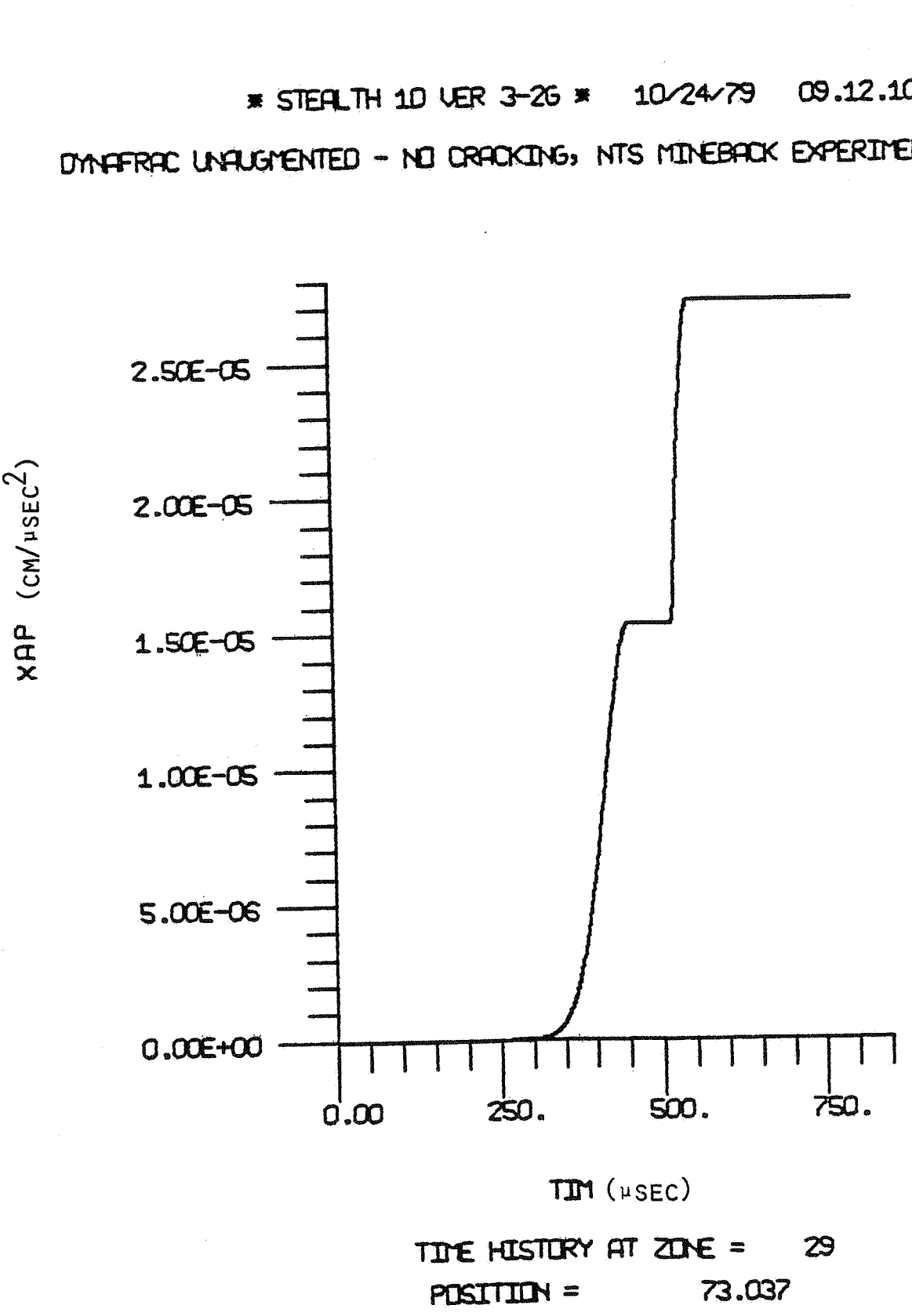

Figure 20c. NTS DYNAFRAC - Radially 2½' Peak Acceleration-Time History.

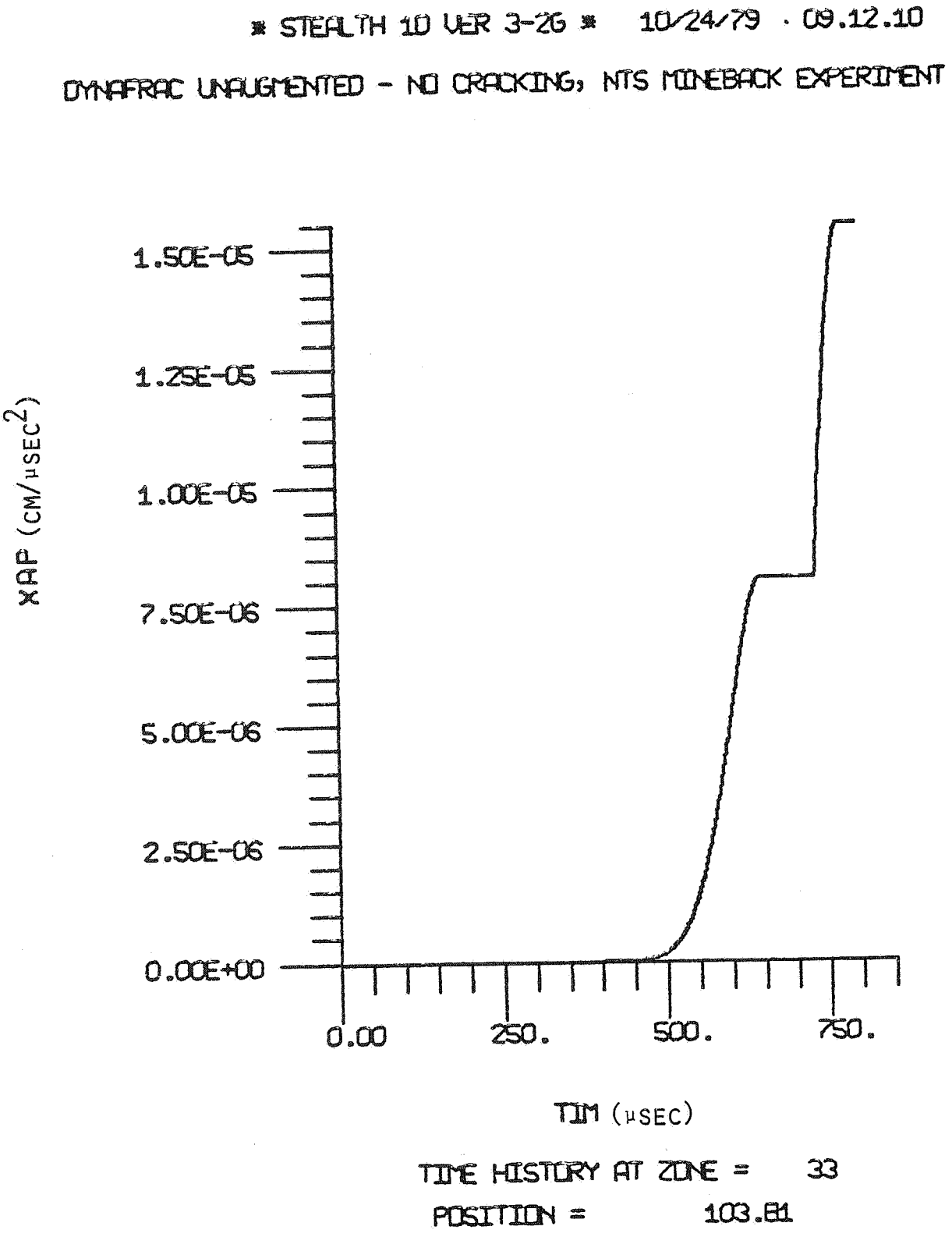

Figure 20d. NTS DYNAFRAC - Radially 3½' Peak Acceleration-Time History.

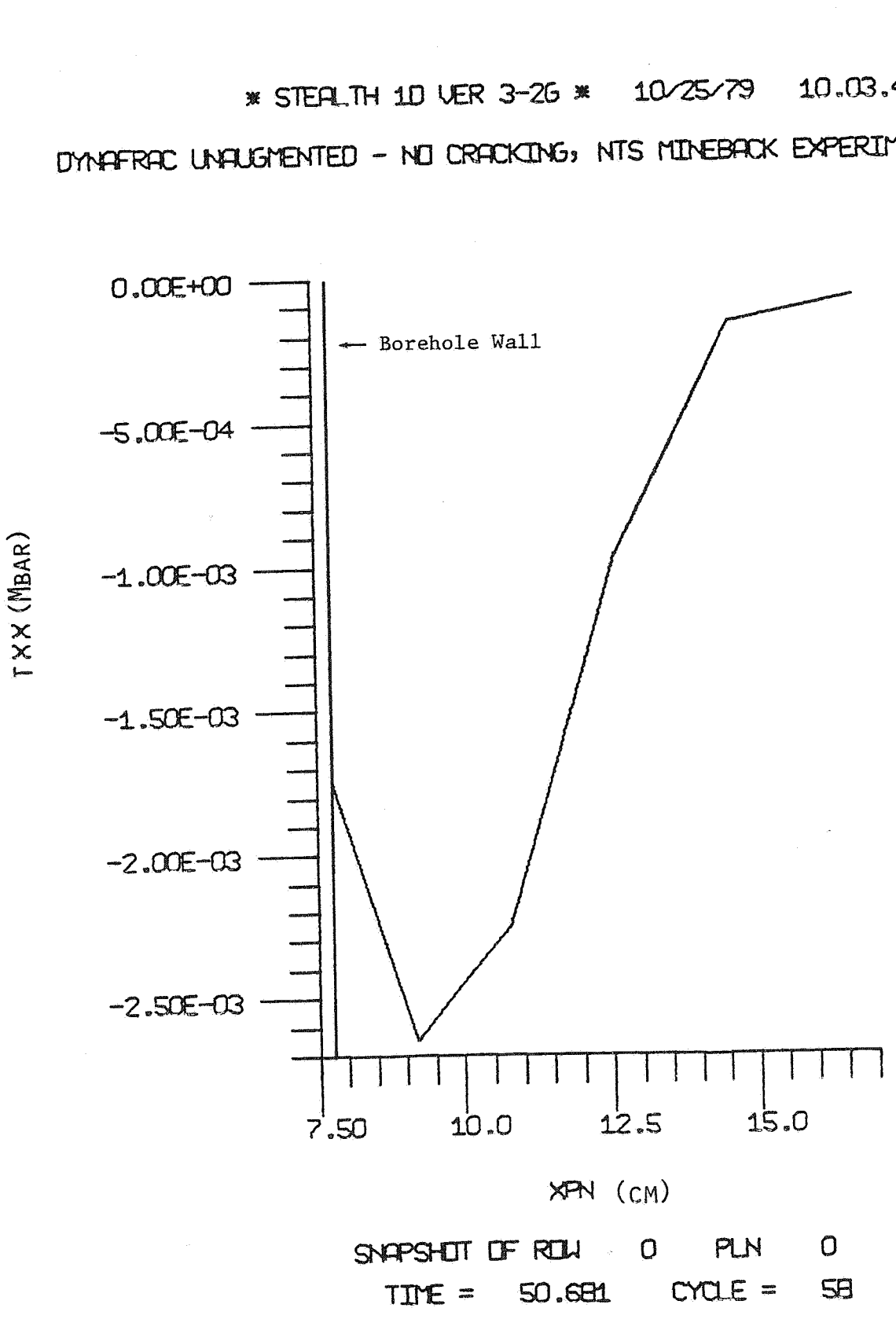

Figure 21a. NTS DYNAFRAC - Radial Stress Snapshot at 50 μsec.

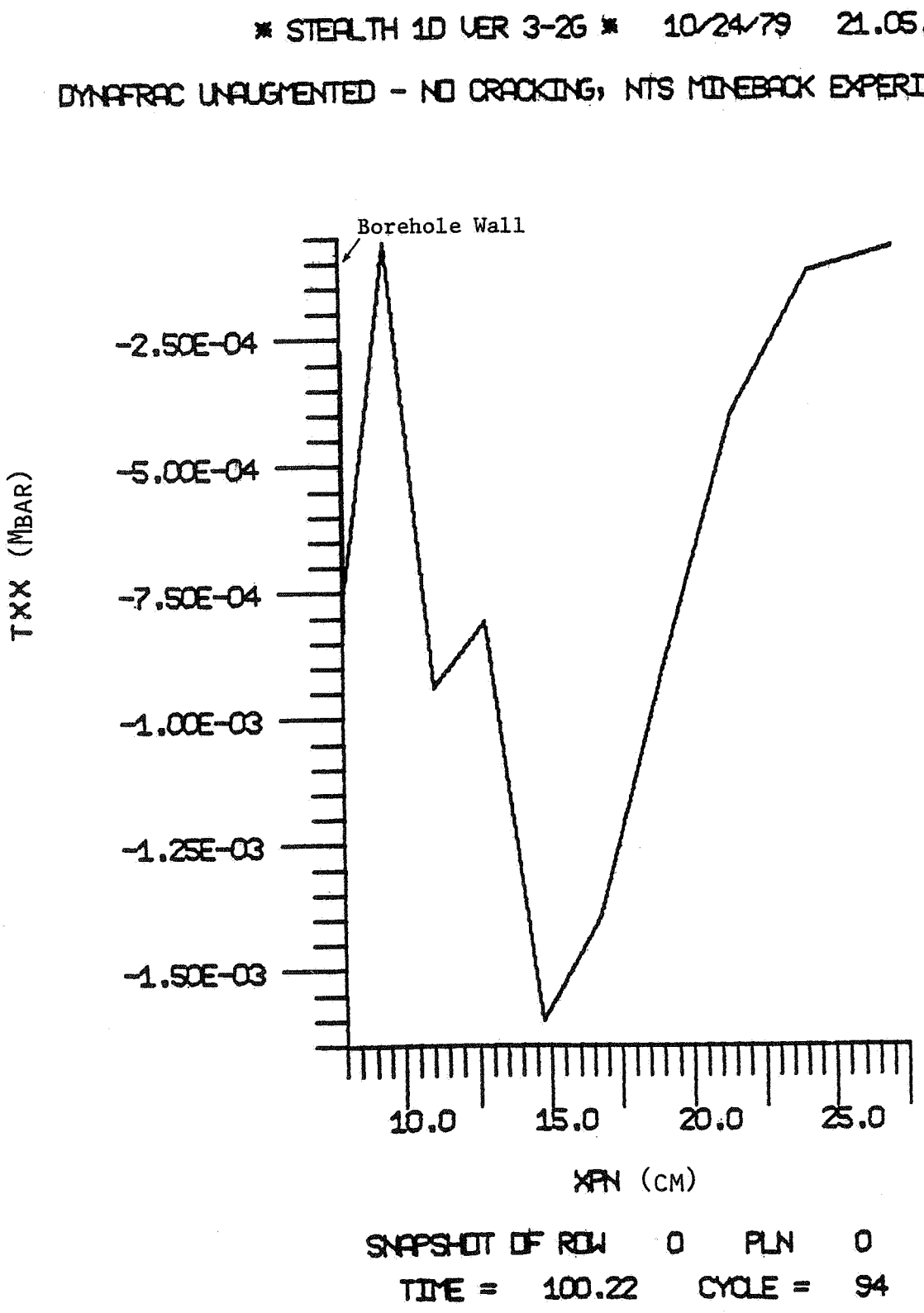

Figure 21b. NTS DYNAFRAC - Radial Stress Snapshot at 100 μsec.

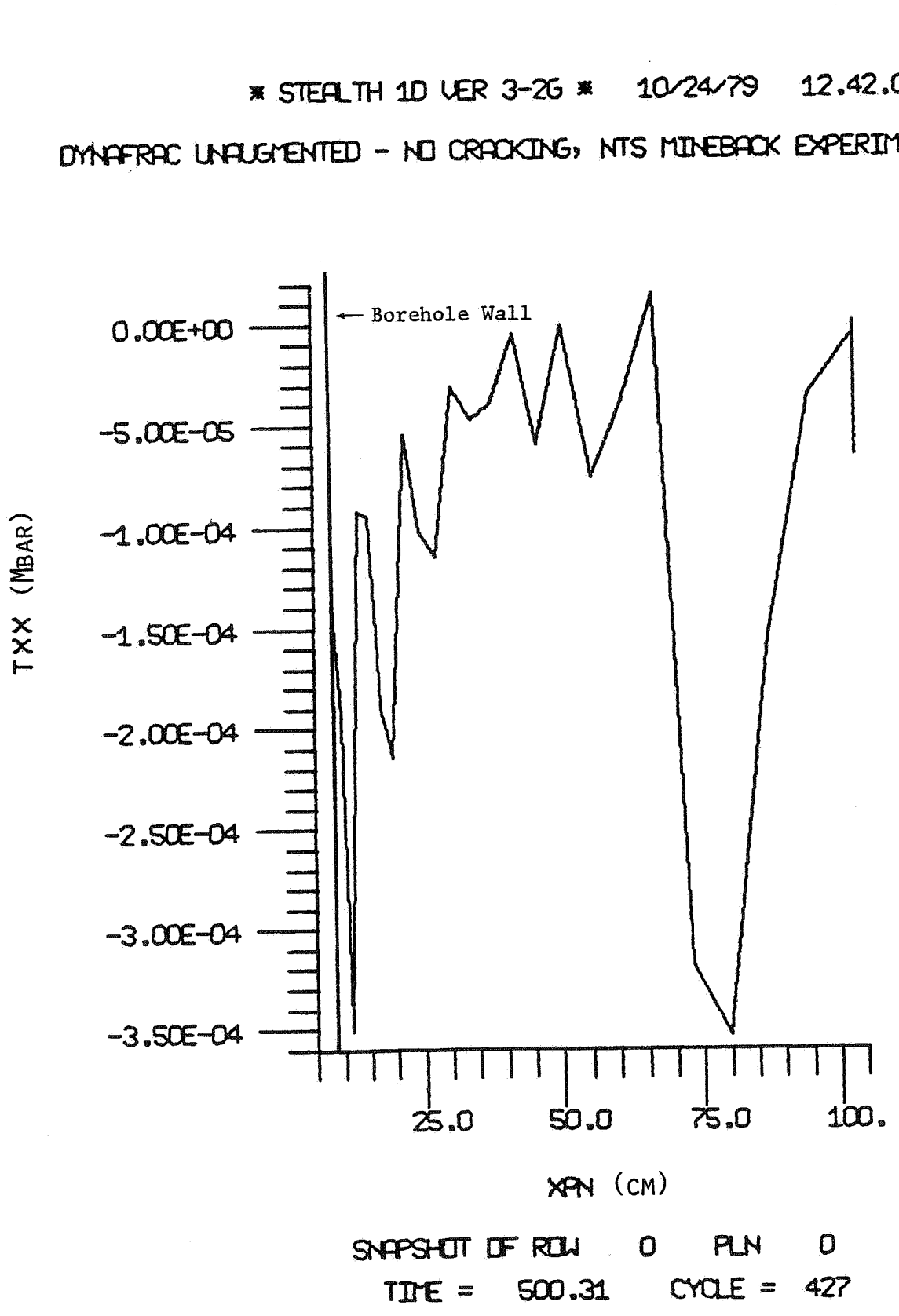

Figure 21c. NTS DYNAFRAC - Radial Stress Snapshot at 500 μsec.

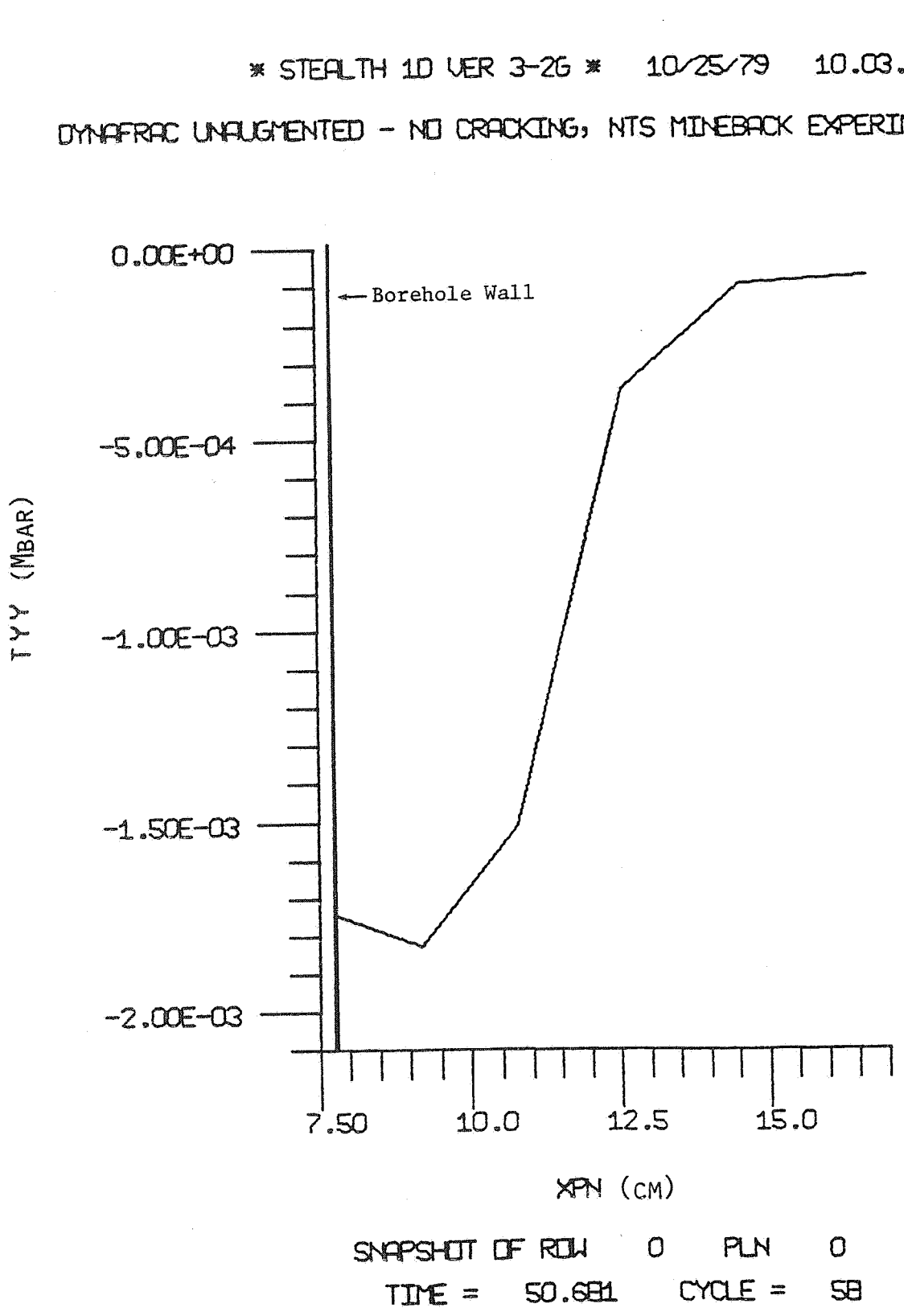

Figure 22a. NTS DYNAFRAC - Hoop Stress Snapshot at 50 μsec.

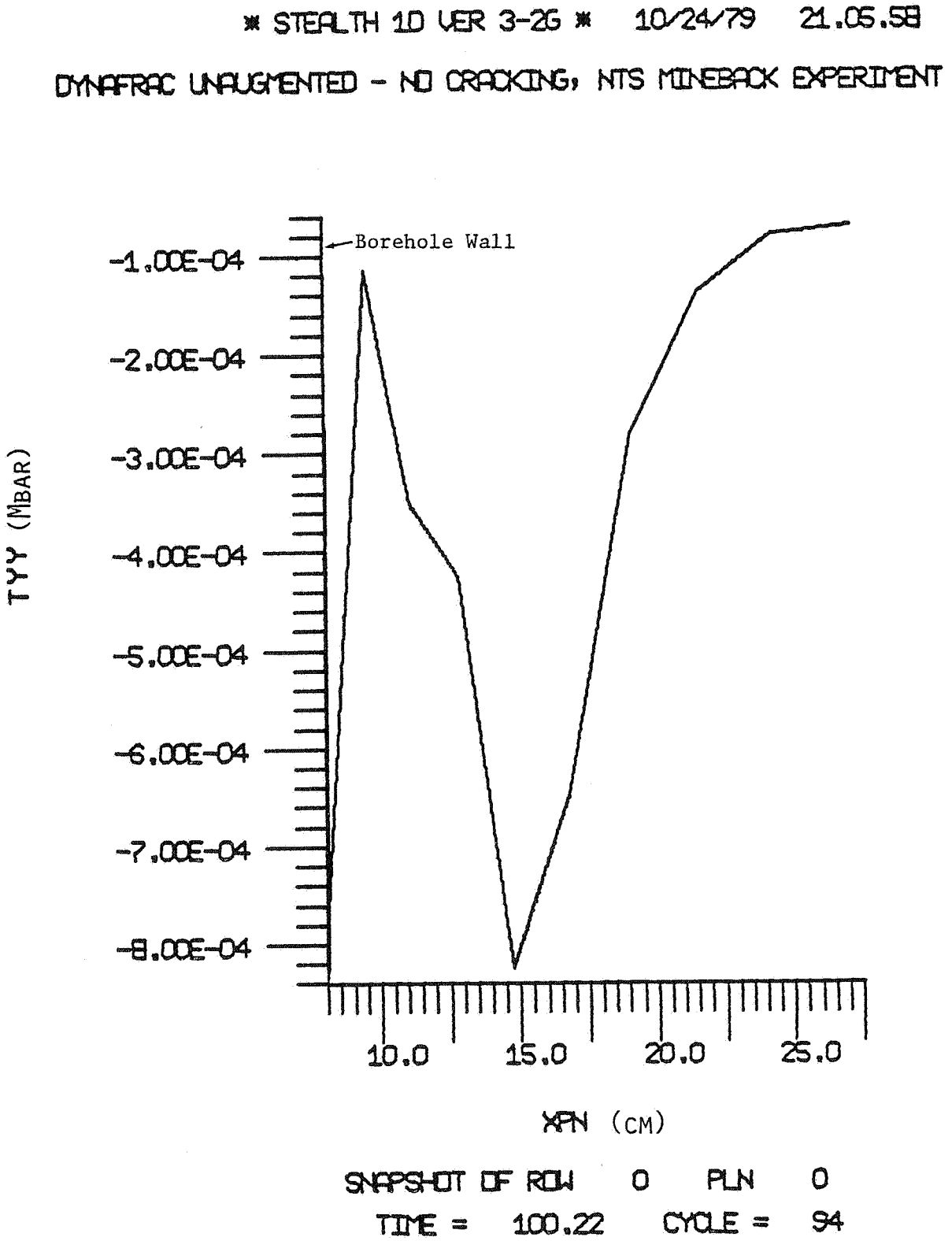

Figure 22b. NTS DYNAFRAC - Hoop Stress Snapshot at 100 μsec.

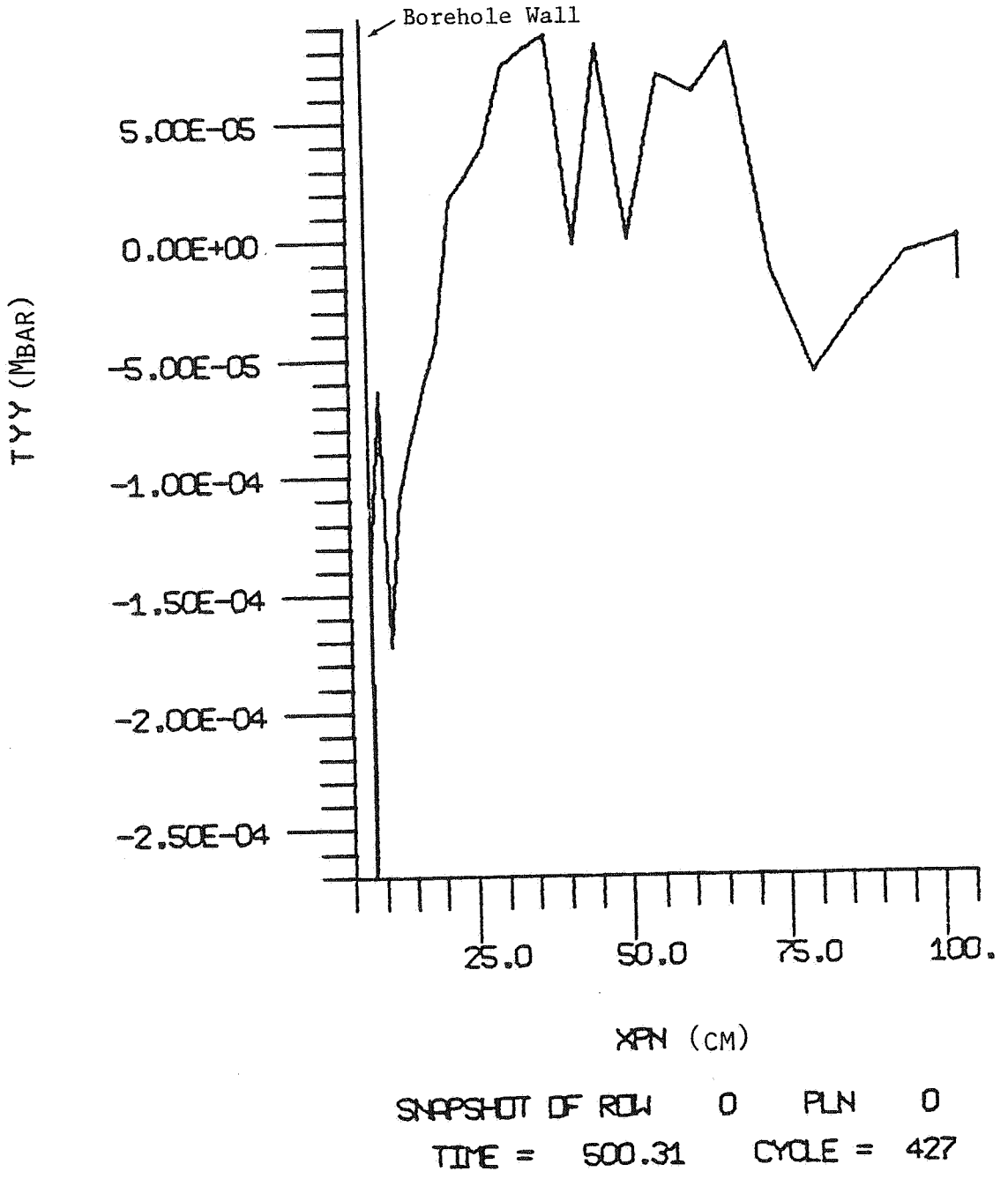

Figure 22c. NTS DYNAFRAC - Hoop Stress Snapshot at 500 μsec.

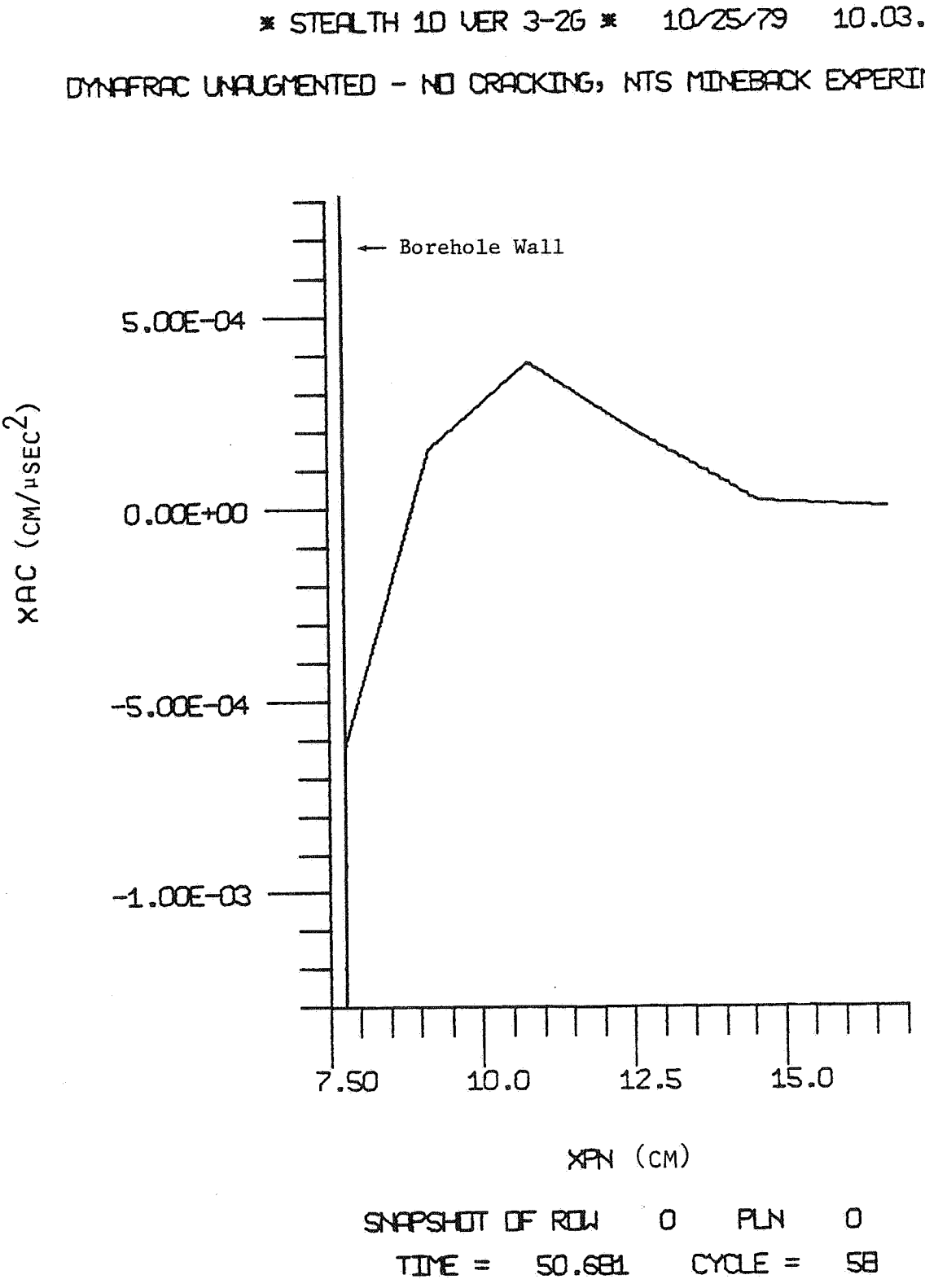

Figure 23a. NTS DYNAFRAC - Acceleration Snapshot at 50 μsec.

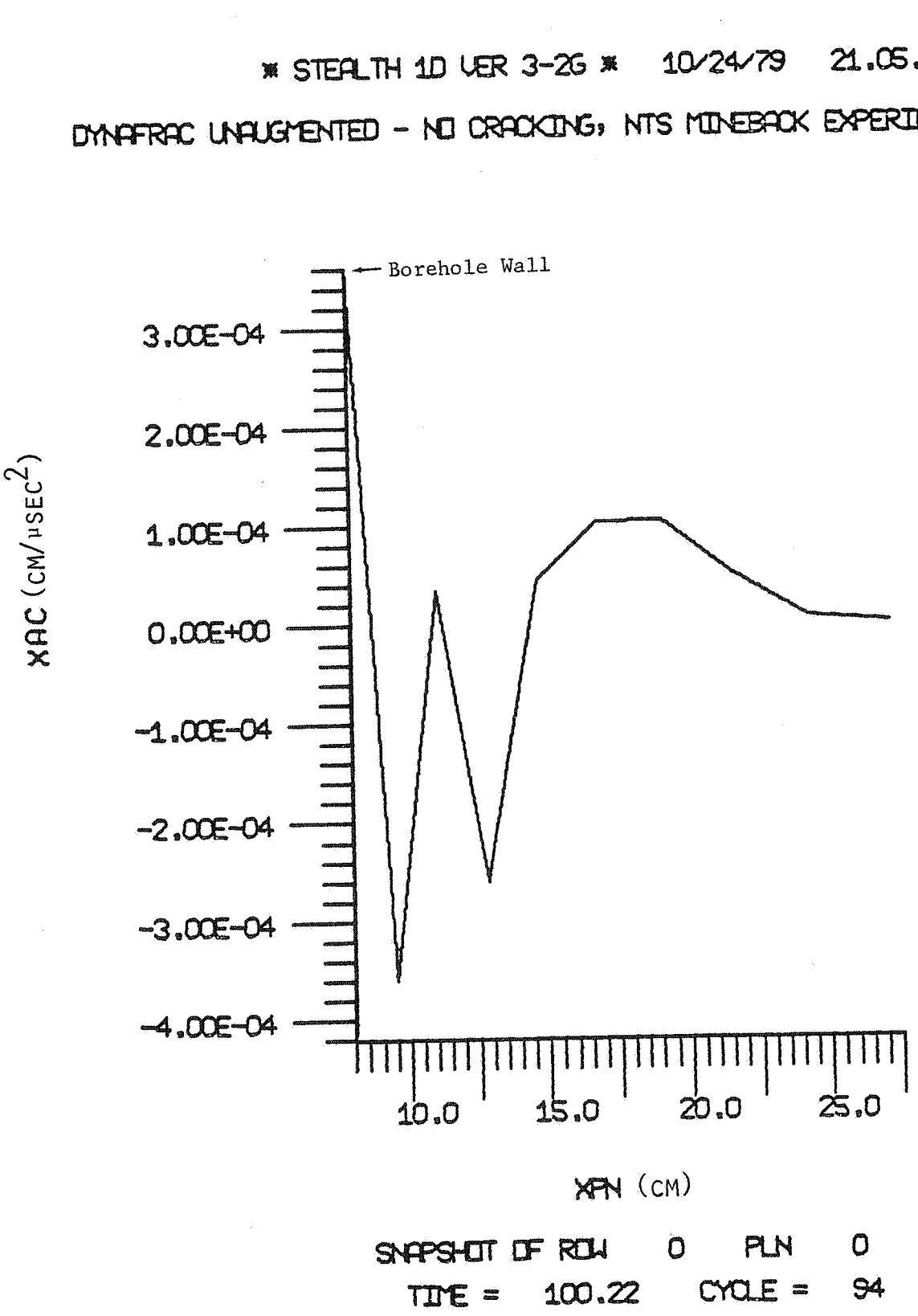

Figure 23b. NTS DYNAFRAC - Acceleration Snapshot at 100 μsec.

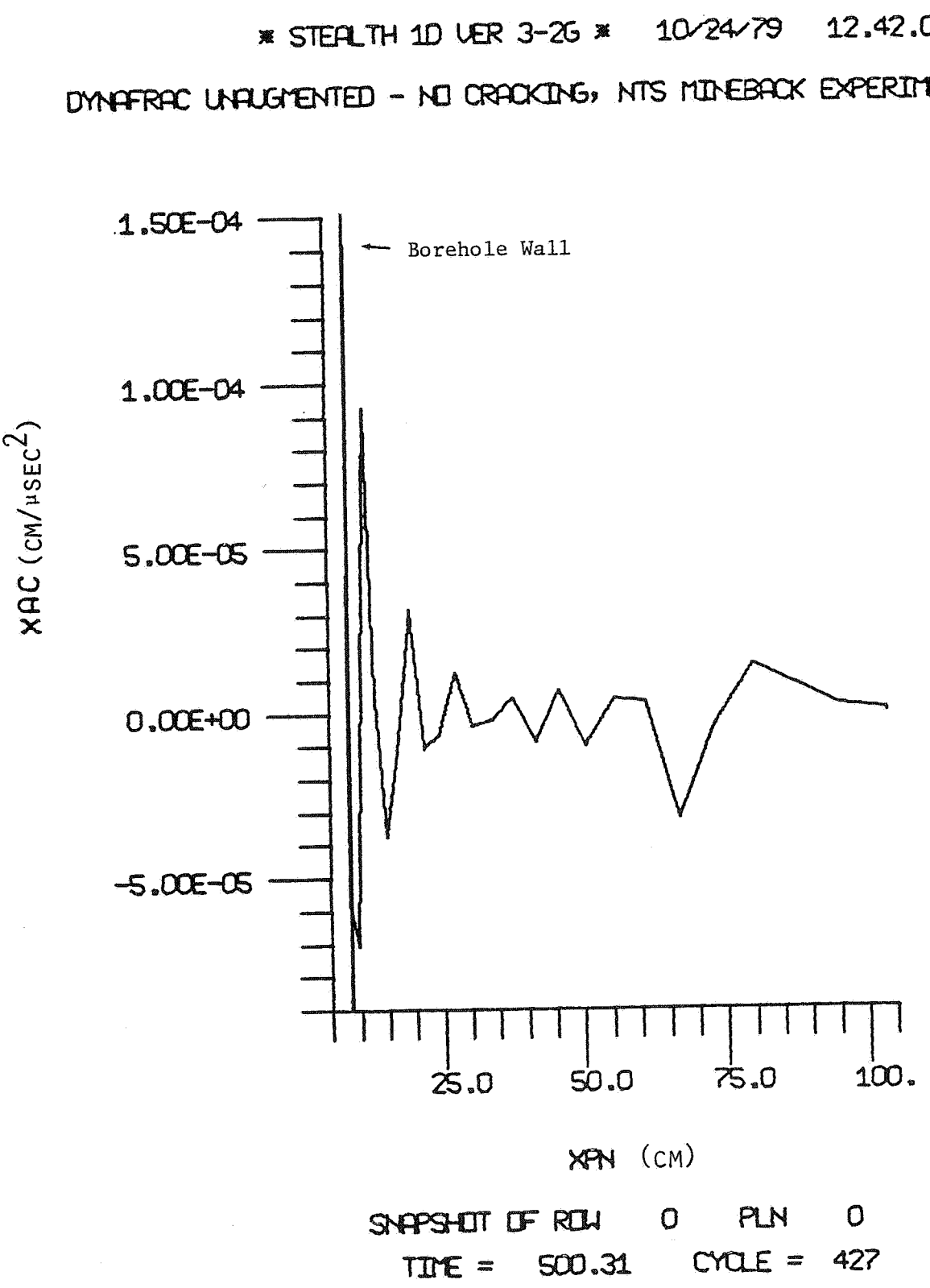

Figure 23c. NTS DYNAFRAC - Acceleration Snapshot at 500 μsec.

SECTION 5

SUMMARY, CONCLUSIONS AND RECOMMENDATIONS

5.1 Summary These efforts were directed towards the development of a numerical tensile failure model that could be used to make a parameter sensitivity study of the EGSP wellbore stimulation methods for gas recovery in Devonian shale. As a preliminary effort to site-specific modeling in Devonian gas shales, calculations were performed using the NTS Multi-Frac Mineback Experiments as the geometry, boundary conditions and material properties of the models.

Several major accomplishments were achieved during this task. These include:

- development of a Crack and Void Strain (CAVS) tensile failure model for one-dimensional fracture analysis using the one-dimensional geometries available in SAI's STEALTH 1-D finite-difference code.
- modification of the original CAVS tensile failure criteria to improve its representation of multiple fracture development by introducing a logic that adjusts the material's tensile strength (both for crack initiation and crack propagation) according to the degree of cracking that has occurred.
- adding a submodel to CAVS to allow for cracking propping when a crack is reclosed and to require energy to be expended during this process.
- adding a submodel to CAVS to allow for crack pressurization when a crack void strain is in communication with the fluid pressures of the borehole.
- performing a parameter sensitivity analysis to determine the effect that the material properties of the rock has on crack development, to include the effects of yielding and compaction.

Using the CAVS model and its submodels, a series of STEALTH calculations were then performed to estimate the response of the NTS unaugmented Dynafrac experiment. Pressure, acceleration and stress time histories and snapshot data were obtained and should aid in the evaluation of these experiments. Crack patterns around the borehole were also calculated and should be valuable in a comparison with the fracture patterns observed during mineback.

5.2 Conclusions The following conclusions can be drawn as a result of this study:

1. Exceeding the yield strength, particularly near the borehole, results in irretrievable deformation (plastic flow) and/or compaction and should be minimized as it causes stress redistribution that can severely limit tensile fracture.

2. The rock yield surface is a critical parameter in the cracking predicted by CAVS. A lower yield strength will result in a larger plastic deformation around the borehole causing stress redistributions which will result in more crack development near the borehole but not extend away from the borehole. A larger yield strength by contrast will cause less stress redistribution and reduces the number of cracks and extend them further away from the borehole into the formation.

3. Irretrievable compaction near the borehole plays an important role in the cracking response as indicated in conclusion 1. An accurate definition of the compaction equation-of-state appears to be important in these preliminary analyses. Modeling the rock's equation-of-state as linear and elastic without describing different paths for unloading and reloading results in less near-field compaction and the creation of a small number of long cracks. Modeling the rock's equation-of-state as non-linear and non-elastic, to provide a more accurate description of its behavior results in more near-field compaction and the creation of a large number of short cracks near the borehole.

4. Greatly exceeding the relatively low tensile strength of the rock by applying large tensile stresses does not significantly assist the cracking process. A crack will initiate and propagate by only exceeding the appropriate tensile strength. Additional crack development and crack extension can be improved if the tensile strength of the rock is only slightly exceeded and held for a longer period of time.

5. Crack propping, either by asperity interference or introduced proppants, directly influences the residual crack void strain and indirectly influences crack extension through crack pressurization. As the shock wave passes the zones immediate to the borehole the hoop tensile stresses generated by the shock are relaxed and the stresses again become compressive. Without a propping mechanism, either natural or introduced, a "skip-zone" commonly occurs around the borehole where cracks that were once open reclose, cutting off communication of the borehole with cracking that has occurred and remains open further from the borehole. By introducing a propping mechanism the residual void strain is accordingly increased. The increased void strain does not directly influence crack extension but because a non-zero crack void strain exists crack pressurization is possible which assists extension.

6. Crack pressurization has the most beneficial effect of the parameters analyzed. During early times (less than 250 μsec), in the unaugmented Dynafrac case, the shock wave caused by the dynamic explosive loading in the borehole initiates and propagates cracks to about 40 cm. Late time (after 250 μsec) cracking will continue to about 80 to 120 cm depending on the pressure profile in the crack, if the shock wave generated cracks are communicating with the borehole and are pressurized by the fluids of the borehole. Calculations which incorporated the crack pressurization model were run for as much as 10,000 μsec to observe the stability and convergence of crack extension as the

borehole pressure decreased to levels that could no longer drive the crack.

7. The nature of the stimulating pressure profile and fracture pressure profile as related to the rock yielding properties can significantly modify the fracture pattern around a borehole.

8. Understanding the phenomenology of explosive/propellant stimulation treatments can be greatly enhanced using time-explicit finite-difference numerical calculations.

9. The factors that influence the cracking pattern in wellbore stimulation treatments have been demonstrated. Comparative evaluations can now be performed between various commercial stimulation treatments with specific pulse characteristics and between hypothetical pulse-tailored pressure profiles.

5.3 Recommendations Having demonstrated the applicability of the CAVS tensile failure model as a means of numerically modeling the EGSP wellbore stimulation techniques, numerous refinements are now in order to improve and add to its capabilities in predicting dynamic fracture and fragmentation of rock. The theoretical basis of CAVS is well-founded, based on the fundamental principles of elasticity, and provides a solid foundation upon which to build a numerical anslysis tool which can model the many interactions of dynamic rock fracture caused by explosive loading conditions. Part of these improvements have been made as a result of this study and are described in Section 5.1.

Many additional factors need to be considered in a complete quantitative evaluation of the many fracture stimulation techniques being proposed or actively considered. The physical processes believed to be advantageous to each technique can be more specifically defined to establish the relative and absolute value of these processes. Initial efforts, however, should be devoted to the critical assessment of the numerical models, in a general sense, so that the many interactions of dynamic fracture and fragmentation, which these models describe accurately represent the physical processes of the event. At the same time, it is equally important that continued efforts be directed toward laboratory and field experiments which will provide the material properties required by these models.

The following list summarizes many of the factors that should be considered in the complete development and evaluation of the CAVS tensile failure model and its use in the fracture technology evaluation for the Eastern Gas Shales Project.

I. Rock Properties
   A. Elastic Properties
      1. stratigraphic variation
      2. influence of natural fractures
      3. differences in static and dynamic properties and rate dependency
      4. anisotropic properties (e.g. due to preferred orientation of natural fractures)

   B. Strength
      1. tensile
         a. rate dependence
         b. stratigraphic variation
         c. effect of pore pressure
         d. planes of weakness (i.e. bedding, natural fractures)
         e. fracture energy approach
         f. stress intensity factor approach
         g. sealing effect
         h. exceeding tensile strength by a large amount
      2. yielding
         a. rate dependence
         b. effect of pore pressure
         c. degree of saturation
         d. cap model
         e. history dependence

   C. Production Characteristics
      1. self-propping fractures
      2. natural fractures
      3. influence of different modes of failure on permeability

4. 2-D effects on self propping
5. gas production characteristics
6. compatibility of fracture model and reservoir model
7. influence of compaction

II. Explosive Properties

A. Characteristics

1. burn rate
2. continuous gas generation
3. pulse shape (i.e. rise time, peak amplitude, decay time, pulse width, decay shape)

B. In Borehole

1. propellant/borehole ratio
2. fluid compressibility/viscosity and flow characteristics
3. multiple shots
4. 2-D effect along borehole
5. compaction/yielding

C. In Fractures

1. detonatability
2. flow characteristics of gas
3. detonation/deflagration
4. fracture face damage
5. explosive viscosity and distribution
6. *in situ* stress effects
7. pressure profile
8. leak-off

III. State of Stress

A. *In Situ*

1. differences in principal stresses
2. effect of pore pressure

B. Induced

1. stress field modifications by displaced explosives
2. peak pulse above *in situ* stresses but below yield surface
3. borehole pressure and consequent yielding and compaction
4. fracture pressure and far field propagation

REFERENCES

1. Butters, S.W., Jones, A.H., and Dropek, R.K., "Material Properties of Nevada Test Site Tuff and Grout-With Emphasis on the Mighty Epic Event," November 1976, DNA4235F. Prepared by Terra Tek, Inc., Salt Lake City, Utah. Defense Nuclear Agency, Washington, D.C.

2. Daneshy, A.A., "On the Design of Vertical Hydraulic Fractures," January 1973, J. Pet. Tech. pp. 83-97.

3. Fitzgerald, R., "The Kinefrac Process in Operation," Internal Technical Report 103, Kinetech Corporation, Sacramento, California.

4. Fourney, W.L., Parker, D.B., and Holloway, D.C., "Crack Propagation Due to Explosive Detonation in Fluid Filled Boreholes," January 1979, University of Maryland, College Park, Maryland.

5. Goodman, R.E., Methods of Geological Engineering in Discontinuous Rocks, 1976, West Publishing Company, San Francisco, California.

6. Hofmann, R., "STEALTH, A Lagrange Explicit Finite-Difference Code for Solids, Structural and Thermohydraulic Analysis," EPRI NP-260, Vol. 1, User's Manual, Electric Power Research Institute, Palo Alto, California, August 1976. Prepared by Science Applications, Inc., San Leandro, California.

7. Hofmann, R., "STEALTH, A Lagrange Explicit Finite-Difference Code for Solids, Structural and Thermohydraulic Analysis, " EPRI NP-176-1, Electric Power Research Institute, Palo Alto, California, April 1978. Prepared by Science Applications, Inc., San Leandro, California.

8. Lee, E.L., Hornig, H.C., and Kury, J.W., "Adiabatic Expansion of High Explosive Detonation Products", UCRL-50422, May 1968. Lawrence Radiation Laboratory, University of California, Livermore, California.

9. Maxwell, D.E., "Refined Equation-of-State of Water," Internal Memorandum, February 1971, Physics International Company, San Leandro, California.

10. Maxwell, D.E., "The CAVS Tensile Failure Model," Internal Report SATR 79-4, April 1979. Science Applications, Inc., San Leandro, California.

11. McHugh, S.L., Murri, W.J., Seaman, L., Curran, D.R., and Keough, D.D., "Fracture of Devonian Shale by Tailored Pulse-Loading," December 1978, Stanford Research Institute International, Menlo Park, California.

12. McHugh, S.L., and Keough, D.D., "The Effect of Explosive Gases on the Fracture Process in Geologic Solids," Proceedings of Third Eastern Gas Shales Symposium, October 1979, pp. 415-424.

13. Moore, E.T., Mumma, D.M., and Seifert, K.D., "DYNAFRAC-Application of a Novel Rock-Fracturing Method to Oil and Gas Recovery," PIFR-827, April 1977, Physics International, San Leandro, California.

14. Schmidt, R.A., personnel communique, April 1979, Sandia Laboratories, Albuquerque, New Mexico.

15. Warpinski, N.R., Schmidt, R.A., Walling, H.C., Cooper, P.W., and Finley, S.J., "High Energy Gas Frac," SAND78-2342, December 1978, Sandia Laboratories, Albuquerque, New Mexico.

APPENDIX A

DESCRIPTION OF THE STEALTH CODES

A.1 Features of STEALTH

The STEALTH* computer code system consists of three continuum mechanics equation solvers, three data analyzers, and one graphics package. The names of the specific codes are STEALTH 1D, STEALTH 2D, STEALTH 3D, ADAPRO 1D, ADAPRO 2D, ADAPRO 3D and GRADIS.

STEALTH 1D, 2D, and 3D are one-, two-, and three-dimensional explicit finite-difference codes which numerically solve the time-dependent, nonlinear thermomechanical, partial differential equations of continuum mechanics. The numerical equations are cast in several coodrinate systems, using the Lagrange (material) frame of reference. Space- and time-centered difference equations result in second-order accurate solutions in both space and time. Pressure discontinuities (shocks) are handled by smearing out the discontinuity with a von Neumann quadratic artificial viscosity; zone-to-zone oscillations (noise) may be damped out by using a linear artificial viscosity; and grid instability (hourglassing) is controlled by a "tensor-triangle" artificial viscosity. Zone tangling is controlled by a "tickle" rezoner. Stability is automatically regulated by the Courant stability criterion. Non-dynamic problems utilize dynamic relaxation to optimize solution convergence.

ADAPRO 1D, 2D, and 3D are the Archive DAta PROcessors for the STEALTH 1D, 2D, and 3D codes, respectively. GRADIS is the GRAphic DISplay package which is used by STEALTH and ADAPRO.

Four volumes of documentation, which present theory, input, and sample problems, have been published. The titles of these volumes are:

---

*"Solids and Thermal hydraulics codes for EPRI Adapted from Lagrange TOODY and HEMP," developed for Electric Power Research Institute by Science Applications, Inc. under Contract RP307.

Volume 1	User's Manual
Volume 2	Sample and Verification Problems
Volume 3	Programmer's Manual
Volume 4	GRADIS Manual

The STEALTH User's Manual is common to the 1D, 2D, and 3D codes. Input instructions and output formats are identical, and standard models in one code are available in the others. Hooks for user-provided subroutines which override standard models can be found in all three codes. In many instances, a user-supplied subroutine for the 1D code can be used unchanged in the 2D or 3D code.

There are seven standard one-dimensional geometries available in STEALTH 1D:

(1) plane strain or slab symmetry
(2) cylindrical or line symmetry
(3) spherical or point symmetry
(4) planar pipe flow geometry
(5) cylindrical, variable height geometry
(6) thin rod geometry
(7) thin plate geometry

There are three standard two-dimensional geometries available in STEALTH 2D:

(1) 2D plane strain (translational symmetry)
(2) 2D plane stress (translational symmetry)
(3) axial symmetry

The three-dimensional code is asymmetric. Grid generation in any of these geometries may be performed by using standard input and/or user-supplied subroutines.

Material models include the ability to include equation of state (mean properties), strength (deviatoric mechanical properties), and heat transfer (thermal properties). Standard options include:

Equation of state (mean properties)

Pressure can be a function of relative volume (or density) and internal energy (or temperature). Tabular relations are also allowed.

Strength (deviatoric mechanical properties)

Deviatoric stress can be a function of strain and/or strain rate. Yield stress, shear modulus, and spall criteria can be functions of thermodynamic variables such as temperature, pressure, density, etc. Tabular relations are also allowed. Deviatoric stress states may be adjusted to the yield surface by any user-supplied algorithm. The standard algorithm is the Prandtl-Reuss flow rule using the second stress deviator invariant as the criterion for plastic flow.

Heat transfer (thermal properties)

Heat flux can be a function of temperature and user-defined properties. The standard heat flux model is a Fourier conduction with temperature-dependent conductivity.

In addition to many standard constitutive models, STEALTH can accept user-supplied models. These models can be programmed into STEALTH in several different ways at the user's discretion. Simple variations of the standard modeling format can be achieved by using the provided user subroutines. Complex models are often more easily coupled to STEALTH by simply replacing the existing solution of the constitutive equations with a self-standing model. Either of these procedures is easily executed in STEALTH.

Boundary conditions are divided into two categories and have the following options available:

Mechanical

Prescribed pressure or velocity histories can be applied to any boundary. Free and fixed boundaries are sub-cases of these capabilities. Interactive boundaries may include sliding without friction and void opening and closing with pseudo-cohesion. Interaction may occur between two grids or between a grid and a prescribed geometric constraint (e.g., a rigid wall).

Thermal

Prescribed temperature or heat flux histories can be applied to any boundary. Isothermal and adiabatic are sub-cases of these capabilities.

A fundamental design feature in STEALTH is its ability to interact with other codes. Weak and strong coupling logics are already programmed into wall-point (rigid body) interaction and Lagrange grid interaction subroutines, respectively. Similar logics may be used to couple STEALTH to finite-element codes, shell codes, and even Eulerian codes. Lagrange-Euler coupling requires a special use of the tickle rezoner to rezone interface points. Shell and finite-element coupling are more straightforward additions to STEALTH, using wall-point logic.

The tickle rezoner, which makes possible the performance of calculations in a Lagrangian, Eulerian, or hybrid mode, is a major STEALTH capability. The rezoner gives STEALTH an ALE-like (Arbitrary Lagrange Eulerian) character which is useful on both hydrodynamic and large-distortion solid mechanics problems. The basic philosophy of the tickle rezoner is to gently and continuously alter the positions of grid points into more favorable locations. It is designed to operate automatically in time and on a point-by-point basis. When the position of an interior point is moved to a new position, the zones surrounding it are rezoned with mass and internal energy being conserved. For free boundary points, stress can be conserved at the expense of conserving mass and energy. It is also possible, through standard options,

to alter velocities of neighboring points to conserve a region's momentum or kinetic energy when the rezoned point's velocity has been changed to preserve the velocity field.

In addition to the tickle rezoner, a dezone capability exists in STEALTH. This capability allows the user to remove interior mesh lines at restart time. Strict mass and internal energy conservation are used to merge zones.

Extensive output and display capabilities are available. This sophisticated plot package, GRADIS, can provide time histories, spatial snapshots, mesh configuration plots, isometric controus, and contour, vector, and tensor plots. In addition to plots, several modes of printed output are available. These include data printed by grid point, data printed by region, subroutine trace information, and formatted COMMON block dumpts. Finally, options exist for storing archive data and for writing restart dumps.

ADAPRO provides STEALTH with a post-processing capability. Archive data that are written by STEALTH during a simulation can be stored, and then read by ADAPRO at some later time. As standard options, ADAPRO can print and/or plot any saved data in exactly the same way that STEALTH does by utilizing the same input records that are used in STEALTH. ADAPRO can also produce subset archieve data files. Its greatest asset, however, is its flexibility in performing data reduction tasks. For example, it is possible to interface a user-supplied spectral analysis code to ADAPRO in order to create frequency domain plots from time history data that were saved during a STEALTH run.

A.2 Summary

The explicit finite-difference method is fundamentally a numerical simulation technique and can be used in several different modes. It can augment data from experiments; it is a useful tool in the design and calibration of field tests; and, finally, it can facilitate the understanding of material response characteristics.

The explicit approach offers more flexibility than some current methods because it is not restricted to solid's or fluid's methods, large- or small-strain models, static or dynamic response techniques, etc. It is all of these capabilities combined. Only economic considerations dictate when an alternative approach should be used.

There are several important reasons for the existence of a user-oriented, well documented system of explicit codes. First, these codes can be used to help check or normalize analytical techniques; second, these codes can be used in their own right to solve problems that cannot be solved by any other method; and third, well documented explicit codes can be used to become familiar with the technology and to form the base for new developments utilizing the explicit approach.

The STEALTH 1D, 2D, and 3D codes have been designed with the intent to satisy these requirements.

☆U.S. GOVERNMENT PRINTING OFFICE: 1983-646-069/681